Stratified shallow flow modelling

Thesis

Sébastien E. Bourban, Ingénieur

(Mathématiques Appliquées et Modélisation Numérique)

Stratified Shallow Flow Modelling

PhD Thesis

October 2013

The Open University

Affiliated Research Centre: HR Wallingford, UK

Discipline: Environmental and Mechanical Engineering

Supervisors:

Prof Alistair G.L. Borthwick and

Dr Alan J. Cooper

Director of studies:

Prof Paul Samuels

External examiners:

Dr Peter Sweby and

Prof Nigel Wright

ORIGINAL COPY TIGHTLY BOUND

PAGE NUMBERING AS ORIGINAL

Acknowledgements

I would like to thank most sincerely both my supervisors, Prof Alistair G.L. Borthwick and Dr Alan J. Cooper, for their continuous engagement and support in expanding my areas of research and as a result my personal knowledge, as well as for their constant encouragement over the last seven years.

I would also like to thank those who worked under my supervision, in particular DPhil Michael S. Turnbull and Dr Christopher J. Cawthorn, for their help in the prototyping of my research outcomes, and Jean-Michel Hervouet and Dr Riadh Ata for making their time available to argue numerical methods and implementation with me.

In addition, I would like to express my gratitude to HR Wallingford as an Affiliated Research Centre of the Open University and to the Open University itself, for giving me the opportunity to conduct and for sponsoring my research toward a PhD degree.

I would also like to thank my co-workers and supervisors while at the Canadian Hydraulics Centre in Ottawa and at HR Wallingford in the UK, for accommodating my leaves of absence and for the priority given to my research work while outside the office hours.

Last but not least, I would like to acknowledge not having taken enough time to enjoy the company of my partner, Noémie Durand, and our 6-year old son and would like to thank them for their enduring and understanding of my primary occupation while at home.

Abstract

Environmental hydraulics covers a very wide range of applications, including free surface flows in rivers, estuaries and lakes. To find engineering solutions to environmental hydraulics problems, 3D numerical modelling is nowadays widely used. However, the computation of sharp spatial gradients (such as found in stratified estuaries and lakes, around plumes near outfalls along rivers and coasts or in exchange areas of high shear), and the modelling of these processes along steep bathymetric slopes (such as found at the edge of dredged channels or of the continental shelf) remains a challenge. In addition, crude assumptions (such as the hydrostatic assumption) are often made to the primary differential equations in order to simplify the problem and enable long term prediction of environmental hydraulic changes.

In this thesis, a robust adaptive mesh displacement (AMD) method is implemented and validated against the lock exchange case in particular. The AMD method aims at vertically focusing nodes within each water column to capture sharp gradients, while reducing the number of nodes or requiring prior knowledge of the flow structure. Second, a direct computation of dynamic pressure is introduced based on the equation of vertical momentum and validated against the analytical potential flow theory solution of a source-sink pair. Dynamic pressure is necessary to model de-stratification recirculation devices, or flow over dredge channel, or solitary waves, for instance. This direct computation method makes the hydrostatic assumption redundant. Third, a new advection scheme is implemented, whose main advantage is simplicity averaging over Riemann problems without solving them, while excessive

numerical viscosity is compensated for by using high-resolution MUSCL type reconstruction.

Recommendations are made in this thesis to extend the advection scheme developed herein for tracer advection to the non-linear shallow water equations, to the diffusion terms and to turbulence closure laws within the same finite element framework.

Content

BLANK PAGE IN ORIGINAL

Chapter 1 – Introduction

This Chapter provides an introduction to stratified shallow flow modelling in the context of environmental hydraulics, followed by the aim and objectives of the research work, a discussion of the evolution of the research strategy, and concludes with a synopsis of the thesis.

Environmental hydraulics covers a very wide range of activities, including but not only physical and numerical modelling of free surface flows in rivers, coastal waters and estuaries and lakes. Modelling of free surface flows include, for instance, modelling dam breaches and flash floods, modelling reservoir stratification and algal blooms, geomorphological evolution of estuaries, fresh-salt water exchanges in estuaries, modelling tidal and wave energy resources, impact of dredging and disposal activities, wave agitation in harbours, tsunami propagation coastal inundations, etc.

This thesis focuses on numerical modelling within a subset of environmental hydraulics activities. Depending on the dimension of the problem, numerical modelling is carried out using one-, two-, or three-dimensional solvers (1D, 2D, and 3D respectively), each applied to a wide range of environmental hydraulics activities. For the past 17 years, the author of the present work has been developing and using numerical 3D solvers for free surface flow applications in many parts of the world, and in particular for applications related to the subset of stratified shallow flow modelling.

Ch.1-1. Stratified shallow flows

Shallow flows here refer to the natural bias between the vertical and horizontal scales of the world of environmental hydraulics, which is here sufficiently close to a thin flat disk. The water bodies considered vary vertically from a few meters to a several tens of meters while at the same time vary horizontally from a few hundreds of meters to several hundreds of kilometres.

Stratified shallow flows here refer to the presence of at least two layers of different densities, either one above the other (uniform flows) or one wedging under the other (non-uniform flows), leading to 3D processes. Density differences can be the result of a combination of variations in water temperature, salinity or sediment concentrations. In a typical estuary, for instance, the denser layer underneath is the result saltier waters coming from the sea while the lighter layer above the result of warmer waters coming from the land. Estuaries with high sediment content could develop an additional fluid mud layer near the bottom. Contrarily, in the ocean, hotter waters can convey saltier waters to the surface while colder fresh waters would plunge toward the ocean floor. Density differences can result in gravity current such as underflows of waste waters in streams preventing natural aerobic degradation, underflow of sediments behind hydropower dams clogging sluices and turbines, anaerobic condition in lakes and seas posing a serious stress to all aquatic like forms or the formation of sub-surface waves during the filling of locks.

Industrialisation, climate change, population growth, development of riverine and coastal areas greatly impact the environment and, in particular, water and its quality. Modelling stratified shallow flows in environmental hydraulics aims at predicting and mitigating numerous practical 3D problems and their solutions.

Ch.1-1.1. State of the art of stratified flow modelling

Already in the sixties, the US Bureau of Reclamation (1966) reported that the state of the art in stratified flow modelling was dynamic with many national institutions and organisations around the world involved. At the time, future research by its Hydraulics Branch was to consist of general studies concerning the influence of intake geometry on selective withdrawal from stratified reservoirs.

Almost 50 years later, many national institutions and organisations worldwide remain active, with as many 3D free surface solvers. While free surface numerical modelling is nowadays widely used to find engineering and / or environmental solutions to problems, the number of solvers available indicates that the state of the art remains as dynamics as it used to be, with its gaps, strengths and weaknesses.

Ch.1-1.2. Modelling gaps in the current state of the art

A relatively extensive review of 3D free surface solvers known to the author to date has been carried out and assembled as preparation for the present research work. Where possible the source code was downloaded. The complete list of twenty four 3D solvers reviewed is included in Appendix B. Although incomplete, the list illustrates differences and commonalities of the principal features between solvers and provides an overview of the present state of the art. It should be noted that the list and its associated analysis was also in part used by HR Wallingford in an internal research and development strategy document (Curington & Bourban, 2009), and the 2D/3D Flow Modelling Advances strategy implemented under the leadership of the author of

the present work.

In summary, the mathematical description of the physics of free surface flows is a relatively mature field, with most solvers based on the continuity and Navier-Stokes equations (see Section Ch.3-1.1) or, by extension, the Reynolds-Averaged continuity and Navier-Stokes equations aimed at turbulent flows, and where the free surface is directly calculated and related to the pressure field under the hydrostatic assumption.

However, numerical methods and assumptions remain divided and in constant evolution. For instance, the list of 3D hydrodynamic solvers can be split into two distinct categories: those with the vertical structure of the mesh based on a sigma-stretched transformation and those based on fixed horizontal levels. This categorisation reflects the inadequacy of either numerical method to be universally applicable, with only a few exceptions implementing a hybrid representation dependent on the water depth.

In addition, the list shows that the majority of 3D solvers use the hydrostatic assumption (mainly because these are based on previous generations of computers), and either a mixing length theory or the turbulence closure model of Mellor Yamada (1982) level 2.5. Most of these solvers are implemented with the "Arakawa C" scheme (Arakawa & Lamb, 1977) applied either to finite difference and/or finite volume formulations. All 3D solvers known to the author to date which implement a non-hydrostatic formulation do so by deriving a Poisson equation of the dynamic pressure from the 3D mass conservation equation.

Further, the list also shows that, except for COHERENS (which is a coupled solver soon to become implicit), all solvers involve decoupled and semi-implicit solutions of the continuity and Navier-Stokes equations (or by extension the continuity and Reynolds-averaged Navier-Stokes equations.) whether in their advective or divergent form.

Several solvers differ from each other solely in that they implement one or a few distinctive features such as the Krauss-Turner mixed layer diagnosis algorithm (Krauss & Turner, 1967) or the "Arakawa A" spatial discretisation scheme (Arakawa & Lamb, 1977). Last but not least, a handful of solvers, such as ADCIRC, ICOM-FLUIDITY and TELEMAC, are based on the finite element method formulated on unstructured meshes. Unstructured meshes are also used by certain finite volume solvers such as FVCOM.

Ch.1-1.3. Significant advances required

Three gaps, for which significant advances could be made, have been identified below based on the author's previous experience. Each of these gaps was associated one research objective also introduced here.

Categorisation of 3D solvers

Having collected information on many 3D shallow water solvers (see Appendix B) using by major national and international organisations, it is clear that virtually all solvers fall into only two mutually exclusive categories, depending on the vertical discretisation: (a) those with fixed horizontal layers; and (b) those with sigma-stretched transformation. For illustration purposes, Figure 1.1 shows a comparison between vertical cross sections through an arbitrary domain with fixed layers and sigma-stretched transformation, left and right respectively.

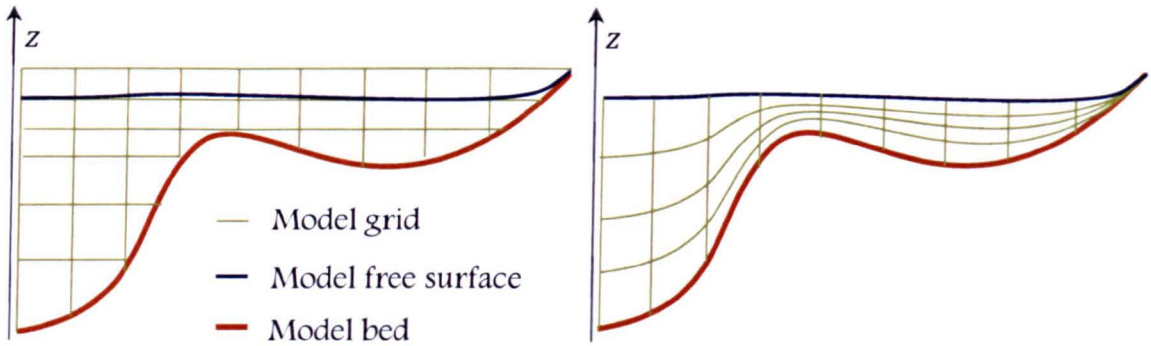

Figure 1.1 – Fixed horizontal layers and sigma-streched transformation

In the case of fixed horizontal layers, the 2D mesh representing the entire domain as projected on a horizontal plan is intersected with the varying depth of the water domain. Layers are defined as horizontal slices of constant thickness made of all elements above the bottom of the domain. Depending on the depth, a water column as more or less elements and the bottom of the domain ends up fitted with steps depending on where the horizontal slices intersect.

Solvers with fixed horizontal layers are applicable to modelling stratification in deep lakes such as the Coquitlam Reservoir holding the drinking waters for the Vancouver area, Canada but are presently incapable of modelling friction-driven sediment transport as a continuous map following the bathymetry over large estuarial mudflats and wetlands.

In the case of a sigma-stretched transformation, the 2D mesh representing the bottom of the domain is extruded vertically into a volume between the surface defining the bottom and the surface defining the water free surface. A constant number of intermediate surfaces can further discretise the vertical columns resulting in a layered mesh, where one layer is defined as the volume between two adjacent surfaces. Each surface is supported by 2D unstructured mesh; all surfaces are stacked one above the other and project to the same 2D mesh.

Solvers with sigma-stretched transformation are applicable to modelling large

estuaries such as the Severn Estuary in the UK, with wetting and drying (mudflats, wetlands) over vast areas but are presently incapable of modelling horizontal stratification over steep bathymetry slopes as the mesh follows somewhat the bathymetry and the free surface rather than the thermal / saline layering of the water column.

Moreover, for applications such as the Congo River Mouth with its underwater canyon piercing through the east African continental shelf, neither types of solvers are presently suitable to model it all.

The first of the three research objectives was therefore to develop a novel numerical method allowing a greater flexibility of the vertical representation within 3D solvers to automatically adapt to the evolving physics of the model, specifically to stratified flows.

The novel method (so-called AMD method) is introduced in Ch.3-2.10. The chosen mathematical framework is of the Navier Stokes equations combined with tracer-driven density or gravitational flows. The chosen numerical framework is the open TELEMAC system.

Absence of appropriate numerical schemes

Again, based on the information drawn from the same collection of 3D shallow water solvers (see Appendix B), the second problem identified is that only a handful of models implement a numerical scheme that is monotonic, at least second order accurate, capable of capturing the strong gradients present in stratified waters, and implicit for long term simulations (short definitions of these numerical characteristics are presented in Section Ch.2-1 of Chapter 2). A literature review of numerical schemes that could be appropriate to 3D stratified shallow flows (see Chapter 2)

confirmed that the combination of these numerical properties within the same formulation is difficult to achieve. Even so, these numerical capabilities are important in order to predict stratification processes, for instance, of the appearance, movement and breakdown of stratified waters under the influence of natural forces (winds, tides, etc.) or artificial forces (recirculation devices, thermal outlets, etc.).

In practice, numerical modellers are presently confronted with having to make choices that meet one principal physical aspect while missing on the others, for instance, advancing tidal fronts versus tidal amplification, or flows entrained around the outlet of mixing devices versus long term water quality time scale.

The second of the three research objectives was therefore to investigate a series of numerical schemes for their application to stratified flows, particularly to multi-dimensional hydrodynamics and tracer advection over long periods of time.

The selected scheme and its novel adaptation within a finite element framework (so-called the BCT scheme) in introduced in Ch.3-2.3. The numerical framework is of the open TELEMAC system. The mathematical framework was restricted to pure three-dimensional tracer advection equation, although its generalisation to the Navier Stokes equation is been implemented in collaboration with the author of the present thesis.

Computationally intensive non-hydrostatic assumption

Finally, the information drawn from the collection of 3D shallow water solvers (see Appendix B), highlighted that many 3D free surface shallow water solvers do not implement a non-hydrostatic pressure term, and those which do do so via the resolution of a Laplace equation, which is computationally prohibitive for long term simulations. However, dynamic pressure has a very important influence on flows in deep waters and in stratified waters subject to natural or artificial forcing. For instance,

modelling of de-stratification devices in reservoirs, such as bottom outlets, jet-circulations, or bubble diffusers requires non-hydrostatic pressure.

The third of the three research objectives was therefore to develop a novel method to calculate dynamic presume without resolving to the solution to the Laplace equation.

The novel method is introduced in Ch.3-1.8. The chosen mathematical framework is of the Navier Stokes equations. The chosen numerical framework is of the finite difference coupled solver SULIS.

Ch.1-2. Research aim and objectives

The aim of this thesis is to improve the applicability of existing 3D solvers to a wider spectrum of problems in order to model both short and long term evolution of stratified flows as observed in environmental hydraulics while avoiding compromising on key features of these types of flows.

Consequently, three research objectives were developed following a gap analysis based on past consultancy and research work experience by the author of the present thesis. These are as follows:

- To develop a novel numerical method allowing a greater flexibility of the vertical representation within 3D solvers to automatically adapt to the evolving physics of the model, specifically to stratified flows;

- To develop numerical advection schemes for stratified flow modelling that are monotonic, at least second order accurate, non-diffusive in advecting sharp gradients, fully or at least semi implicit, and correctly represent non-linear 2D and

3D flows and if possible be also applicable to diffusion terms and / or multiple equation turbulence closure methods; and

- To develop a novel method to directly calculate dynamic presume without having to resolve to the solution to the Laplace equation.

The development of these methods and schemes were validated against practical applications such as the lock exchange problem, the interaction between sources and sinks within a water column or the advection of tracer profiles.

Finally, for reasons highlighted in the following historical evolution of the thesis, both SULIS and TELEMAC were used as numerical frameworks for the implementation of certain new concepts developed through the present work: SULIS in the earlier part, TELEMAC in the later part of the research work.

Ch.1-3. Research evolution

Prior to starting with this research work, the author wrote the finite difference implicit coupled 3D solver, SULIS (Bourban, 1997) to study long term water quality processes and recirculation in deep reservoirs. The author also worked on the finite element semi-implicit 3D solver, TELEMAC (Hervouet, 2007) to examine the hydrodynamics of coastal and estuarial waters. The knowledge and experience gained over more than a decade would later guide choices made at the start of this research work.

For the first half of the present work, the author aimed at significantly upgrading the numerical framework of the 3D solver SULIS (within a finite differences context). The original intention was to work on the latest shock capturing methods and monotonic high order time integrators and their application to the 3D hydrodynamics and tracer

transport equations. Further, it was anticipated that SULIS would be modified so it would be based on triangular meshes and the solver parallelised. During that time, SULIS was re-written by the author in a conservative form and a new non-hydrostatic approach implemented and validated (see Section Ch.4-2).

However, following the departure of the author from Canada to join HR Wallingford in UK, the research strategy changed. The research objectives remained the same, but the anticipated involvement of the author on similar numerical developments moved to TELEMAC (within a finite elements context) resulted in a repositioning of the present work away from SULIS. Throughout the evolution, the research work focused on the implementation of new algorithms aimed at improving the representation of stratified free surface flows.

Ch.1-4. Synopsis

Chapter 2 presents a literature review focusing on implicit numerical schemes capable of capturing sharp gradients for application to stratified waters. Chapter 3 details the governing mathematical equations and boundary conditions noting the assumptions. A new approach is introduced for the computation of dynamic pressure in 3D non-hydrostatic solvers. Details are given of the advection scheme chosen for implementation in the open TELEMAC system and its extension to 3D adaptive layering. Chapter 4 presents the verification and validation tests used to confirm the accuracy and applicability of the new algorithms. Examples related to practical environmental hydraulics are considered including the source-sink flow and the lock-exchange problem. Chapter 5 lists the primary conclusions of the research work and offers recommendations. Appendix A lists all symbols used in the thesis. Appendix B

lists the merits and drawbacks of twenty four existing 3D free surface solvers.

Appendix C details some aspects of some of the analytical solutions available to hydrodynamic equations, including those based on potential flow theory and solutions to the Laplace equation.

Chapter 2 – Literature review

This Chapter 2 reviews the literature currently available on implicit numerical schemes capable of computing and maintaining sharp gradients for application to stratified estuaries and lakes, to plume dispersion along rivers and coasts and to areas of high shear. A detailed discussion of the various numerical schemes reviewed is provided in terms of their potential to fulfil the objectives of the present research work, in particular their horizontal and vertical representation and the degree to which each scheme represents shocks, is accurate, monotonic, implicit and suited to three-dimensional and non-linear applications. For clarity, the definition of these numerical scheme characteristics is reminded in the first section.

Ch.2-1. Scheme characteristics

Ch.2-1.1. Accurate

Scheme accuracy is a mathematical measure based on the numerical analysis of the convergence of the scheme for varying discretisation assumptions. The analysis of the convergence measures whether and how a discrete solution converges to an analytical solution when the space discretisation tends to the continuum. The rate of convergence also defines the order of the scheme, hence the naming convention 1st order accurate (linear convergence), for instance, or 2nd order accurate (parabolic

convergence). Roaches (1998) details and opposes various definitions of accuracies and associated errors and ties (order) accuracy to the verification process, or solving the equation right whether or not the equation and its solutions bear any relation to a physical problem.

One of the objectives of the thesis is to select high order accurate schemes, as they allow for a coarser discretisation while remaining accurate, hence faster computation time for long term environmental hydraulics applications.

Ch.2-1.2. Treatment of sharp gradients (or discontinuities)

In the field of free surface environmental hydraulics, sharp gradients or discontinuities can be found in many forms. For instance:

- In a lake or reservoir for instance, a hotter thermal layer can develop at the surface creating a sharp gradient in vertical temperature profile with the colder layer below. At the interface of the two layers, the mixing is considerably reduced, in turn preventing the colder layer from re-oxygenating with the surface. As the water is being replenished form the watershed or discharged, the interface moved vertically with the free surface, up or down respectively.
- In the propagation of a dam breach down a valley or a tsunami wave up on the coast a sharp gradient or discontinuity in the free surface level can be observed at the front of the water wave. In this case, the parallel is made with shock waves produced in a shock tube used to produce high velocity and high temperature gas over a short period of time, a description of which is produced by Hughes & Brighton (1999), for instance.

The numerical treatment of sharp gradients remains a difficult problem with at least two sorts of approaches: shock-fitting and shock-capturing methods. Shock-fitting methods explicitly track the position of the interface and its shock wave characteristics. The interface is treated as a discontinuity and the equations are solved on either side to high order accuracy. However, for complex flows in three-dimension with possible interactions between discontinuities, shock-fitting could become impractical. Rather, shock-capturing methods represent discontinuities naturally, by numerical design of the conservative form of the equation (see Ch.3-1.2), which makes these more appropriate to complex three-dimensional flow problems. The drawback is that shock-capturing methods highlight inherent spurious numerical oscillations near the discontinuity and loss of accuracy with dissipation needed to suppress these oscillations. Rawat and Zhong (2009), for instance, offer a comparison of the two approaches and conclude on the advantages of using hybrid approaches for high accuracy solution in complex flow problems tracking the front based on wave characteristics.

One of the objectives of the thesis is to select a numerical scheme capable of modelling advection of sharp gradients or discontinuities in the conservation variables. While the thesis highlights the development of a three-dimensional numerical scheme for application to the linear laws of tracer advections, the selected scheme has been studied in the wider context of non-linear laws for future application to the hydrodynamics. Preference has been given to numerical schemes highlighting higher order accuracy on either side of the discontinuities, while fitting the discontinuity within as small a gap as possible based on the characteristic shock waves.

Ch.2-1.3. Monotonic

A numerical scheme is said monotonic when an arbitrary norm of the discretised solution does not increase as the solution evolves over time. A monotonic scheme guarantees that physical maximum and minimum values of conservation variables would be preserved, preventing the solution from over-shooting or oscillating about sharp gradients for instance. An example of norm highlighted in this thesis if the so called Total Variation Diminishing (TVD) norm, which ensures that two neighbouring local minima-maxima values cannot be farther apart than they were originally. An example of method to ensure monotonicity is the use of filters or flux limiters to cap sharp gradients depending on surrounding profiles. A list of such flux limiters found in the literature is reproduced in this Chapter 2.

One of the objectives of the thesis is to select monotonic schemes to avoid computation of non-physical solutions. For instance, in an estuary, salinity varies sharply at the interface between denser seawaters and lighter fresh waters. A non-monotonic second order centred scheme could expand into the non-physical domain of negative salinity, which is to be avoided.

Ch.2-2. Scheme representation

Ch.2-2.1. Classification

Numerical modelling of flow problems in the Eulerian framework essentially involves the solution of the governing partial differential equations in discrete form on a grid at prescribed locations (finite difference methods), or cells (finite volume, finite element and spectral methods). In the context of finite difference solvers of the 2D shallow

water equations, Arakawa and Lamb (1977) defined 5 discretisation schemes, i.e. 5 possible positionings of the primary variables u, v and h when discretised on a regular grid (see Figure 2.1, Schemes A to E). The definition of the symbols u, v and h can be found in Appendix A.

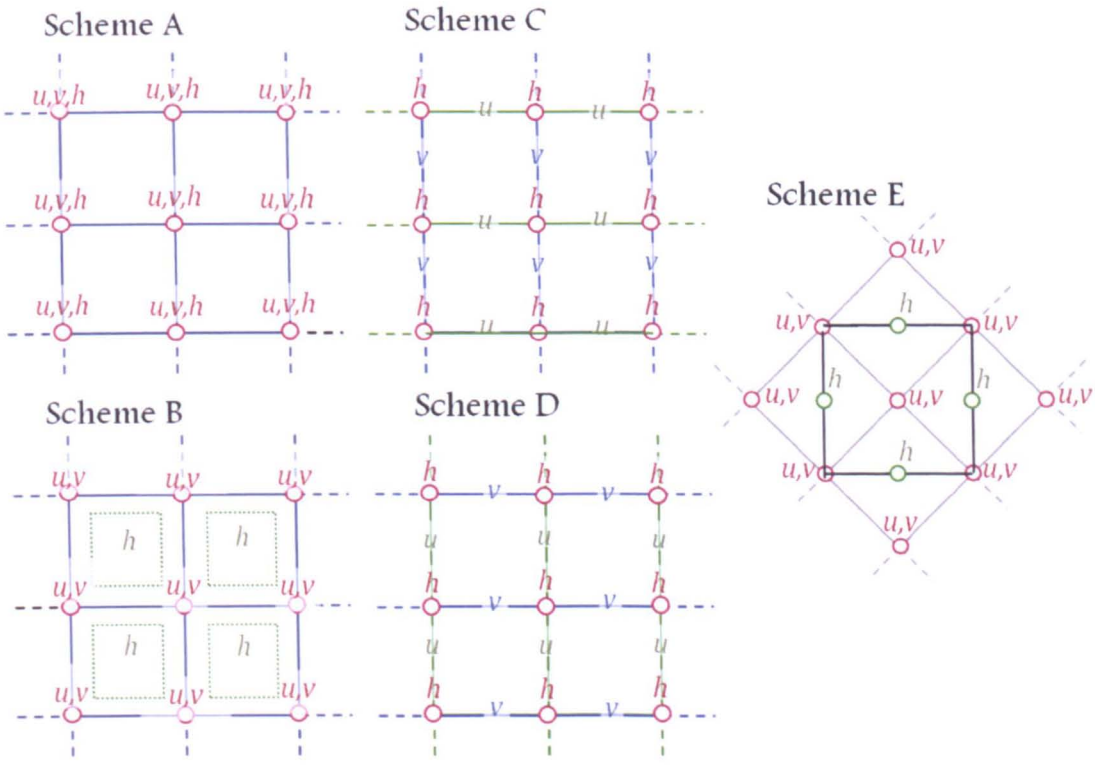

Figure 2.1 – Possible discretisation schemes of Arakawa & Lamb (1977)

Arakawa and Lamb compared the relative behaviour of the 5 schemes to the ideal continuum solution with respect to order accuracy, stability and conservation properties, where stability is achieved if small perturbation errors in the solution do not result in the perturbation errors to increase as the solution evolves with time. They demonstrated that these properties depend on the relative position of the primary variables and on the definition of the gradients of these primary variables given that stencil.

Arakawa and Lamb (1977) chose the *von Neumann* method to estimate the space discretisation error of each scheme on a linearised version of the 2D shallow water equation model. The *von Neumann* method determines the stability of a scheme

through studying the behaviour of admissible harmonic solutions, i.e. the solution is assumed proportional to $e^{[i(kx-\upsilon t)]}$, wher k e is the wave number in the x direction, and υ the angular frequency of the inertia-gravity. It was used by Arakawa and Lamb to extract the angular frequency of inertia-gravity waves. Arakawa and Lamb found that Scheme B and Scheme C were most accurate and that Scheme D was, in that particular case, least accurate compared to the ideal solution. Further comparison between the numerical analytical solutions of an initial value problem demonstrated that Scheme C performed best, in term of accuracy, stability and conservation properties.

It should be noted that several of these schemes were established before the publication by Arakawa and Lamb. For instance, Lilly (1964) obtained the discrete conservation of mass, momentum, kinetic energy and thermal advection based on Scheme A. Harlow and Welch (1965) demonstrated the conservation of mass, momentum and kinetic energy of their solver of the divergence form of the Navier-Stokes equations, based on Scheme C, through its application to two variations of the classical dam breach problem.

Since 1977, many authors have used Arakawa and Lamb's classification. Most 3D solvers reviewed in this thesis (see Section B.3 in Appendix B) are based on the Arakawa C scheme except DieCAST, which is based on the Arakawa A scheme (see Section B.3.5 in Appendix B). It is noted that, the solver SULIS (Bourban, 1997), used as numerical framework for the implementation of dynamic pressure term (see Section Ch.3-1.8 in Chapter 3), is based on Scheme C.

Ch.2-2.2. Interesting observations for wetting and drying applications

In the context of wetting and drying, Falconer and Owens (1987) obtained "much more realistic predictions of the time-varying water surface elevations" by locating the water depth h at the same place as both velocity components, while keeping the free surface as defined by Scheme C. The number of bathymetry points is doubled, hence leading to better representation of the bathymetry and topography of the model. In this particular case, the error analysis undertaken by Arakawa and Lamb is still valid since it is based on the linearised version of the 2D shallow water equations, where the water depth h is assumed constant. With the product uh and vh on each u and v side of the cell seen as the flux through that side, the work undertaken by Falconer and Owens seems to confirm the appropriateness of a conservative "finite volume" form of the finite difference method applied to the continuity and Navier-Stokes equations.

Ch.2-2.3. One additional discretisation scheme

Following on the observations made by Falconer and Owens (1987) an additional sixth scheme, Scheme F (see Figure 2.2) could be developed where the free surface h would be placed at both u and v locations, hence doubling the number of nodes for that variable.

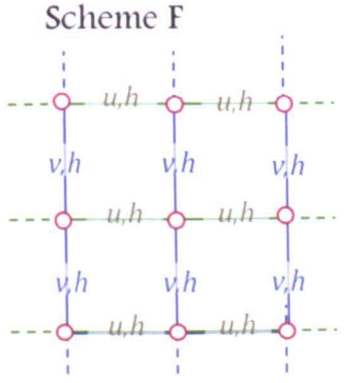

Figure 2.2 – Proposed Scheme F, expanding on Arakawa & Lamb (1977)

The same analysis of space discretisation error on the angular frequency of the inertia-gravity waves as that of Arakawa and Lamb (1977) leads to two possible models depending on the computation of the gradient of h in the momentum equation:

Scheme Fa (2.1)

$$\partial u/\partial t - f\bar{v}^{xy} + (g/d)\overline{(\delta_x h)}^{x} = 0 \qquad \partial v/\partial t + f\bar{u}^{xy} = 0$$

$$\partial h/\partial t + (H/d)\overline{(\delta_x u)}^{x} = 0$$

Scheme Fb (2.2)

$$\partial u/\partial t - f\bar{v}^{xy} + (g/d)\overline{(\delta_x h)}^{y} = 0 \qquad \partial v/\partial t + f\bar{u}^{xy} = 0$$

$$\partial h/\partial t + (H/d)\overline{(\delta_x u)}^{x} = 0$$

Arakawa and Lamb (1977) define f as the Coriolis coefficient, H as the mean value of the water depth h, d as the grid step (based on a regular grid). The gradients are defined by $(\delta_x w)_{i,j} \equiv w_{i+\frac{1}{2},j} - w_{i-\frac{1}{2},j}$ and the average $(\bar{w}^{x})_{i,j} \equiv \frac{1}{2}\left(w_{i+\frac{1}{2},j} + w_{i-\frac{1}{2},j}\right)$, for any quantity w and i and j indices of the grid points along the x and y-axis. All the other symbols can be found in Appendix A.

Therefore, if the solution is assumed proportional to $e^{[i(kx-vt)]}$, where k is the wave number in the x direction, then the angular frequency v of the inertia-gravity waves are given by:

$$(v/f)^2 = cos^2(kd/2) + (\lambda/d)^2 sin^2(kd) \tag{2.3}$$

for Scheme Fa, which is the same as Scheme D, and therefore has its properties, and

$$(v/f)^2 = cos^2(kd/2) + 4(\lambda/d)^2 sin^2(kd) \tag{2.4}$$

for Scheme Fb, which is the same as Scheme C, and therefore has its properties.

Arakawa and Lamb (1977) define the radius of deformation $\lambda = \sqrt{gH}/f$.

Therefore, stability of the proposed scheme is achieved when the spatial gradients of

the free surface are taken from the adjunct and perpendicular sides (Scheme Fb) rather than the opposite sides (Scheme Fa). Besides, Scheme Fb has a natural means to turn on or off fluxes at the interface of two cells in cases involving wetting and drying, as the variation of the water depth h at the cell side could be seen as the opening of a gate between ponds.

Ch.2-2.4. Generalisation to unstructured meshes

A natural generalisation of the Arakawa Scheme C and the additional Scheme F on an unstructured mesh of triangular elements is achieved by removing one edge from the square cell while keeping the velocity (defining the flux through the sides of the cells) perpendicular to the sides. These are here referred to Scheme C^T and Scheme F^T respectively (see Figure 2.3).

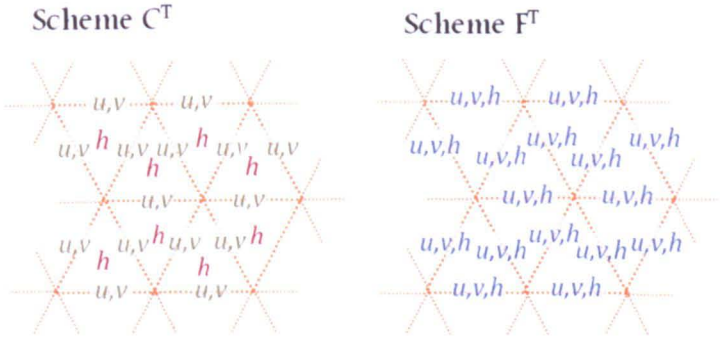

Figure 2.3 – Generalisation to unstructured meshes, Scheme C^T and new Scheme F^T

It is noted for the additional Scheme F^T that the condition on the gradients of h for stability arises naturally from the adjunct and cross flow sides rather than the opposite sides that do not exist any longer.

Finally, it is noted that Scheme C^T is commonly used with solvers based on Finite Volume methods, where the fluxes are defined through the edges of the mesh and the

conservation variable as representative of the triangle value. Similarly, the additional Scheme F^T is commonly used with solvers based on Finite Element methods where all variables are discretised at the same position.

Ch.2-2.5. Vertical regular and irregular grids

Appendix B lists the merits and drawbacks of twenty four existing 3D free surface solver, with a clear split into two categories: those based on fixed horizontal layers (also called z-coordinate), and those based on a sigma-stretched transformation (also called σ-coordinate). A few exceptions (such as MICOM and SELFE) implement a hybrid representation dependent on the water depth, in order to decrease the spacing between mesh planes in regions of sharp vertical variations.

The split into two categories reflects the inadequacy of either category to be universally applicable to problems of environmental hydraulics:

- Sigma-stretched transformations are often used in cases where the bathymetry is non-uniform, smoothly varying and affects the flows, for instance in coastal and estuarial applications. It permits a continuous computation of the shear stress at the bottom and a simpler treatment of the free surface. Use of the σ-coordinate leads to large errors in the evaluation of horizontal gradients near steep slopes. Haney (1991) for instance, analysed the error due to hydrostatic inconsistency associated with computing the pressure gradient force over steep topography. Mellor et al. (1994) demonstrated that the pressure gradient error decreases as the square of both the vertical and horizontal grid size.

- Horizontal layers are often used to model stratification in applications to ocean,

deep lake and reservoir flows. What is a concern for the σ-coordinate method is an advantage for the z-coordinate approach and vice-versa. Cornelissen (2004), for instance, offers a substantial numerical modelling comparison of the application of the two methods to various cases of stratified waters and concludes on the same dichotomy for universal application to stratified flows.

In order to find a compromise, researchers have worked on either: (1) developing bottom fitting algorithms to correct the computation or shear stresses in the z-coordinate system; or (2) correcting the artificial mixing produced by the σ-coordinate near steep slopes; or (3) developing hybrid coordinate systems gradually switching one into the other depending on the physics of the problem.

In Case (1), Chen (2002)'s work is notable for describing the application to a piecewise linear bottom, which could either include discontinuities (staircase bottom) or not (continuous bottom). The solver SULIS (Bourban, 1997), used as numerical framework for the implementation of the dynamic pressure term (see Chapter 3 Section Ch.3-1.8), follows this Case (1).

In Case (2), Stelling and van Kester (1994) introduced a numerical method to compute diffusion and horizontal gradients of the pressure terms, based on a filter similar to those developed for monotonicity in horizontal advection terms. Although not presented here nor published yet, a new numerical scheme of the horizontal diffusion terms was similarly prototyped in TELEMAC-3D by M.S. Turnbull under the leadership of the present author. Flux limiters similar to those developed for the advection terms (see Chapter 3 Section Ch.3-2.1) were used to characterise horizontal layering of a stratified water column while the mesh followed the slope of the bed.

In Case (3), Fortunato and Baptista (1996) introduced "a loose vertical equivalent to horizontal unstructured grids", also called the Localised Sigma Coordinates (LSC)

method, for which the nodal placement is independent for each vertical.

In principle, Case (3) resembles the adaptive mesh displacement (AMD) approach presented in Chapter 3 Section Ch.3-2.10. The AMD approach also allows nodal locations within one water column to be virtually independent of the nodal locations in the neighbouring water column. A purpose-built smoothing diffusion term is used to prevent the intermediate surfaces to be too steep. The principal idea of the AMD approach is to decrease the spacing between layers in regions of sharp vertical variations while maintaining a fixed number of layers. The work of Winslow (1966) who first introduced this type of method in a 1D model is notable, together with the more detailed description of the Winslow's "variable diffusion" approach by Tang and Tang (2003). The solver TELEMAC-3D, used as numerical framework for the implementation of the tracer advection schemes (see Chapter 3 Section Ch.3-2.3), was also used for the implementation of the AMD approach.

Ch.2-3. Implicit and shock capturing schemes

Ch.2-3.1. Monotonic, non-diffusive, shock capturing advection

One of the goals of the present work is to identify an advection scheme that remains monotonic, yet is non-diffusive, shock-capturing and is second order at least, while also compatible with a fully implicit 3D framework. In the case where the conserved quantity is a tracer (such as temperature, salinity, sediment concentration, etc.) the conservation laws are linear. In the case where the conserved quantity is momentum, the conservation laws are non-linear. A scheme that is applicable to both linear and non-linear laws is pursued in this thesis.

The problem at hand is related to the choices made to interpolate fluxes and gradients with respect to the discretised locations of the primary variables. It is well described by several authors including Abbott and Basco (April 1997), Blumberg and Mellor (1987) or Toro, et al., (1994). The conservation laws are a system of partial differential equations of a conserved dependent quantity along the 1D x-axis is written:

$$\frac{\partial T}{\partial t} + \frac{\partial F(T)}{\partial x} = 0 \tag{2.5}$$

where T is the conserved dependent quantity, F is the flux of T,

and t is time and x is distance.

Using 1st order forward Euler time integration Eq. (2.5) becomes:

$$T_j^{n+1} = T_j^n - \frac{\Delta t}{\Delta x}\left[F_{j+\frac{1}{2}}^n - F_{j-\frac{1}{2}}^n\right], \tag{2.6}$$

where $F_{j+\frac{1}{2}}^n$ is the flux at the interface between cells j and $j+1$, Δt is a temporal step and Δx is the spatial increment along the 1D x-axis.

Use of both first and second order schemes in space for the flux term can be grouped into one definition of the flux as follows:

$$F_{j+\frac{1}{2}}^n = \left(u_{j+\frac{1}{2}}^n - \gamma\left|u_{j+\frac{1}{2}}^n\right|\right)\cdot\left(T_j^n + T_{j+1}^n\right)/2 \tag{2.7}$$

where ($\gamma = 1$) for upwind schemes, which are monotonic but highly diffusive, or ($\gamma = 0$) for central difference schemes, which are less diffusive but non-monotonic.

As mentioned previously (see Section Ch.2-1.3) non-monotonic schemes could lead to unrealistic solutions where physical maximum and minimum values of conservation variables would not be guaranteed. Contrarily, accurate advection of a sharp gradient is particularly important in the context of stratification in reservoirs and estuaries. And so a numerical model of stratified flows must be able to minimize the distortion of features in the profile of the conservation field, satisfying the shock-capturing (or

shape-preserving) property of an advection scheme.

Finding the ideal advection scheme is tightly linked to the following three aspects, the combination of which will give the scheme its final properties:

- First, the nature of the interpolation of the conserved quantity at the interface between neighbouring cells: (a) in classical centred schemes, the conserved quantity at the interface is defined as the weighted average of the quantities within each cell; (b) in classical upwind schemes, the flux is skewed towards the direction from which the information flows and the conserved quantity at the interface is defined as the value of the neighbouring cell depending on direction of the flow (the sign of the velocity component); and (c) in classical Riemann solvers, a discontinuity is assumed at the interface, and left and right quantities are used to reconstruct the solution.

- Second, the re-interpolation or reconstruction of the advected solution on the original mesh. In certain schemes (such as the flux-corrected transport schemes by Boris (1971) and discussed below) advection is processed in two stages: (a) the physical transport (or advection) stage which includes interpolation back onto the original mesh and; (b) the posteriori flux correction (anti-diffusion) stage, which could itself be subject to a flux limiter. In other schemes (such as the Riemann solvers discussed below) the interpolation is combined with the definition of the flux and its limiters. Generally speaking, the numerical diffusion is very large during that process.

- Finally, a numerical strategy is used to satisfy monotonicity, shock-capturing and / or shock-fitting, stability, implicitness, conservation, and clipping regardless whether the strategy relates to the definition of the flux and / or the definition of the gradients of the conservation quantities. Many of the early 1D schemes based

on 1st order time integrators have spawned from the Total Variation Diminishing (TVD) condition (such as the ULTIMATE QUICKEST scheme by Leonard (1979) discussed later), and ensure monotonicity.

As mentioned earlier (see Section Ch.2-1.3), the Total Variation Diminishing (TVD) condition ensures monotonicity of the advection scheme based on the following oscillation-suppression strategy:

$$\|w(t + \Delta t)\|_{TV} \leq \|w(t)\|_{TV}, \tag{2.8}$$

where $\|.\|_{TV}$ is a norm such that $\|w\|_{TV} = \sum_i |w_i - w_{i-1}|$ for w_i components of w.

The TVD condition ensures that two neighbouring minima-maxima values cannot be farther apart after advection than they were originally. For its relevance later in this thesis, an example of high order procedure limiting the fluxes of the conservation quantities to satisfy the TVD condition is the MUSCL method (Monotonic Upwind Schemes for Conservation Laws) introduced by van Leer (1979). A flux limiter is used to vary the solution between high and low resolution schemes while limiting the solution gradients to prevent spurious oscillations. The work of Sweby (1984) is also notable for its comparison of several flux limiters dependent on consecutive gradients of the solution. Griffiths (2007) posted on Wikipedia a series of plots showing limiter functions in relation to Sweby's 2nd order TVD region (see Figure 2.4), of which the minmod limiter, referred to later in this document, is one of.

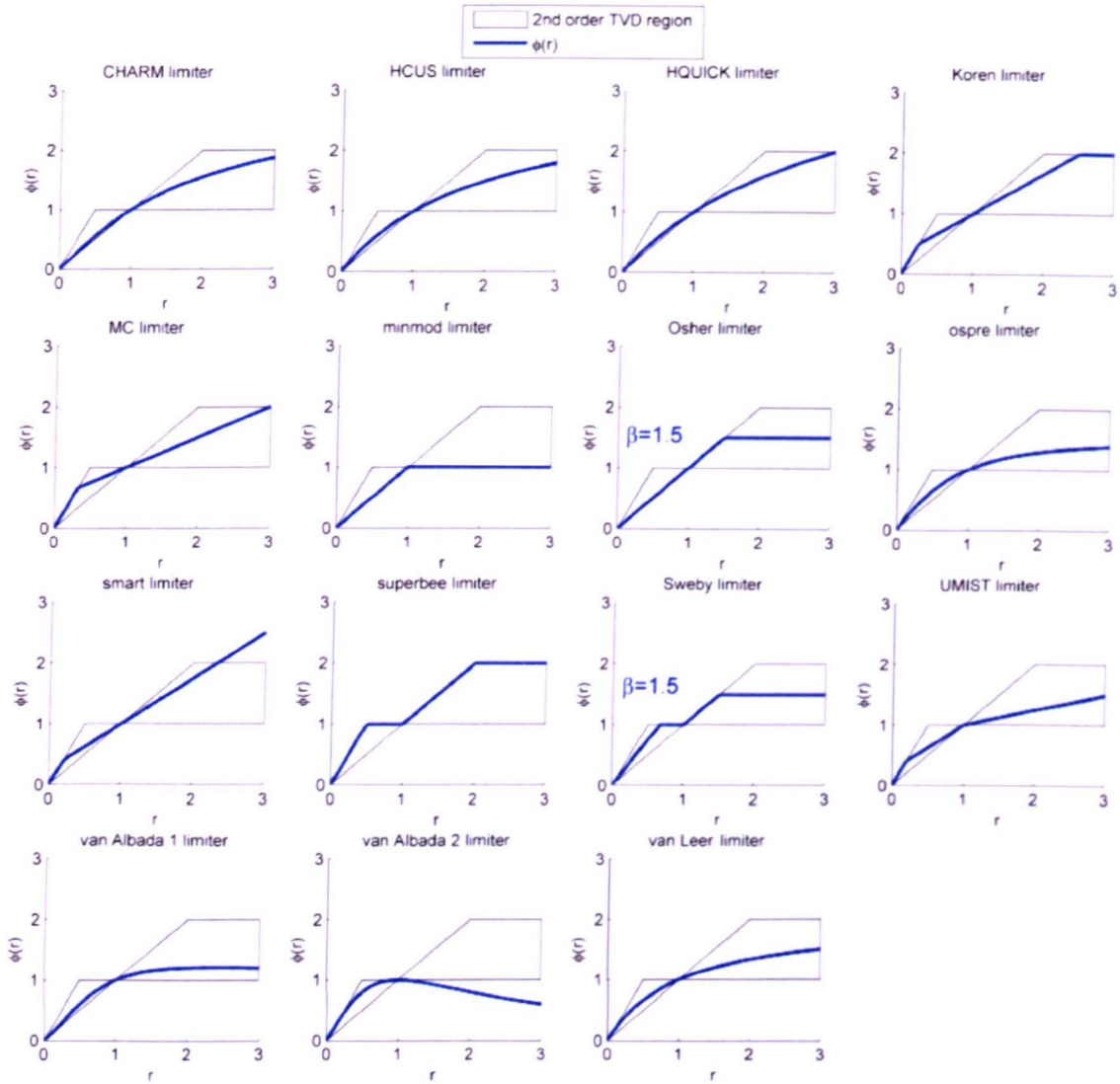

Figure 2.4– Limiter functions in relation to Sweby's 2nd order TVD region

The Strong Stability Preserving (SSP) condition was also proposed as an extension of the TVD condition by Gottlieb, et al. (2001) for generalisation to higher order time integrators.

Finally, Rauch (1986) highlighted in a short communication that the TVD condition fails in the theoretical study of systems of conservation laws in higher dimensions. In these cases, the TVD condition is substituted by a mean entropy decreasing criterion, as discussed by Bouchut et al. (1996), for instance.

For illustrative purposes, three approaches are here presented in chronological order:

(a) The Flux Corrected Transport scheme (see Section Ch.2-3.2); (b) High order polynomial splines interpolation methods (see Section Ch.2-3.3), and (c) Schemes based on (approximate) Riemann solvers (see Section Ch.2-3.4). Where possible these will be referenced for comparison with the approach presented herein.

Ch.2-3.2. The Flux Corrected Transport schemes

Boris (1971) and Boris and Book (1973) introduced the Flux Corrected Transport (FCT) algorithm consisting of two major stages: a transport (or advection) stage, followed by a correction (or anti-diffusive) stage. It should be noted that the same article was also re-published later (Boris & Book, 1997).

Within the transport stage, the physical fluxes are computed by following the movement of the conserved quantity in a Lagrangian sense. The resulting profile is then re-interpolated on the original Eulerian grid (see Figure 2.5), the later step producing a very large diffusion term.

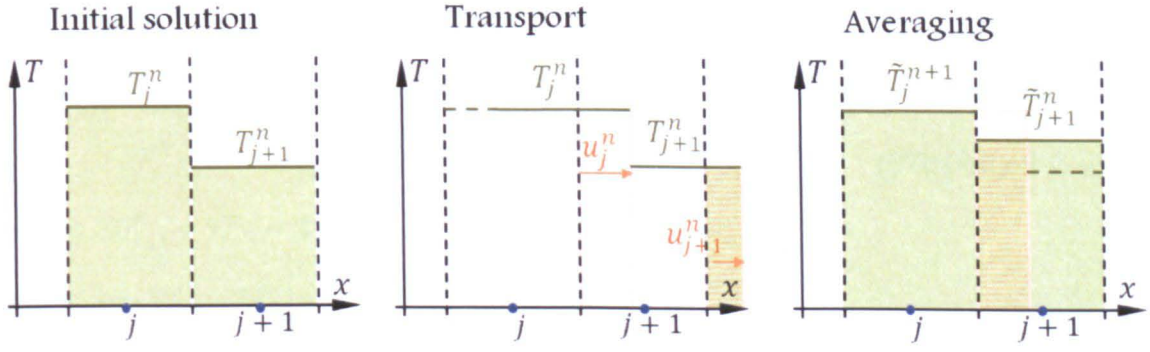

Figure 2.5 – Flux Corrected Transport Stage I, (Boris & Book, 1973)

The anti-diffusive stage therefore subtracts the surplus diffusion terms but not without limiting undesirable effects: a limiter to the anti-diffusive term is introduced by correcting the fluxes transported (origin of the FCT name). The principle of the limiter

is to prevent the tracer value T from going beyond the values at neighbouring points.

The resulting algorithm, SHASTA (Boris & Book, 1973) for Sharp And Smooth Transport Algorithm, is written in two stages as follows along the 1D x-axis:

➤ Stage 1: Transport (or advection)

$$\tilde{T}_j^{n+1} = \tfrac{1}{2}Q_-^2\left(T_{j-1}^n - T_j^n\right) + \tfrac{1}{2}Q_+^2\left(T_{j+1}^n - T_j^n\right) + (Q_+ + Q_-)T_j^n \tag{2.9}$$

with $Q_\pm = \left(\frac{1}{2} \mp u_j^* \frac{\Delta t}{\Delta x}\right) / \left[1 \pm \left(u_{j\pm1}^* - u_j^*\right)\frac{\Delta t}{\Delta x}\right]$ and where the advection velocity is linearly interpolated at the interface depending on its sign:

$$u_j^* = \left(1 - \tfrac{1}{2}\left|u_j^{n+\frac{1}{2}}\frac{\Delta t}{\Delta x}\right|\right)u_j^{n+\frac{1}{2}} + \tfrac{1}{2}\left|u_j^{n+\frac{1}{2}}\frac{\Delta t}{\Delta x}\right|u_{j+1}^{n+\frac{1}{2}} \qquad \text{if } u_j^{n+\frac{1}{2}} \geq 0, \text{ and}$$

$$u_j^* = \left(1 - \tfrac{1}{2}\left|u_j^{n+\frac{1}{2}}\frac{\Delta t}{\Delta x}\right|\right)u_j^{n+\frac{1}{2}} + \tfrac{1}{2}\left|u_j^{n+\frac{1}{2}}\frac{\Delta t}{\Delta x}\right|u_{j-1}^{n+\frac{1}{2}} \qquad \text{if } u_j^{n+\frac{1}{2}} < 0.$$

All other parameters have been defined previously.

➤ Stage 2: Correction (anti-diffusion)

$$T_j^{n+1} = T_j^n - \left(f_{j+\frac{1}{2}}^c - f_{j-\frac{1}{2}}^c\right) \text{ where} \tag{2.10}$$

$$f_{j+\frac{1}{2}}^c = sign\left(\delta_{j+\frac{1}{2}}\right) max\left\{0, min\left\{sign(\delta_{j+\frac{1}{2}})\delta_{j+\frac{1}{2}},\ \tfrac{1}{8}\left|\delta_{j+\frac{1}{2}}\right|,\ sign(\delta_{j+\frac{1}{2}})\delta_{j+\frac{3}{2}}\right\}\right\}$$

with $\delta_{j+\frac{1}{2}} = \tilde{T}_{j+1}^{n+1} - \tilde{T}_j^{n+1}$, and all other parameters have been defined previously.

"With both stages conservative and positive, their interaction enables FCT algorithms to treat strong gradients and shocks without the usual dispersive generated ripples."
(Boris & Book, 1973)

Ch.2-3.3. High order polynomial spline interpolation methods

The work of Leonard (1979) and (1991) is here chosen for its excellent performance in 1D, and for comparison with approaches developed in the present work.

Leonard (1979) first introduced the QUICKEST scheme (Quadratic Upstream Interpolation for Convective Kinematics with Estimated Streaming Terms) expanding the interpolation of conserved quantity up to the 8th order using polynomial splines partially centred and upwinded. Leonard writes (transformed for the reader to previously used notations):

- For the first two orders:

$$F_{j+\frac{1}{2}}^{n\ (1^{st})} = u_{j+\frac{1}{2}}^{n} \cdot \frac{1}{2}\left[\left(T_{j+1}^{n} + T_{j}^{n}\right) - sign(c_{j+\frac{1}{2}})\left(T_{j+1}^{n} - T_{j}^{n}\right)\right], \qquad (2.11)$$
$$F_{j+\frac{1}{2}}^{n\ (2^{nd})} = u_{j+\frac{1}{2}}^{n} \cdot \frac{1}{2}\left[\left(T_{j+1}^{n} + T_{j}^{n}\right) - c_{j+\frac{1}{2}}\left(T_{j+1}^{n} - T_{j}^{n}\right)\right]$$

where the function $sign()$ is the sign function, and $c_{j+\frac{1}{2}}$ is the Courant number $\frac{\Delta t}{\Delta x} u_{j+\frac{1}{2}}^{n}$.

All others have been defined previously,

- For the following two orders:

$$F_{j+\frac{1}{2}}^{n\ (3^{rd})} = F_{j+\frac{1}{2}}^{n\ (2^{nd})} - u_{j+\frac{1}{2}}^{n} \cdot \frac{1}{3!}(1 - c_{j+\frac{1}{2}})\left[\mathfrak{D}_{j+\frac{1}{2}}^{2} - \frac{1}{2} sign(c_{j+\frac{1}{2}})\delta_{j+\frac{1}{2}}^{3}\right] \qquad (2.12)$$
$$F_{j+\frac{1}{2}}^{n\ (4^{th})} = F_{j+\frac{1}{2}}^{n\ (2^{nd})} - u_{j+\frac{1}{2}}^{n} \cdot \frac{1}{3!}(1 - c_{j+\frac{1}{2}}^{2})\left[\mathfrak{D}_{j+\frac{1}{2}}^{2} - \frac{1}{4} c_{j+\frac{1}{2}}\, \delta_{j+\frac{1}{2}}^{3}\right]$$

where $2\mathfrak{D}_{j+\frac{1}{2}}^{2} = \left(T_{j+2}^{n} - 2T_{j+1}^{n} + T_{j}^{n}\right) + \left(T_{j+1}^{n} - 2T_{j}^{n} + T_{j-1}^{n}\right) = T_{j+2}^{n} - T_{j+1}^{n} - T_{j}^{n} + T_{j-1}^{n}$

and $\delta_{j+\frac{1}{2}}^{3} = T_{j+2}^{n} - 3T_{j+1}^{n} + 3T_{j}^{n} - T_{j-1}^{n}$

- And for the 5th and 6th orders:

$$F_{j+\frac{1}{2}}^{n\ (5^{th})} = F_{j+\frac{1}{2}}^{n\ (4^{th})} + u_{j+\frac{1}{2}}^{n} \cdot \frac{1}{5!}(1 - c_{j+\frac{1}{2}}^{2})(4 - c_{j+\frac{1}{2}}^{2})\left[\mathfrak{D}_{j+\frac{1}{2}}^{4} - \frac{1}{2} sign(c_{j+\frac{1}{2}})\, \delta_{j+\frac{1}{2}}^{5}\right] \qquad (2.13)$$
$$F_{j+\frac{1}{2}}^{n\ (6^{th})} = F_{j+\frac{1}{2}}^{n\ (4^{th})} + u_{j+\frac{1}{2}}^{n} \cdot \frac{1}{5!}(1 - c_{j+\frac{1}{2}}^{2})(4 - c_{j+\frac{1}{2}}^{2})\left[\mathfrak{D}_{j+\frac{1}{2}}^{4} - \frac{1}{6} c_{j+\frac{1}{2}}\, \delta_{j+\frac{1}{2}}^{5}\right]$$

where $2\mathfrak{D}_{j+\frac{1}{2}}^{4} = T_{j+3}^{n} - 3T_{j+2}^{n} + 2T_{j+1}^{n} + 2T_{j}^{n} - 3T_{j-1}^{n} + T_{j-2}^{n}$

and $\delta_{j+\frac{1}{2}}^{5} = T_{j+3}^{n} - 5T_{j+2}^{n} + 10T_{j+1}^{n} - 10T_{j}^{n} + 5T_{j-1}^{n} - T_{j-2}^{n}$

- And finally for the 7th and 8th orders:

$$F_{j+\frac{1}{2}}^{n\ (7^{th})} = F_{j+\frac{1}{2}}^{n\ (6^{th})} \qquad (2.14)$$
$$-u_{j+\frac{1}{2}}^{n} \cdot \frac{1}{7!}\left(1 - c_{j+\frac{1}{2}}^{2}\right)\left(4 - c_{j+\frac{1}{2}}^{2}\right)\left(9 - c_{j+\frac{1}{2}}^{2}\right)\left[\mathfrak{D}_{j+\frac{1}{2}}^{6} - \frac{1}{2} sign\left(c_{j+\frac{1}{2}}\right)\delta_{j+\frac{1}{2}}^{7}\right]$$
$$F_{j+\frac{1}{2}}^{n\ (8^{th})} = F_{j+\frac{1}{2}}^{n\ (6^{th})}$$

$$+u^n_{j+\frac{1}{2}} \cdot \frac{1}{7!}(1-c^2_{j+\frac{1}{2}})(4-c^2_{j+\frac{1}{2}})(9-c^2_{j+\frac{1}{2}})\left[\mathfrak{D}^6_{j+\frac{1}{2}} - \frac{1}{8}c_{j+\frac{1}{2}}\,\delta^7_{j+\frac{1}{2}}\right]$$

where $2\mathfrak{D}^6_{j+\frac{1}{2}} = T^n_{j+3} - 3T^n_{j+2} + 2T^n_{j+1} + 2T^n_j - 3T^n_{j-1} + T^n_{j-2}$

and $\delta^7_{j+\frac{1}{2}} = T^n_{j+3} - 5T^n_{j+2} + 10T^n_{j+1} - 10T^n_j + 5T^n_{j-1} - T^n_{j-2}$.

However, while the high orders of the QUICKEST scheme improve the accuracy of the solution, the polynomial splines result in a non-monotonic solution. Leonard (1991) later admitted that "Clearly, these results are disappointing". He therefore formulated a gradient limiting strategy applicable to any order of QUICKEST and other explicit conservative advection schemes, achieving sharp monotonic resolution of the step without corrupting the other profiles: the ULTIMATE strategy. He concluded that the ULTIMATE QUICKEST 3rd order upwind scheme was highly satisfactory for most flows of practical importance.

It should be highlighted that the ULTIMATE QUICKEST scheme is generic to problems of higher dimension. For instance, Lin and Falconer (1997) evaluated the performance of the 3rd order scheme in 2D with an application to the tracer advection in the Humber Estuary, UK. Because their scheme is based on an explicit strategy and its recommended 3rd order has a wide stencil, it was not kept as the final candidate for the present work, although it is included in comparisons (see Section Ch.3-2).

Ch.2-3.4. Schemes based on (approximate) Riemann solvers

In the case of non-linear laws, Riemann solvers are used to determine the solutions of the Riemann problem, in other words determining the fan of waves spawned at the discontinuity of a step function. Assuming an initial piecewise representation of a function (accepting discontinuities between neighbouring cells as opposed to using a polynomial interpolation), the advected function result of Eq. (2.6) can be interpreted

as a superposition of as many Riemann problems as there are discontinuities between neighbouring cells.

Godunov (1959) first introduced a conservative first order upwind scheme based on finding the advection solution to a step function. The work is summarised by Roe (1981) as follows: "Godunov supposed that the initial data could be replaced by a piecewise constant set of states with the discontinuities at the interface of two cells/nodes. He then found the exact solution to this simplified problem. After some time steps, he replaced the exact solution by a new piecewise constant approximation, whilst preserving integral properties of the conserved variable." It is noted that although Godunov's paper was published before those of Boris (1971) and Leonard (1979), the application of Godunov's work to high order multi-dimensional shock capturing schemes was only published later with the arrival of simpler iterative procedures, such as proposed by van Leer (1979).

In any case, these approaches are similar to other two-stage approaches with:

- Stage 1: Starting from a piecewise constant set of states with discontinuities at the interface of cells, use a Lagrange type resolution of a Riemann problem (following particles along characteristic curves) at all interface sides to define the exact fluxes over a small time period so to avoid interaction between the fluxes within the cells.

- Stage 2: Reconstruct a piecewise constant set of states by projecting the new solution onto the original grid of cells whilst preserving integral properties of the conserved variables.

In practice, finding the exact solution to this simplified problem requires the design of an iterative numerical procedure involving a system of differential equations of the flux function (or evaluating the eigenvalues of the Jacobian matrix representing the

advection) as well as limiters to maintain numerical properties such as monotonicity.

Again, many choices are available regarding the stages and steps included in these approaches. For the reconstruction of Stage 2, for instance, higher order schemes build on more precise piecewise approximations of the solution with higher order schemes and wider stencils. These are based on combining numerical methods, some of which were developed in the context of upwind schemes such as WENO (Weighted Essentially Non-Oscillatory), with methods that were taken from the central differencing framework. The work of Aboiyar et al. (2006) is notable for its original use of polyharmonic splines instead of the traditional polynomial WENO reconstructions. The work of Levy et al. (2000) is also highlighted for the development of a total variation bounded condition (as opposed to diminishing) and the so called Centred WENO scheme.

To solve the Riemann problem of Stage1, the problem is usually posed along the 1D x-axis for the parallel made with waves produced in a shock tube used to produce high velocity and high temperature gas over a short period of time, for instance by Hughes & Brighton (1999).

Figure 2.6 shows an illustration of the structure of the solution of a Riemann problem with characteristics curves in the $x - t$ plane starting from the discontinuity between cells j and $j + 1$.

Riemann fan

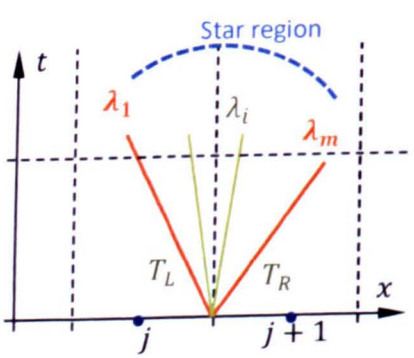

Figure 2.6 – Structure of the solution of a Riemann problem

The characteristics curves represent either rarefaction, shock or contact discontinuity waves depending on the advection within what is called the star region (see Figure 2.6). Each characteristic curve is defined by one of the eigenvalues of the Jacobian matrix representing advection. There are 3 waves in the case of 2D shallow water equations and just 2 in 1D shallow water equations. In the case of 3D problems, the Riemann solver becomes rather more complex. In order to simplify the problem, the design of approximate Riemann solvers started with the work of Roe (1981), followed by Harten et al. (1983) and more than 10 years later by Toro et al. (1994). In particular,

- The HLL scheme (Harten, et al., 1983) assumes only one intermediate wave state between the left and right wave speeds. This assumption was shown to be correct for a 2-equation system (such as the 1D shallow water equations) but not for higher dimensions.

- The HLLC scheme (Toro, et al., 1994), a modified version of the HLL scheme Contact waves, assumes two intermediate wave states, i.e. three wave speeds. Later, Batten et al. (1997) suggested algorithms for computing the wave speeds required by HLLC, resulting in a positively conservative scheme.

Because schemes based on approximate Riemann solvers remain complex and difficult to expand to 3D and the Navier-Stokes equations, the HLLC approximate Riemann solver was not kept as final candidate for the present work. In the context of scalar transport, the work of Ahmad et al. (2007) is noted, however, for an implementation of a Godunov type scheme to unstructured meshes combined with a Runge-Kutta high order time integration.

Ch.2-3.5. Schemes based on averaging Riemann solvers

As observed so far, a large number of advection schemes exist, several of which are potentially good candidates for implementation in SULIS and TELEMAC. Most high-resolution schemes for hyperbolic conservation laws are based on upwind differencing. The most recent schemes based on (approximate) Riemann solvers remain complex and time consuming because they have to identify the waves spawned from the Riemann fan.

Instead, the approach taken herein is based on the latest evolution by Kurganov, et al., (2001) of a series of schemes first introduced by Nessyahu and Tadmor (1990). As described in Section Ch.3-2, the use of second order piecewise linear approximants (instead of the first order piecewise constant) compensates for the excessive viscosity and results in a family of second order accurate, central difference schemes. The main advantage is simplicity with no Riemann problems solved, while excessive numerical viscosity is compensated for by using high-resolution MUSCL type reconstruction.

The Nessyahu and Tadmor (1990) scheme was further refined by Kurganov and Tadmor (2000), and advanced to a 1D centred-upwind form by Kurganov, et al., (2001). The latter scheme is based on bounding the minimum and maximum speeds of the Riemann solver and averaging over the Riemann fan. Again, the scheme does not need to solve the Riemann problem, and as a result, it can be extended to multiple dimensions and sets of equations with a relatively minimal effort. Kurganov and Tadmor (2000) also showed that the scheme is applicable to the diffusion terms as well as advection. The centred-upwind form was later generalised to a 2D unstructured finite volume form by Kurganov and Petrovna (2004).

Ch.2-4. Time integration

As discussed previously, both SULIS and TELEMAC-3D (see Sections B.1 and B.2 respectively) use a first order time integrator, whether fully implicit or semi-implicit. One of the goals of the present work is to retain advection schemes compatible with time integrators that are implicit, the main idea being that the size and complexity of the matrix representing the problem should not be a barrier to the choice of the time integrator. Even though the implementation of a higher order time integrator is not part of the research objectives, higher order time integrators would be welcomed to increase time order accuracy of either SULIS or TELEMAC 3D solver.

For reference, commonly used high order time integrators include multi-step and Runge-Kutta methods, both of which are extensively discussed, including in their implicit form, by Hairer, et al (1987) and Hairer & Wanner (1991). Also, implicitness has been the subject of many publications, some less optimistic than others. For instance, Gottlieb, et al. (2001) concluded on the non-existence of SSP (Strong Stability Preserving) implicit multi-step or Runge-Kutta methods of order higher than 1. Later Gottlieb (2005) added that if the explicit Euler terms are included, the methods obtained would be SSP but only under a CFL restriction similar to explicit methods. Conversely, Ferracina & Spijker (2005) highlighted a 2^{nd} order singly diagonally implicit Runge-Kutta method with a CFL greater than 4, having first extended the representation of Shu-Osher (1988) and (1989) of general Runge-Kutta methods.

Several high order time integration schemes exist, the most promising of which are based on the Runge-Kutta method:

- First, this method allows explicit, semi-implicit, explicit-implicit formulations

allowing use of direct matrix resolution technique, and fully implicit formulations.

- Second, the Runge-Kutta scheme can preserve monotonicity under certain conditions, although theoretical proofs have only been found for explicit and semi-implicit formulations (with respect to the total variation norm).

It should also be noted that second order Runge-Kutta schemes only make use of two time levels, equivalent to the scheme presently implemented in SULIS (backward Euler) and TELEMAC-3D (semi implicit). The order of accuracy is obtained through the computation of intermediate solutions. In comparison, high order schemes that make use of more than two time levels such as Leapfrog allow the growth of one or more time splitting errors with own amplification factors. Filters for non-physical errors can be used (for instance the leapfrog scheme used in a trapezoidal correction, which aggressively damps the non-physical solution) although the accuracy of the integrator is reduced to lower orders.

It is noted that, having chosen to switch numerical framework from the finite difference solver SULIS to the finite element solver TELEMAC, the implementation of a higher order time integrator was deemed too complex with dramatic impact on all modules of the TELEMAC system for it to be included in the present work.

Chapter 3 –
Mathematical and numerical framework

As discussed in Chapter 2, the 3D numerical modelling of free surface flows is a relatively mature field, mostly based on the continuity and Navier-Stokes equations where the free surface is directly calculated and related to the pressure field under the hydrostatic assumption. The projection method usually extends the work to non-hydrostatic pressure fields. The present Chapter first presents the mathematical framework, in particular the Navier-Stokes equations and its various forms followed by the numerical framework including a description of the numerical solver.

Ch.3-1. Mathematical framework

In this section, particular attention is given to the theoretical representation of the continuity and Navier-Stokes equations for applications to stratified waters. In the context of environmental hydraulics and with a specific focus on deep reservoir stratification and recirculation devices, the hydrostatic assumption and the computation of the dynamic pressure will be revisited.

It is noted that, although diffusion and by extension turbulence closure are presented here, the work will focus on advection.

Ch.3-1.1. The advective form of the equations

The continuity and Navier-Stokes equations are fundamental equations of motion for an incompressible fluid (for which changes in density do not relate to the pressure). The Navier-Stokes equations are established in an Eulerian (fixed referential) Cartesian (orthogonal) 3D space from the vector balance between two sums:

(a) The sum of changes in momentum of the mass within a control volume of fluid and in fluxes of momentum through the sides of that same control volume and;

(b) The sum of all external forces acting throughout the body of the fluid (such as gravity and Coriolis forces) and of all external forces acting on the surface of the control volume of fluid (such as pressure and viscous forces).

The viscous forces are expressed in the form of linear functions of the velocity gradients, so-called the Newtonian fluid assumption, given an isotropic molecular dynamic viscosity coefficient. The dynamic viscosity is eventually replaced by the turbulent dynamic viscosity, which leads to the Navier Stokes equations in their advective form (or non-conservative form):

$$\rho\frac{\partial u}{\partial t}+\rho\left(u\frac{\partial u}{\partial x}+v\frac{\partial u}{\partial y}+w\frac{\partial u}{\partial z}\right)=-\frac{\partial p}{\partial x}+\mu\left(\frac{\partial^2 u}{\partial x^2}+\frac{\partial^2 u}{\partial y^2}+\frac{\partial^2 u}{\partial z^2}\right)+F_x \tag{3.1}$$

$$\rho\frac{\partial v}{\partial t}+\rho\left(u\frac{\partial v}{\partial x}+v\frac{\partial v}{\partial y}+w\frac{\partial v}{\partial z}\right)=-\frac{\partial p}{\partial y}+\mu\left(\frac{\partial^2 v}{\partial x^2}+\frac{\partial^2 v}{\partial y^2}+\frac{\partial^2 v}{\partial z^2}\right)+F_y \tag{3.2}$$

$$\rho\frac{\partial w}{\partial t}+\rho\left(u\frac{\partial w}{\partial x}+v\frac{\partial w}{\partial y}+w\frac{\partial w}{\partial z}\right)=-\frac{\partial p}{\partial z}+\mu\left(\frac{\partial^2 w}{\partial x^2}+\frac{\partial^2 w}{\partial y^2}+\frac{\partial^2 w}{\partial z^2}\right)+F_z \tag{3.3}$$

where (x, y, z) defines the axis of the 3D space, t defines the time, ρ is the fluid density, μ is the dynamic viscosity coefficient, and where F_x, F_y and F_z represent the three components of the body forces. The four hydrodynamic variables are the pressure p and the velocity components u, v, and w.

A fourth equation is given by the conservation of mass of fluid in the control volume:

$$\rho\frac{\partial u}{\partial x}+\rho\frac{\partial v}{\partial y}+\rho\frac{\partial w}{\partial z}=S_w \qquad \text{(the continuity equation)} \tag{3.4}$$

where S_w is a generic source or sink of fluid and all other quantities have been defined previously.

For most applications in environmental hydraulics, the three components of the body force are the gravity force component $F_z=-\rho g$ (where g is the gravitational constant) and the Coriolis force components $F_x=\rho f v$ and $F_y=-\rho f u$ (where f is the Coriolis coefficient function of the latitude).

Similarly, with regard to the transport of a tracer T, the conservation of its mass may be written as follows (the *advection diffusion equation*):

$$\rho\frac{\partial T}{\partial t}+\rho\left(u\frac{\partial T}{\partial x}+v\frac{\partial T}{\partial y}+w\frac{\partial T}{\partial z}\right)=S_T+\kappa\left(\frac{\partial^2 T}{\partial x^2}+\frac{\partial^2 T}{\partial y^2}+\frac{\partial^2 T}{\partial z^2}\right) \tag{3.5}$$

where κ is the turbulent (or eddy) diffusivity, or the tracer equivalent of the turbulent dynamic viscosity, and S_T is a generic source or sink of tracer. All other quantities have been defined previously. The advection terms directly correspond to the transport of the tracer along streamlines of the velocity field, while the diffusion terms correspond to energy exchanges induced by shear stresses, or between molecules of different fluid velocity.

The derivation of equations Eq. (3.1) to Eq. (3.5) is the subject of many publications, including Blumberg and Mellor (1987), Beckmann and Haivogel (1993), and Hughes and Brighton (1999). The resulting form is conducive to finite differences because it is characterised by the multiplication of linear gradients with the velocity (or viscosity) components. The author of the present work previously wrote the finite difference 3D

solver SULIS (Bourban, 1997) on the basis of the advective form of the Navier-Stokes equations.

Ch.3-1.2. The divergence form of the equations

The continuity and Navier-Stokes equations are based on the conservation of mass and momentum defined by boundary fluxes within small control volumes, and use of the divergence theorem linking surface integrals with volume integrals. The assumption of a smooth solution, for which all derivatives exist, results in the advective (non-conservative) form of the equations (Eq. (3.1) to Eq. (3.5) in Section Ch.3-1.1). However, in a few particular cases such as hydraulic jumps or strongly stratified water columns, the solution is discontinuous, the derivative terms are undefined and the differential equations are therefore invalid.

As highlighted by Abbott and Basco (April 1997) a different form of the Navier-Stokes equations exists for these situations "in which mass and momentum are used as functions of space and time, in place of velocity and pressure. Such equations can be cast into a conservation form and as such they can be generalized, through the use of integral formulation, so as to hold both continuous and discontinuous flows, thus providing a more general formulation". Toro (1999) re-stated in more detail that, by definition, a partial differential equation is written in its conservative form when its advective term is such that:

$$\frac{\partial \varphi}{\partial t} + \vec{\nabla}.\vec{F}(\varphi) = 0 \qquad (3.6)$$

where φ is the time- and space-dependent quantity, $\vec{F}$ is a flux vector function of φ and $\vec{\nabla}$ is the spatial gradient operator, the scalar product of which with $\vec{F}$ represents the change of the quantity in the control volume.

With regard to the hydrodynamics, the conservative form of the Navier-Stokes equations reads as follows:

$$\frac{\partial \rho u}{\partial t} + \frac{\partial \rho u^2}{\partial x} + \frac{\partial \rho uv}{\partial y} + \frac{\partial \rho uw}{\partial z} = -\frac{\partial p}{\partial x} + \frac{\partial}{\partial x}\left[\nu \frac{\partial \rho u}{\partial x}\right] + \frac{\partial}{\partial y}\left[\nu \frac{\partial \rho u}{\partial y}\right] + \frac{\partial}{\partial z}\left[\nu \frac{\partial \rho u}{\partial z}\right] + F_x \tag{3.7}$$

$$\frac{\partial \rho v}{\partial t} + \frac{\partial \rho uv}{\partial x} + \frac{\partial \rho v^2}{\partial y} + \frac{\partial \rho vw}{\partial z} = -\frac{\partial p}{\partial y} + \frac{\partial}{\partial x}\left[\nu \frac{\partial \rho v}{\partial x}\right] + \frac{\partial}{\partial y}\left[\nu \frac{\partial \rho v}{\partial y}\right] + \frac{\partial}{\partial z}\left[\nu \frac{\partial \rho v}{\partial z}\right] + F_y \tag{3.8}$$

$$\frac{\partial \rho w}{\partial t} + \frac{\partial \rho uw}{\partial x} + \frac{\partial \rho vw}{\partial y} + \frac{\partial \rho w^2}{\partial z} = -\frac{\partial p}{\partial z} + \frac{\partial}{\partial x}\left[\nu \frac{\partial \rho w}{\partial x}\right] + \frac{\partial}{\partial y}\left[\nu \frac{\partial \rho w}{\partial y}\right] + \frac{\partial}{\partial z}\left[\nu \frac{\partial \rho w}{\partial z}\right] + F_z \tag{3.9}$$

where $\nu = (\mu/\rho)$ now represents the kinematic viscosities. The fourth equation, the continuity equation, is as follows:

$$\frac{\partial \rho u}{\partial x} + \frac{\partial \rho v}{\partial y} + \frac{\partial \rho w}{\partial z} = S_w \tag{3.10}$$

Similarly, the divergence (or conservative) form of the *advection-diffusion equation* for the tracer reads:

$$\frac{\partial \rho T}{\partial t} + \frac{\partial \rho uT}{\partial x} + \frac{\partial \rho vT}{\partial y} + \frac{\partial \rho wT}{\partial z} = S_T + \frac{\partial}{\partial x}\left[\chi \frac{\partial \rho T}{\partial x}\right] + \frac{\partial}{\partial y}\left[\chi \frac{\partial \rho T}{\partial y}\right] + \frac{\partial}{\partial z}\left[\chi \frac{\partial \rho T}{\partial z}\right] \tag{3.11}$$

where $\chi = (\kappa/\rho)$ and all other quantities have been defined previously.

For comparison purposes, the author of the present work re-wrote the original finite difference 3D solver SULIS (Bourban, 1997) on the basis of the divergence (conservative) form of the Navier-Stokes equations.

The conservative form of the Navier-Stokes equations is the preferred formulation for most recent developments for discontinuous or shock capturing methods. For instance, its implementation based on finite differences is detailed in user manuals and technical reports associated with the solvers ELCOM, MICOM, MOM, POM, ROMS, UnTRIM, ELCIRC, etc. (see Chapter 2 and Appendix B).

Ch.3-1.3. Equivalence between advective and divergence forms

The equivalence of the linear gradients between the non-conservative and the conservative forms (see Section Ch.3-1.1 and Ch.3-1.2 respectively) assumes constancy of coefficients (density, viscosity and diffusivity). The non-linear terms (convection and advection) are derived from the conservation of the mass of fluid, Eq. (3.10). For instance, the convection (momentum advection) terms in Eq. (3.1) can be re-arranged as follows:

$$\begin{aligned}
&\rho u\frac{\partial u}{\partial x}+\rho v\frac{\partial u}{\partial y}+\rho w\frac{\partial u}{\partial z}\\
&\quad=\frac{\partial \rho u^2}{\partial x}-u\frac{\partial \rho u}{\partial x}+\frac{\partial \rho uv}{\partial y}-u\frac{\partial \rho v}{\partial y}+\frac{\partial \rho uw}{\partial z}-u\frac{\partial \rho w}{\partial z}\\
&\quad=\frac{\partial \rho u^2}{\partial x}+\frac{\partial \rho uv}{\partial y}+\frac{\partial \rho uw}{\partial z}-u\left(\frac{\partial \rho u}{\partial x}+\frac{\partial \rho v}{\partial y}+\frac{\partial \rho w}{\partial z}\right)=0
\end{aligned}$$

Constancy of coefficients and smoothness of the solution are not assumptions in the formulation of the conservative form of the equations anymore. Sharp gradients and discontinuous solutions could therefore be captured in theory.

Ch.3-1.4. Introduction of vorticity in the equation

For completeness, there exists a third form of the Navier-Stokes equations, the so-called rotational form (see the work of Perot (2000), for instance), in which the vorticity of the flow is factorised as follows:

$$\rho\frac{\partial \vec{u}}{\partial t}+\rho(\vec{\omega}\times\vec{u}) \;=\; -\vec{\nabla}\left(p+\frac{1}{2}\rho\vec{u}\cdot\vec{u}\right)-\vec{\nabla}\times(\mu\vec{\omega})+\vec{F} \qquad (3.12)$$

where the vorticity vector $\vec{\omega}$ is defined as the cross product of the spatial gradient $\vec{\nabla}$ and the velocity vector $\vec{u}$, or the curl of the velocity $\vec{\omega}=\vec{\nabla}\times\vec{u}$.

It is interesting to note that a kinetic energy term has been added to the pressure

gradient term in Eq. (3.12) and that the convection term only acts perpendicularly to the velocity. It can indeed be verified that the scalar product $\vec{u} \cdot (\vec{\omega} \times \vec{u}) = 0$.

An implementation of the rotational form of the Navier-Stokes equations on (unstructured) staggered grids is detailed by Perot (2000) and further expanded by Zang et al. (2004). Perot showed that staggered grids are well suited to this form of the equations, and in particular for the natural conservation of kinetic energy, vorticity and rotational energy. Vorticity reflects the fundamental rotational property of a fluid at any level: from ocean recirculation to turbulent eddies near solids, including reservoir recirculation and the swirling of vortices. These physical processes aside, the significance of the rotational form over the divergence form is, however, yet to be established, and in particular its ability to deal with discontinuities.

Ch.3-1.5. Hydrostatic and dynamic pressure

The vast majority of 3D hydrodynamic solvers applied to large-scale environmental hydraulics (see Chapter 2 and Appendix B) are based on the hydrostatic assumption, where the variations in the vertical momentum are small when compared to gravity and vertical pressure gradient. In that case, the third equation of momentum, Eq. (3.9), simplifies to:

$$0 = -\frac{\partial p}{\partial z} - \rho g, \tag{3.13}$$

where g is the gravitational constant, the body force being $F_z = -\rho g$.

The vertical integration of this equation gives the linear pressure distribution (ignoring spatial variation of atmospheric pressure):

$$p(z) = \int_z^\eta \rho g dz + p_{atm}, \tag{3.14}$$

or $p(z) = \rho g(\eta - z) + p_{atm}$ if the density is constant

where p_{atm} is the atmospheric pressure at the free surface η, which in turn leads to the spatial derivatives, $\partial p/\partial x = \rho g \partial(\eta - z)/\partial x$ and $\partial p/\partial y = \rho g \partial(\eta - z)/\partial y$

The hydrostatic assumption therefore helps reduce the size of the system of 3D hydrodynamic equations by replacing the third equation of momentum, Eq. (3.9), by a relationship between the pressure term, the density and the distance below the surface. If the density is constant, the pressure spatial gradients are then replaced in the first two momentum equations Eq. (3.7) and Eq. (3.8) by a gradient in free surface elevation. At this stage, it is important to note that a new variable, the free surface elevation η, has been introduced whole spatial gradients can be replaced by those of the water depth h for problems where the bed is fixed.

Ch.3-1.6. Further simplifications

The vast majority of 3D hydrodynamic solvers applied to large-scale environmental hydraulics (see Chapter 2 and Appendix B) based on the hydrostatic assumption further simplify the solution of the continuity and Navier-Stokes equations by decoupling the system of equations. Within each time step, each hydrodynamic variable is calculated assuming that all the others are known:

- Stage 1: The two velocity components u and v are solved independently based on the first two momentum equations, Eq. (3.7) and Eq. (3.8) respectively and in the absence of free surface gradient, the pressure is zero;
- Stage 2: The free surface h is updated based on the 2D continuity equation of fluid, integrating the continuity equation, Eq. (3.10), over the water column from bottom to top; and

- Stage 3: The velocity component w simply results from the conservation of mass of fluid Eq. (3.10) for each control volume within the water column bounded by the relative positions of the free surface and bottom of the model

Beside the evident gain in calculation time with a series of smaller matrices (if any), the decoupled solution is ideal for semi-implicit and explicit time integration (i.e. virtually all solvers listed in Appendix B but COHERENS and SULIS) or alternate direction integration methods, for which iterative solvers are most often circumvented (the structured version of MIKE-3, for instance, see Appendix B). However, the scope of the present work encompasses some physical processes that are not trivially modelled using a decoupled system of equations. One example is the modelling of source (or sink) terms at a certain depth within the water column. In stratified reservoirs, these terms are used to represent de-stratification devices, such as bottom outlets, jet-circulations, or bubble diffusers, the latter modelled as a series of source and sink terms within the same water column. Under the hydrostatic assumption, the source term solely appears in the 2D vertically averaged continuity equation, when solving for the free surface h (at Stage 2), and when solving for the vertical velocity component w using the continuity equation (at Stage 3).

Figure 3.1 schematises the 3 stages described above plus 1 from the next time step, for a source placed within a water column of 4 cells, and where the velocity field is defined on a staggered mesh for illustrative purposes, with fluxes computed perpendicularly through the sides of the control volume.

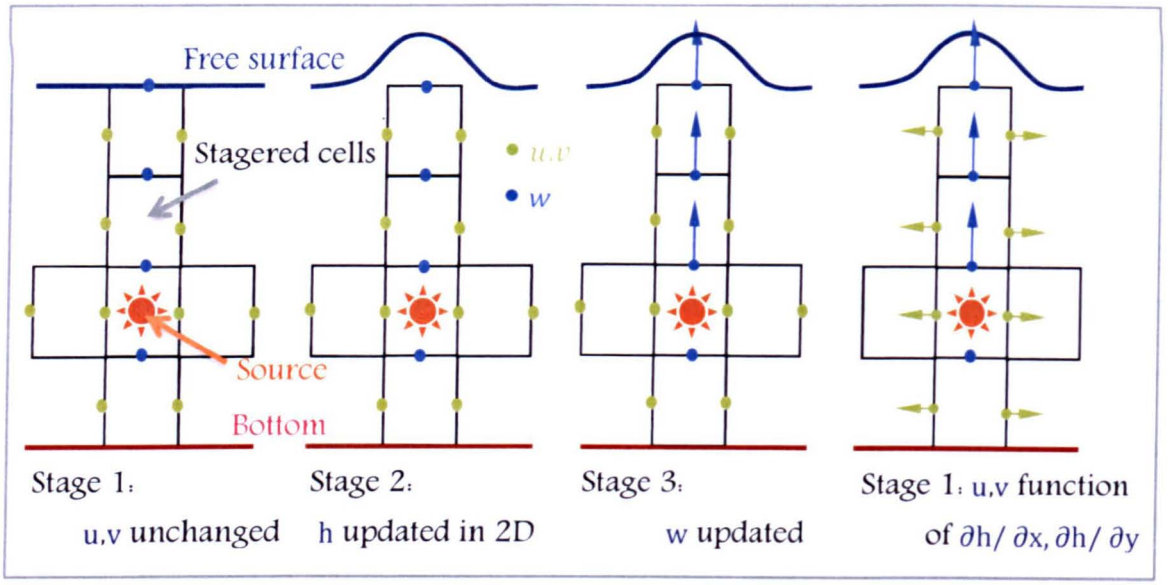

Figure 3.1 – Procedure to update variables in a non-hydrostatic solver

At Stage 3, the source of fluid creates an upward velocity w above the source location with no impact below the source or sideways, which leads to unrealistic w magnitudes. At Stage 1 of the next time step, the horizontal velocity field is the result of the 2D surface gradient terms $\rho g \partial h/\partial x$ and $\rho g \partial h/\partial y$, constant through the depth. These terms do not account for a vertically located source presence. It is only at Stage 1 of the time step after the next that the entrainment terms $\partial uw/\partial z$ and $\partial vw/\partial z$, computed from the vertically constant u and v and unrealistic w above the source triggers a local inward horizontal velocity field around the source. The fluid is drawn towards the source instead of being pushed away from it. With the same reasoning, sink terms within the water column would trigger exactly the opposite response, resulting locally in horizontal velocity components being pushed away from the sink.

Similarly, for a sink of the same magnitude placed above or below the source, Stage 2 results in no changes to the free surface, which would lead in turn (at Stage 1 of the next time step) to no changes in the horizontal velocity field. Further, the entrainment terms $\partial uw/\partial z$ and $\partial vw/\partial z$ in equation Eq. (3.7) and Eq. (3.8) respectively would remain zero as u and v remain zero. The hydrostatic assumption on its own is therefore not applicable to de-stratification devices, such as bottom outlets, jet-

circulations, or bubble diffusers.

Other examples for which the hydrostatic assumption is not valid include deep reservoirs, lakes and fjords, for which the water depth can be of similar order of magnitude to the width of the fluid body. The Coquitlam Reservoir, Canada, providing drinking water to the Greater Vancouver Regional District, for instance, is more than 185 m deep while only being 750 m wide at its deepest.

Ch.3-1.7. Pseudo non-hydrostatic formulation

For such applications, the third equation of momentum, Eq. (3.9), has to be reintroduced in the system and another equation has to be found for the dynamic pressure (as opposed to the hydrostatic pressure on its own). The difficulty resides in the fact that the Navier-Stokes equations are driven by a spatial pressure gradient term but do not solve for the pressure itself. Rather, the system of momentum equation is closed by the continuity equation, which does not include a pressure term.

In order to compute pressure, the vast majority of 3D hydrodynamic solvers applied to large-scale environmental hydraulics having a non-hydrostatic option (see Chapter 2 and Appendix B) use the *projection method* as described, for instance, by Brown et al. (2001) and by Guy and Fogelson (2005). The *projection method* adds the following equation of type Poisson equation to the system to compute the dynamic pressure:

$$\Delta p = \frac{\partial F_x}{\partial x} + \frac{\partial F_y}{\partial y} + \frac{\partial F_z}{\partial z} - \frac{\partial \rho u^2}{\partial x^2} - \frac{\partial \rho v^2}{\partial y^2} - \frac{\partial \rho w^2}{\partial z^2} - 2\frac{\partial \rho uv}{\partial x \partial y} - 2\frac{\partial \rho uw}{\partial x \partial z} - 2\frac{\partial \rho vw}{\partial y \partial z}, \qquad (3.15)$$

where Δp is the Laplacian of the pressure p, also $div(\vec{\nabla} p)$ the divergence of the gradient of the pressure p, also $\frac{\partial^2 p}{\partial x^2} + \frac{\partial^2 p}{\partial y^2} + \frac{\partial^2 p}{\partial z^2}$, and all other quantities have been defined previously.

It should be noted that, given the importance of hydrostatic pressure in environmental hydraulics, the pressure term is sometimes split in two components: a hydrostatic pressure and a dynamic pressure. For instance Song and Haidvogel (1994) or Koçyigit et al. (2002) describe such approach. As a result, the horizontal free surface gradients derivatives, $\rho g \partial h/\partial x$ and $\rho g \partial h/\partial y$ are added to the Navier-Stokes equations instead of inserted in place of the horizontal pressure gradients.

In this context, the horizontal velocity field (u, v) is computed through the first and second momentum equations, Eq. (3.7) and Eq. (3.8) respectively. The free surface elevation is computed through the 2D depth averaged continuity equation, Eq. (3.10). The pressure term p is computed through the projection method, Eq. (3.15). The remaining vertical velocity component w is therefore computed through the continuity equation Eq. (3.10) since the third momentum equation is indirectly included in the *projection method*.

The *projection method*, Eq. (3.15), is derived using the divergence of the momentum, sum of the derivative of each of the 3 equations Eq. (3.7), Eq. (3.8) and Eq. (3.9):

$$\frac{\partial}{\partial x}\left(\frac{\partial \rho u}{\partial t}+\frac{\partial p}{\partial x}\right)+\frac{\partial}{\partial y}\left(\frac{\partial \rho v}{\partial t}+\frac{\partial p}{\partial y}\right)+\frac{\partial}{\partial z}\left(\frac{\partial \rho w}{\partial t}+\frac{\partial p}{\partial z}\right)$$

$$=\frac{\partial}{\partial t}\left(\frac{\partial \rho u}{\partial x}+\frac{\partial \rho v}{\partial y}+\frac{\partial \rho w}{\partial z}\right)+\Delta p \quad (=0)$$

$$=\frac{\partial F_x}{\partial x}+\frac{\partial F_y}{\partial y}+\frac{\partial F_z}{\partial z}-\frac{\partial \rho u^2}{\partial x^2}-\frac{\partial \rho v^2}{\partial y^2}-\frac{\partial \rho w^2}{\partial z^2}-2\frac{\partial \rho uv}{\partial x \partial y}-2\frac{\partial \rho uw}{\partial x \partial z}-2\frac{\partial \rho vw}{\partial y \partial z}$$

$$+\frac{\partial}{\partial x}\left[\nu\frac{\partial}{\partial x}\left(\frac{\partial \rho u}{\partial x}+\frac{\partial \rho v}{\partial y}+\frac{\partial \rho w}{\partial z}\right)\right]+\frac{\partial}{\partial y}\left[\nu\frac{\partial}{\partial y}\left(\frac{\partial \rho u}{\partial x}+\frac{\partial \rho v}{\partial y}+\frac{\partial \rho w}{\partial z}\right)\right]+\frac{\partial}{\partial z}\left[\nu\frac{\partial}{\partial z}\left(\frac{\partial \rho u}{\partial x}+\frac{\partial \rho v}{\partial y}+\frac{\partial \rho w}{\partial z}\right)\right]$$

$(=0)$ $(=0)$ $(=0)$

However, the Poisson equation is computationally time consuming as it leads in 3D to a linear system of equations, with 7 diagonals, which requires a (direct or iterative) linear algebra solver. For that reason, several authors have explored an explicit discretisation of some or all of the components of the pressure gradient within the

Laplacian, therefore reducing the number of diagonals in the linear system. For instance, the work of Namin et al. (2001) is notable for considering both an implicit and semi-implicit methods to replace the vertical pressure gradient component by a simplified version of the third equation of momentum Eq. (3.9).

Ch.3-1.8. Direct non-hydrostatic formulation

Instead of using the projection method, whether computed or simplified as described in the vast majority of 3D hydrodynamic solvers, a new approach is here introduced, where the pressure p is directly computed from the third equation of momentum Eq. (3.9), without transformation:

$$\frac{\partial \rho w}{\partial t} + \frac{\partial \rho uw}{\partial x} + \frac{\partial \rho vw}{\partial y} + \frac{\partial \rho w^2}{\partial z} = -\frac{\partial p}{\partial z} + \frac{\partial}{\partial x}\left[\nu \frac{\partial \rho w}{\partial x}\right] + \frac{\partial}{\partial y}\left[\nu \frac{\partial \rho w}{\partial y}\right] + \frac{\partial}{\partial z}\left[\nu \frac{\partial \rho w}{\partial z}\right] + F_z, \tag{3.16}$$

where all quantities have been defined previously.

In this context, the horizontal velocity field (u, v) is computed through the first and second momentum equations, Eq. (3.7) and Eq. (3.8) respectively. The free surface elevation is computed either through the 2D depth averaged continuity equation, Eq. (3.10) or as a function of w at the surface, together with the dynamic surface boundary conditions. The pressure term p is computed through the third equation of momentum, Eq. (3.16), knowing that the pressure above the free surface is the atmospheric pressure. Finally, the remaining vertical velocity component w is computed through the continuity equation Eq. (3.10), similarly to the solution under the hydrostatic assumption.

The author of the present work wrote the finite difference 3D solver SULIS (Bourban, 1997) on the basis of a fully implicit solver, where all equations are coupled within

one linear algebra system. The 3D continuity equation Eq. (3.10) being linear, the three velocity components u, v and w are defined at the sides of every cell on a 3D staggered mesh and are solved implicitly with equal weights. Any source (or sink) term of the 3D continuity equation at any depth within the water column therefore affects all velocity components in all directions at the same time. The third equation of momentum is solved on the w-sides (except for the bottom of the water column), where the vertical gradient of the pressure term $\frac{\partial p}{\partial z}$ is also defined, based on a central finite difference computation, therefore leading to a pressure term p defined within each cell.

It is noted that the geometric location of pressure term is the same as for finite volume and finite element framework. This approach can therefore be implemented in TELEMAC-3D, in particular.

The validity of the approach taken to compute the dynamic pressure is demonstrated through the comparison against an analytical solution (see Section Ch.4-2).

Ch.3-1.9. Viscosity and turbulent closure methods

In general, turbulence closure is attained when the Reynolds stresses are fully quantified, either by creating a relationship with existing unknowns, such as velocity components (zero-equation model) or by introducing one, two or more unknowns (such as kinetic energy k and viscous dissipation ε) where each unknown adds a further advection-diffusion equation to the system. The popularity of most recent two-equation turbulence models such as the $k-\varepsilon$ Mellor-Yamada model (1982) (referred to in 8 of the 24 3D solvers listed in Appendix B) seems to dampen interest in the mixing length hypothesis of Prandtl, which is now only referenced in earlier work.

Falconer explains in his doctoral thesis (1976) that turbulence closure is achieved in a first step by assuming a direct relationship between the velocity components and the eddy viscosity (or Reynolds stresses): the Prandtl hypothesis for instance, assumes that the relationship coefficient is function of the mixing length taken from the theory of gas dynamics. Other instances introduce mixing length as a more or less complex function of the Richardson number (the ratio of buoyancy and inertia). The arbitrary nature of the mixing length coefficient spawned one-equation turbulence closures, introducing the kinetic energy k. In this case, the eddy viscosity varies with the square root of the kinetic energy but is also function of an empirical length scale. Falconer (1976) concludes that there is no advantage to use a one-equation model over the simpler mixing length model because the arbitrary or empirical nature of the mixing length remains.

In order to remove the presence of an arbitrary mixing length scale, two-equation turbulence closures are developed. For instance a viscous dissipation ε can be defined and added to the system of equations, or a specific dissipation ω can also be introduced and combined to the kinetic energy. An empirical function then links the kinetic energy and the viscous dissipation or the specific dissipation back to the eddy viscosity.

Turbulence closure methods are numerous. In addition to the two-equation turbulence closure of Mellor-Yamada (1982) the following three publications are noted for completeness of the mathematical framework:

- Large and Gent (1999) introduced a series of zero-equation models, including the so-called κ-profile parameterisation;
- Kantha and Carniel (2003) present a generic two-equation turbulence closure, which enables to simulate any desired length scale equation including those in the

$k-\varepsilon$ and $k-\omega$ as well as $k-kl$, $k-k\tau$ and variations; and

- McDonough (2004) presents a more general appreciation of turbulent processes for the fluid flows.

Nonetheless, the present research work does not investigate these but primarily focus on advection.

Ch.3-2. Numerical framework

The numerical framework is based on a series of advection schemes first introduced by Nessyahu and Tadmor (1990) in a 1D centred finite difference form, further refined by Kurganov and Tadmor (2000), and advanced to a 1D a centred-upwind form by Kurganov, et al. (2001). The centred-upwind form was later generalised to a 2D unstructured finite volume form by Kurganov and Petrovna (2004).

These schemes are based on semi-implicit finite differences, the common objective being to integrate the solution over the non-smooth Riemann fan rather than trying to solve the discretised equations explicitly. Of particular interest here, this integration over the Riemann fan allows a natural generalisation of the schemes to multiple dimensions and multiple sets of equations for which the eigenvalue structure of the problem is not obvious to Riemann fan solving schemes. Further, the most recent forms by Kurganov et al. (2000), (2001), and (2004) admit a conservative form, which correspond to finite volume schemes when in an explicit context.

For practical reason in this thesis, the names of schemes will be distinguished from one another by the initials of theirs authors, a convention that is also used in the above literature.

Ch.3-2.1. Advection, 1D finite difference, numerical diffusion

For the hyperbolic conservation law, Lax (1954) and Friedrichs (1954) introduced the following first-order explicit yet stable central difference scheme (the LF-scheme) along the 1D x-axis:

$$w_j^{n+1} = \frac{1}{2}\left[w_{j+1}^n + w_{j-1}^n\right] - \frac{\Delta t}{2\Delta x}\left[f\left(w_{j+1}^n\right) - f\left(w_{j-1}^n\right)\right], \tag{3.17}$$

which leads to infinite numerical viscosity $\sim w_{xx}(\Delta x)^2/(2\Delta t)$ as $\Delta t \to 0$, having written the above in its viscous form

$$\frac{w_j^{n+1} - w_j^n}{\Delta t} + \frac{\left[f\left(w_{j+1}^n\right) - f\left(w_{j-1}^n\right)\right]}{2\Delta x} = \frac{(\Delta x)^2}{2\Delta t}\frac{\left[\left(w_{j+1}^n - w_j^n\right) - \left(w_j^n - w_{j-1}^n\right)\right]}{(\Delta x)^2}$$

In order to decrease excessive first-order dissipation of the LF-scheme, Nessyahu and Tadmor (1990) observed that the average component of Eq. (3.17) could be written as a second-order piecewise linear average and that the difference of fluxes could be averaged over the non-smooth Riemann fans using a staggered cell of fixed width Δx (see Figure 3.2). Finally, implicitness was also introduced in the difference of fluxes by using the mid-point rule, second order in time.

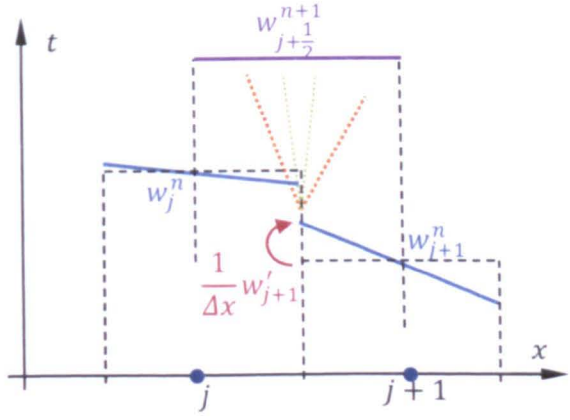

Figure 3.2 – Nessyahu & Tadmor (1990), Staggered integration over the Riemann fan

As a result, a two-substep time integration approximation is constructed (the NT-

scheme) where the intermediate step is discretised on the adjoining stencil such that:

$$w_{j+\frac{1}{2}}^{n+1} = \bar{w}_{j+\frac{1}{2}}^{n} - \frac{\Delta t}{\Delta x}\left[f\left(w_{j+1}^{n+\frac{1}{2}}\right) - f\left(w_{j}^{n+\frac{1}{2}}\right)\right] \tag{3.18}$$

where $\bar{w}_{j+\frac{1}{2}}^{n}$ is a 2nd order integration of the form $\frac{1}{2}[w_{j+1}^{n} + w_{j}^{n}] - \frac{1}{8}[w_{j+1}^{n\prime} - w_{j}^{n\prime}]$ with $w_i^{n\prime}/\Delta x$ an approximate slope at grid point i and where $w_i^{n+\frac{1}{2}} := w_i^n - \frac{\Delta t}{2\Delta x} f_i^{n\prime}$ with $f_i^{n\prime}/\Delta x$ the numerical derivative of the function f.

To prevent oscillatory behaviour, Nessyahu and Tadmor (1990) recommended that slope and derivative terms be calculated using the non-linear minmod limiter, $w_i^{n\prime} := minmod([w_i^n - w_{i-1}^n], [w_{i+1}^n - w_i^n])$, where:

$$minmod\{z_j\} := \begin{cases} min_j\{z_j\} & if\ z_j > 0\ \forall j \\ max_j\{z_j\} & if\ z_j < 0\ \forall j \\ 0 & otherwise \end{cases} \tag{3.19}$$

With this, the NT-scheme is second-order in time and space. However, the numerical viscosity, $\sim w_{xxxx}(\Delta x)^4/(2\Delta t)$, tends to infinity away from extrema as $\Delta t \to 0$ even though its value for a finite time step is considerably smaller than the that obtained using the LF-scheme (see also Figure 3.4 and Figure 3.5 for a comparative illustration of the schemes applied to the non-linear Burgers' equation).

In order to further decrease numerical viscosity, or at least bound its dependency on Δt, Kurganov and Tadmor (2000) presented a modified version of the scheme (the KT-scheme) shrinking the region over which the Riemann fan is integrated. Instead of using a staggered cell of fixed width Δx, Kurganov and Tadmor (2000) used a tighter bound based on the maximum of the local speeds of wave propagation (see Figure 3.3).

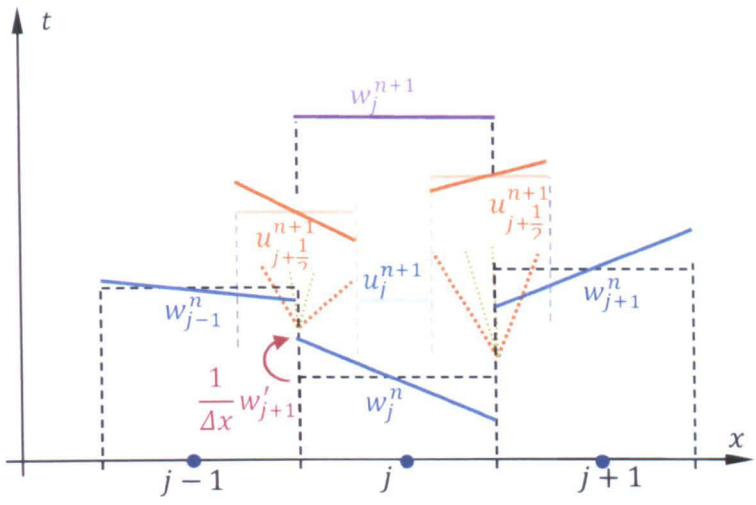

Figure 3.3 – Kurganov and Tadmor (2000), Bounding the Riemann fan integration

Again, a second-order piecewise linear approximation is constructed, summing up the contributions over two non-smooth Riemann fans and the one smooth region as follows:

$$w_j^{n+1} = \frac{\Delta t}{\Delta x} a^n_{j-\frac{1}{2}} u^{n+1}_{j-\frac{1}{2}} + \left[1 - \frac{\Delta t}{\Delta x}\left(a^n_{j-\frac{1}{2}} + a^n_{j+\frac{1}{2}}\right)\right] u_j^{n+1} + \frac{\Delta t}{\Delta x} a^n_{j+\frac{1}{2}} u^{n+1}_{j+\frac{1}{2}} + \frac{\Delta x}{2}\left[\left(\frac{\Delta t}{\Delta x} a^n_{j-\frac{1}{2}}\right)^2 w'_{j-\frac{1}{2}} - \left(\frac{\Delta t}{\Delta x} a^n_{j+\frac{1}{2}}\right)^2 w'_{j+\frac{1}{2}}\right] \tag{3.20}$$

where the left and right terms, $u^n_{j\pm\frac{1}{2}}$, are defined given by the staggered integration term of the NT-scheme in Eq. (3.18), while the middle term ,u_j^{n+1}, is what is left of the piecewise linear term in the middle of the j-th cell. In the KT-scheme, $a^n_{j\pm\frac{1}{2}}$ is the maximum local speed of propagation at the discontinuity $x_{j\pm\frac{1}{2}}$ disregarding the direction of the propagation.

As demonstrated by Kurganov and Tadmor, one of the main advantages of the KT-scheme is that the following semi-discrete formulation can be derived, written in conservative form as:

$$\frac{d}{dt} w_j(t) = -\frac{1}{\Delta x}\left[H_{j+\frac{1}{2}}(t) - H_{j-\frac{1}{2}}(t)\right] \tag{3.21}$$

where the numerical flux is given by:

$$H_{j\pm\frac{1}{2}} := \frac{1}{2}\left[f\left(w^{>}_{j\pm\frac{1}{2}}\right) + f\left(w^{<}_{j\pm\frac{1}{2}}\right)\right] - \frac{a_{j\pm\frac{1}{2}}}{2}\left[w^{>}_{j\pm\frac{1}{2}} - w^{<}_{j\pm\frac{1}{2}}\right],$$

with intermediate values

$$w^{>}_{j\pm\frac{1}{2}} := w_{j+\frac{1\pm1}{2}} - \frac{\Delta x}{2} w'_{j+\frac{1\pm1}{2}} \text{ and } w^{<}_{j\pm\frac{1}{2}} := w_{j-\frac{1\mp1}{2}} + \frac{\Delta x}{2} w'_{j+\frac{1\mp1}{2}},$$

in which the superscripts > and < are the right and left sides respectively of the discontinuity.

As a result, this formulation is simpler than the fully discretised form and can therefore be extended to multi-directional problems and to higher order time integrators and represent other terms such as diffusion. Moreover, the conservative form of the KT-scheme also corresponds to a finite volume scheme when in an explicit context.

Kurganov, Noelle and Petrovna (2001) enhanced the central differencing KT-scheme by introducing the left and right local speeds of propagation (as opposed to disregarding the direction of the speed), thus further shrinking the width of the non-smooth region over the Riemann fan. As a result the KP-scheme is central-upwind. Kurganov and Lin (2007) further improved the KP-scheme by making an anti-diffusive correction to the final spatial summation step based on a method used in partial characteristic decomposition. The semi-discrete formulation of the resulting KL-scheme is written as follows:

$$\frac{d}{dt} w_j(t) = -\frac{1}{\Delta x}\left[H_{j+\frac{1}{2}}(t) - H_{j-\frac{1}{2}}(t)\right] \tag{3.22}$$

where the numerical flux is given by:

$$H_{j\pm\frac{1}{2}} := \frac{1}{2}\left[\frac{a^{<}_{j\pm\frac{1}{2}} f\left(w^{>}_{j\pm\frac{1}{2}}\right) + a^{>}_{j\pm\frac{1}{2}} f\left(w^{<}_{j\pm\frac{1}{2}}\right)}{a^{>}_{j\pm\frac{1}{2}} - a^{<}_{j\pm\frac{1}{2}}}\right] - a^{>}_{j\pm\frac{1}{2}} a^{<}_{j\pm\frac{1}{2}}\left[\frac{w^{>}_{j\pm\frac{1}{2}} - w^{<}_{j\pm\frac{1}{2}}}{a^{>}_{j\pm\frac{1}{2}} - a^{<}_{j\pm\frac{1}{2}}} - q_{j\pm\frac{1}{2}}\right],$$

with correction term $q_{j\pm\frac{1}{2}} := minmod\left(\frac{w^{>}_{j\pm\frac{1}{2}} - u^{int}_{j\pm\frac{1}{2}}}{a^{>}_{j\pm\frac{1}{2}} - a^{<}_{j\pm\frac{1}{2}}}, \frac{u^{int}_{j\pm\frac{1}{2}} - w^{<}_{j\pm\frac{1}{2}}}{a^{>}_{j\pm\frac{1}{2}} - a^{<}_{j\pm\frac{1}{2}}}\right)$ and

intermediate velocity $w^{int}_{j\pm\frac{1}{2}} := \frac{a^{>}_{j\pm\frac{1}{2}} w^{>}_{j\pm\frac{1}{2}} - a^{<}_{j\pm\frac{1}{2}} w^{<}_{j\pm\frac{1}{2}} - \left\{f\left(a^{>}_{j\pm\frac{1}{2}}\right) - f\left(a^{<}_{j\pm\frac{1}{2}}\right)\right\}}{a^{>}_{j\pm\frac{1}{2}} - a^{<}_{j\pm\frac{1}{2}}}$

between $w^{>}_{j\pm\frac{1}{2}}$ and $w^{<}_{j\pm\frac{1}{2}}$, in which all other quantities have been defined previously.

The semi-discrete formulation of the KL-scheme is identical to that of the KP-scheme except for the extra term $q_{j+\frac{1}{2}}$.

By means of an illustration, the numerical schemes introduced are implemented as 1D-solvers of the non-linear Burgers' equation (1948). We consider a case where the solution temporally converges to a discontinuity from an initial sinusoid. The characteristics of the models illustrated are based on a regular grid of 200 cells over a total length of 2 m, and closed with a circular boundary condition. Figure 3.4 and Figure 3.5 present the numerical solutions for the LF-, NT-, KT- and KP-schemes for a non-dimensional time step Δt equal to half and to one tenth the non-dimensional spatial grid step Δx respectively.

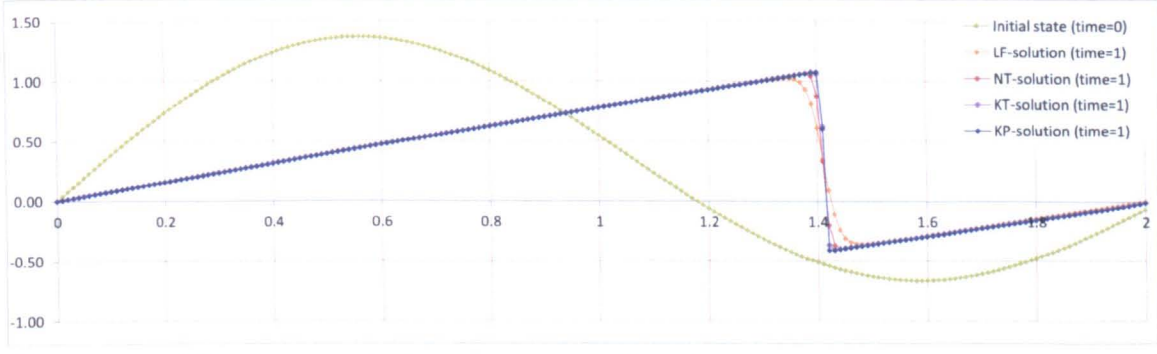

Figure 3.4 – 1D advection, Burgers' equation, $\Delta t = \Delta x/2$

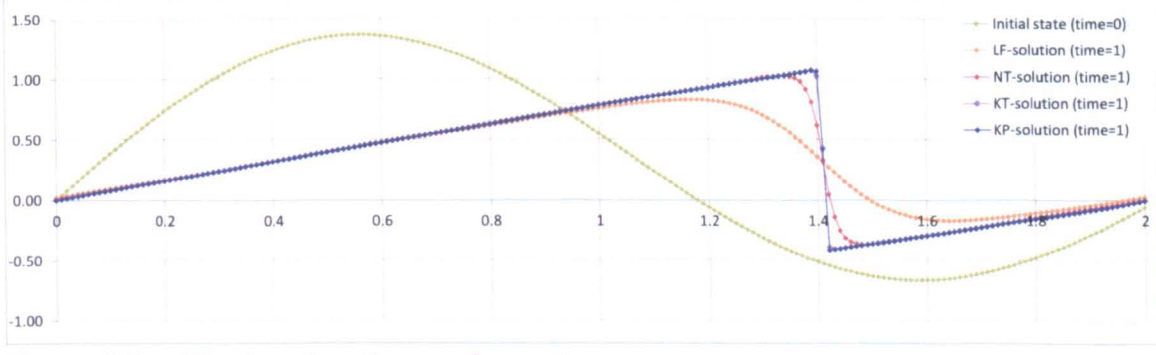

Figure 3.5 – 1D advection, Burgers' equation, $\Delta t = \Delta x/10$

Comparison between Figure 3.4 and Figure 3.5 highlights the increased dissipation when Δt reduces for constant Δx, more so for the LF-scheme than for the NT-scheme, whereas the KT- and KP-schemes seem fairly insensitive in this case. As anticipated, the discontinuity is well represented by the most recent schemes, with only a central

node at the discontinuity.

Ch.3-2.2. 1D linear laws, scheme convergence

The specific case of pure advection (where the flux function is linearly dependent on the quantity being transported) is an application of the movement of tracers in water (including temperature, salinity, sediments). In that case, if the quantity u is transported at a constant uniform speed c, then one of the propagation speeds $a^{>}_{j\pm\frac{1}{2}}$ or $a^{<}_{j\pm\frac{1}{2}}$ is zero and the other is c. Thus the product $a^{>}_{j\pm\frac{1}{2}}a^{<}_{j\pm\frac{1}{2}} = 0$ and the KL- and KP-schemes reduce to a simplified KT-scheme as follows:

$$\frac{d}{dt}w_j(t) = -\frac{c}{\Delta x}\left[w^{<}_{j+\frac{1}{2}} - w^{>}_{j-\frac{1}{2}}\right] = -\frac{c}{\Delta x}\left[w_j + \frac{1}{2}w'_j - w_j + \frac{1}{2}w'_j\right] = -\frac{c}{\Delta x}w'_j \qquad (3.23)$$

where the slope term $w'_j = minmod(w_{j+1} - w_j, w_j - w_{j-1})$.

Because of the limiter, it is difficult to introduce implicitness in the case of pure advection in uniform flows. By comparison, the slope term is written as $\frac{1}{2}[w_{j+1} - w_{j-1}]$ in a central difference scheme such as the LF-scheme (see Eq. (3.17)), which can be written as a fully implicit term.

For verification purposes, the numerical schemes are implemented as 1D-solvers of the pure advection equation. The characteristics of the models considered are based on a regular grid of 800 cells covering a total length of 2 m. The transport speed c is constant and uniform, and set to 0.5 m/s. Four types of initial solution profiles are considered as a function of x along the 1D-axis:

(a) A discontinuity, where the concentration $T_0 = 1$ on the left of $x_{(a)} = 0.1$ m and $T_0 = 0$ on the right;

(b) A linear variation with a triangular profile, where the concentration is

piecewise linear around $x_{(b)} = 0.5$ m, with $T_0(x_{(b)}) = 1$ and a base of 0.25 m where $T_0(x_{(b)} \pm 0.125) = 0$;

(c) A quadratic variation with an elliptic profile, where the concentration is centred around $x_{(c)} = 0.9$ m, with $T_0(x_{(c)}) = 1$ at horizontal tangent and a base of 0.25 m where $T_0(x_{(c)} \pm 0.125) = 0$ at vertical tangents; and

(d) A smoothly varying sine-squared profile, where the concentration is centred around $x_{(d)} = 1.3$ m, with $T_0(x_{(d)}) = 1$ at horizontal tangent and a base of 0.25 m where $T_0(x_{(d)} \pm 0.125) = 0$ at horizontal tangents.

The tracer concentration is transported at speed c for 1 s, covering a distance of 0.5 m. The tracer concentration is imposed at the left boundary at $T(t, x_{=0}) = 1$ (a Dirichlet condition at the inflow) and let free at the right boundary (a Neumann condition at the outflow).

For comparison and reference purposes, Figure 3.6 shows the numerical solutions obtained with the LF-, NT- and KT-schemes for a time step Δt equal to the grid step Δx (Courant number of 0.5). A second-order QUICKEST scheme (Q2-scheme) combining centred and upwind terms over a large stencil, was also implemented using backward-Euler time-integration. The QUICKEST scheme was introduced by Leonard (1979) and further expanded in its ULTIMATE form by the same author (1991). The details of the ULTIMATE QUICKEST schemes are also presented in Ch.2-3.3. The solution predicted by the Q2-scheme is also displayed. For graphical comparison purposes with the analytical solution, the final solution obtained with each scheme is shifted back 0.5 m (moved left) to match the initial condition, which is also the analytical solution.

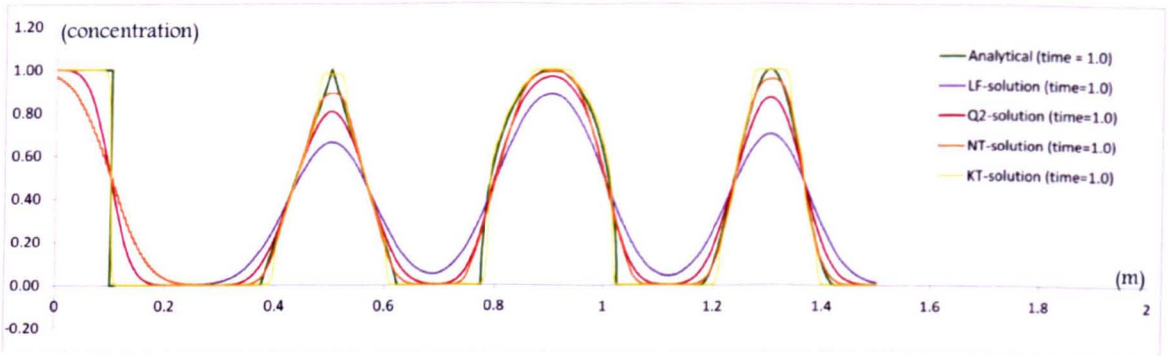

Figure 3.6 – 1D advection of tracer profile, $\Delta t = \Delta x$, $c = 0.5$

The profiles obtained for all schemes except the KT-scheme exhibit increased dissipation in that the profiles' amplitude attenuates as the base widens. In contrast, the solution for the KT-scheme evolves into progressively narrow wave forms with flat crests. Interestingly, the NT-scheme is less dissipative than the Q2-scheme for the same stencil while maintaining monotonicity but it is identical to the LF-scheme in the case of the first step discontinuity.

In order to verify the appropriateness of the chosen paired space and time steps, the next set of figures shows the results of numerical convergence analyses in the norm L2, where numerical convergence is as defined by Morton and Mayers (1994), for instance, and where the norm L2 is defined as the sum of the square of the difference between a given solution and the corresponding analytical solution. These convergence analyses also serve as a verification in the sense defined by Roache (Roache, 1998), and in particular as means to evaluate the order of accuracy of the numerical scheme.

In this case, the Courant number remains unchanged, and both the time step Δt and space step Δx steps are being reduced (divided by 4 each time) so as to observe a gradual convergence toward the continuous (analytical) solution.

Figure 3.7 shows the convergence test profiles obtained for the KT-scheme for 4 pairs of decreasing steps.. In purple, the solution is coarser, with the pair multiplied by 4. In

red, the solution is identical as on Figure 3.6. In orange and yellow, the solution is finer with a pair divided by 4 and 16 respectively. A separate larger figure of these results for the triangle form is shown in Figure 3.11.

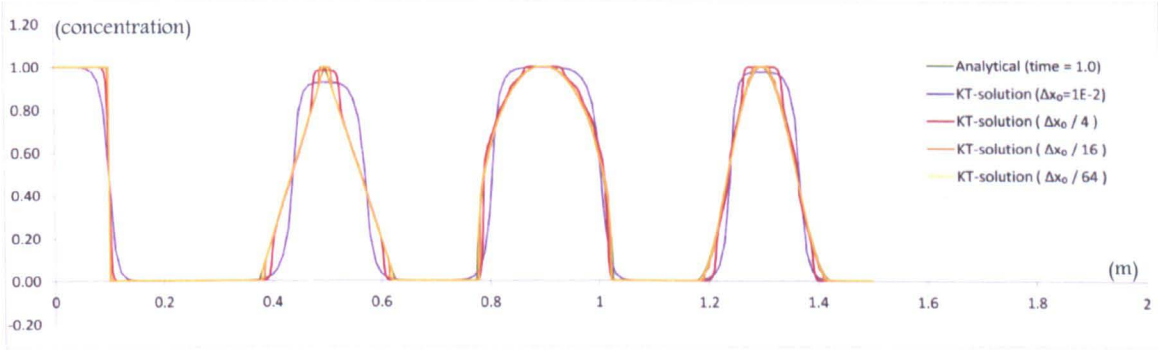

Figure 3.7 – 1D advection of tracer profile, Convergence profiles for the KT-scheme

It is clear that the KT-scheme converges numerically to the physical (analytical) solution when both Δx and Δt tend to 0. For comparison purposes, Figure 3.8 and Figure 3.9 show the same convergence tests for the Q2- and the LF-scheme respectively. Separate larger figures of these results for the triangle form only are shown in Figure 3.13 and Figure 3.15 for the Q2- and the LF-scheme respectively.

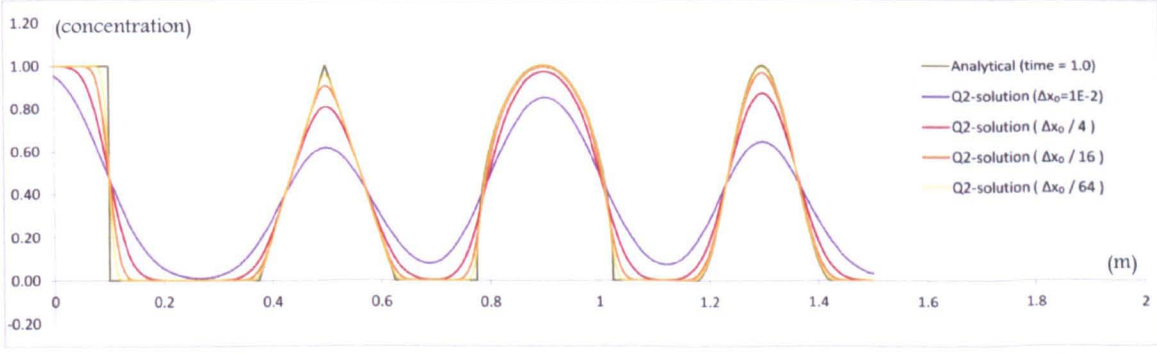

Figure 3.8 – 1D advection of tracer profile, Convergence profiles for the Q2-scheme

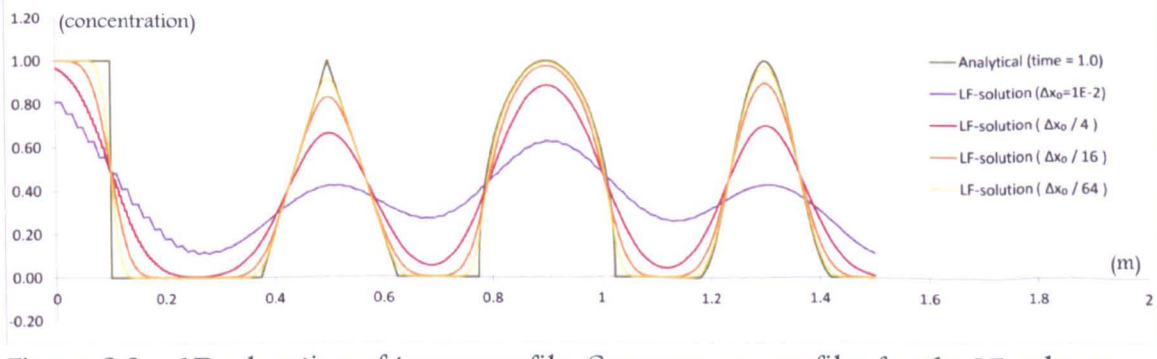

Figure 3.9 – 1D advection of tracer profile, Convergence profiles for the LF-scheme

Here again, it is clear that both these schemes also converge numerically to the analytical solution, albeit not as fast as the KT-scheme.

It should again be noted again that the KT-scheme tends to narrow the base of the individual profile forms distorting their crests into hats, whereas the dissipation of the Q2- and LF-scheme tends to widen the bases and flatten the crests of the profile forms. Consequently, when applied to environmental hydraulic studies, physical diffusion could improve the KT-solution by dissipating hat–shaped crests.

In order to verify the second-order nature of the KT-scheme, the triangular (linear) initial profile form from the convergence analysis above is considered. Figure 3.10 plots the spatial step normalised to its largest value modelled ($4\Delta x_o$) against the error between the computed and the analytical solutions. The point highlighted in orange represents the solution shown previously (Figure 3.6). Key results are listed in Table 1 and Figure 3.11 shows the resulting profile forms.

Name	x-axis Norm L_2	y-axis $1/(4\Delta x_o)$
KT ($4\Delta x_o$)	$6.02_{10}{}^{-01}$	1
KT (Δx_o)	$2.84_{10}{}^{-01}$	0.25
KT ($\Delta x_o/4$)	$1.55_{10}{}^{-01}$	0.625
KT ($\Delta x_o/16$)	$8.19_{10}{}^{-02}$	0.015625
KT ($\Delta x_o/64$)	$4.21_{10}{}^{-02}$	0.00390625

Table 1 – 1D advection of tracer profile, Scheme order analysis of the KT-scheme

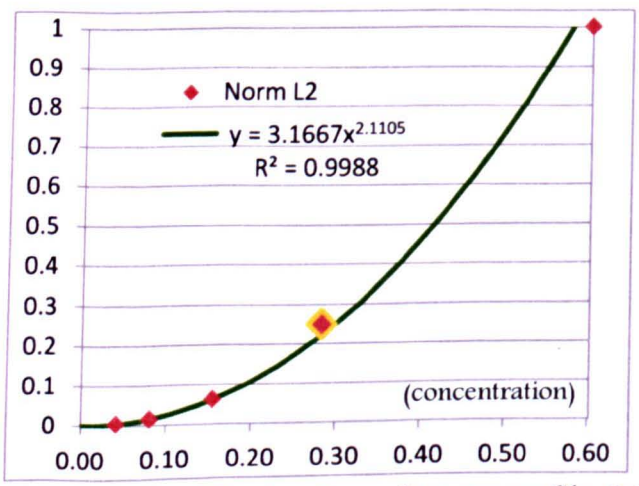

Figure 3.10 – 1D advection of tracer profile, Scheme order analysis of the KT-scheme

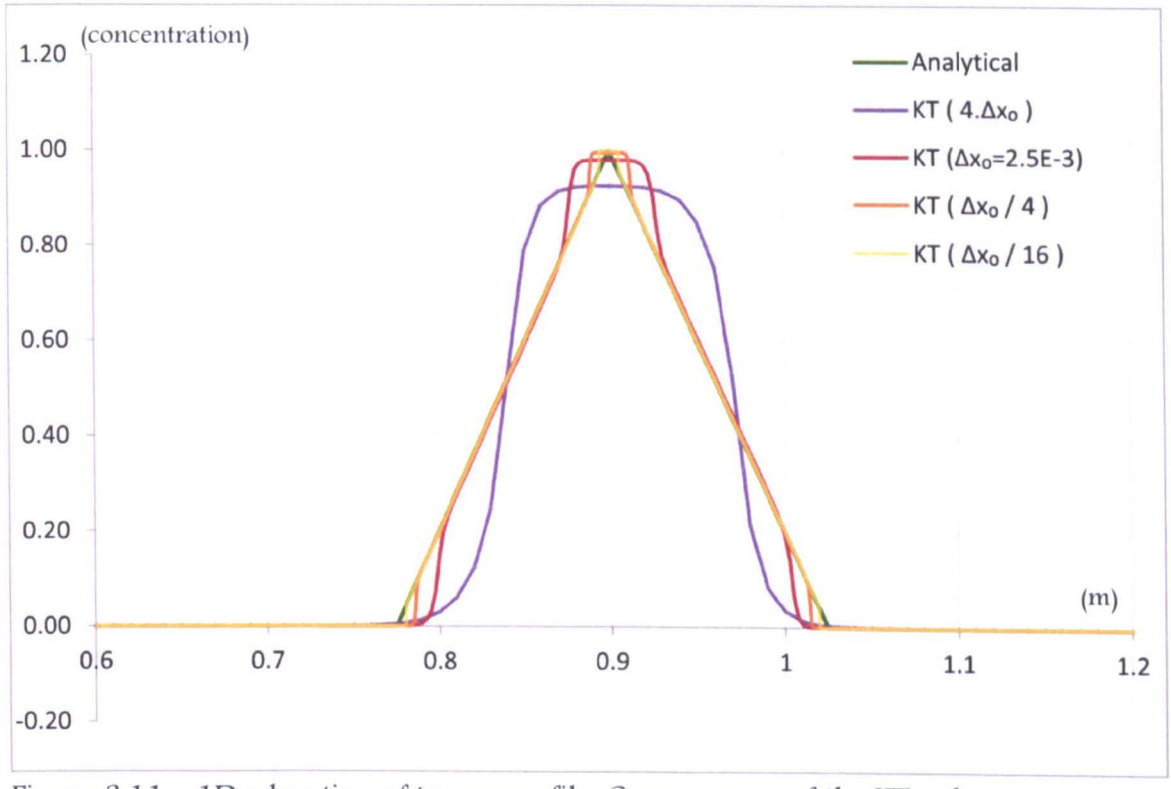

Figure 3.11 – 1D advection of tracer profile, Convergence of the KT-scheme

The results indicate that the KT-scheme is slightly higher than second-order of accuracy within the range of time / space steps chosen. For comparison purposes, Table 2, Figure 3.12, Figure 3.13 and Table 3, Figure 3.14, Figure 3.15 present the same convergence information for the Q2- and the LF-schemes respectively.

Name	x-axis Norm L_2	y-axis $1/(4\Delta x_o)$
Q2 ($4\Delta x_o$)	$8.43_{10}{}^{-01}$	1
Q2 (Δx_o)	$4.90_{10}{}^{-01}$	0.25
Q2 ($\Delta x_o/4$)	$2.44_{10}{}^{-01}$	0.625
Q2 ($\Delta x_o/16$)	$1.22_{10}{}^{-01}$	0.015625
Q2 ($\Delta x_o/64$)	$6.08_{10}{}^{-02}$	0.00390625

Table 2 - 1D advection of tracer profile, Scheme order analysis of the Q2-scheme

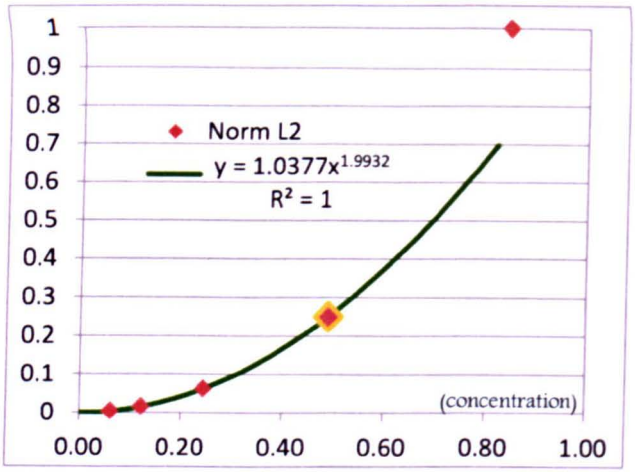

Figure 3.12 – 1D advection of tracer profile, Scheme order analysis of the Q2-scheme

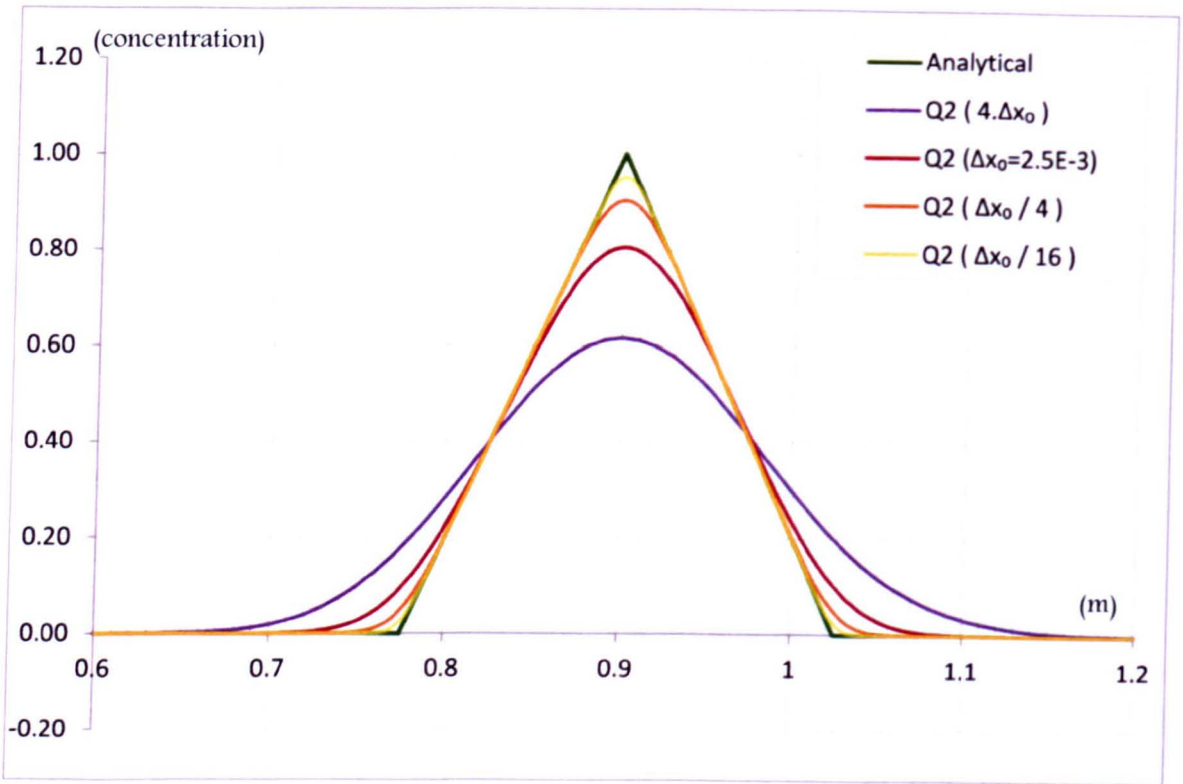

Figure 3.13 – 1D advection of tracer profile, Convergence of the Q2-scheme

Name	x-axis Norm L_2	y-axis $1/(4\Delta x_o)$
LF $(4\Delta x_o)$	$2.46_{10}{}^{+00}$	1
LF (Δx_o)	$2.39_{10}{}^{+00}$	0.25
LF $(\Delta x_o/4)$	$1.30_{10}{}^{+00}$	0.625
LF $(\Delta x_o/16)$	$6.49_{10}{}^{-01}$	0.015625
LF $(\Delta x_o/64)$	$3.24_{10}{}^{-01}$	0.00390625

Table 3 - 1D advection of tracer profile, Scheme order analysis of the LF-scheme

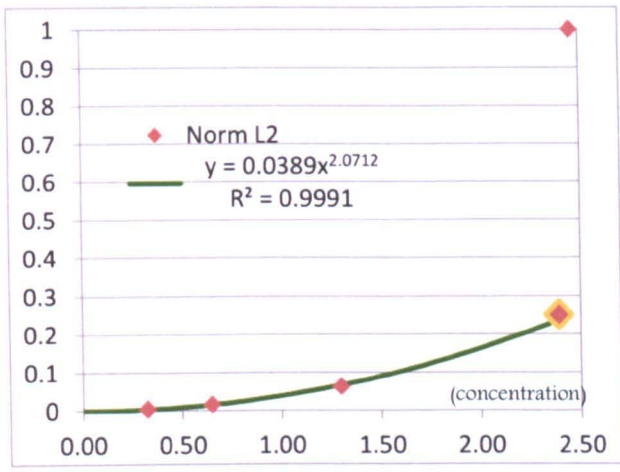

Figure 3.14 – 1D advection of tracer profile, Scheme order analysis of the LF-scheme

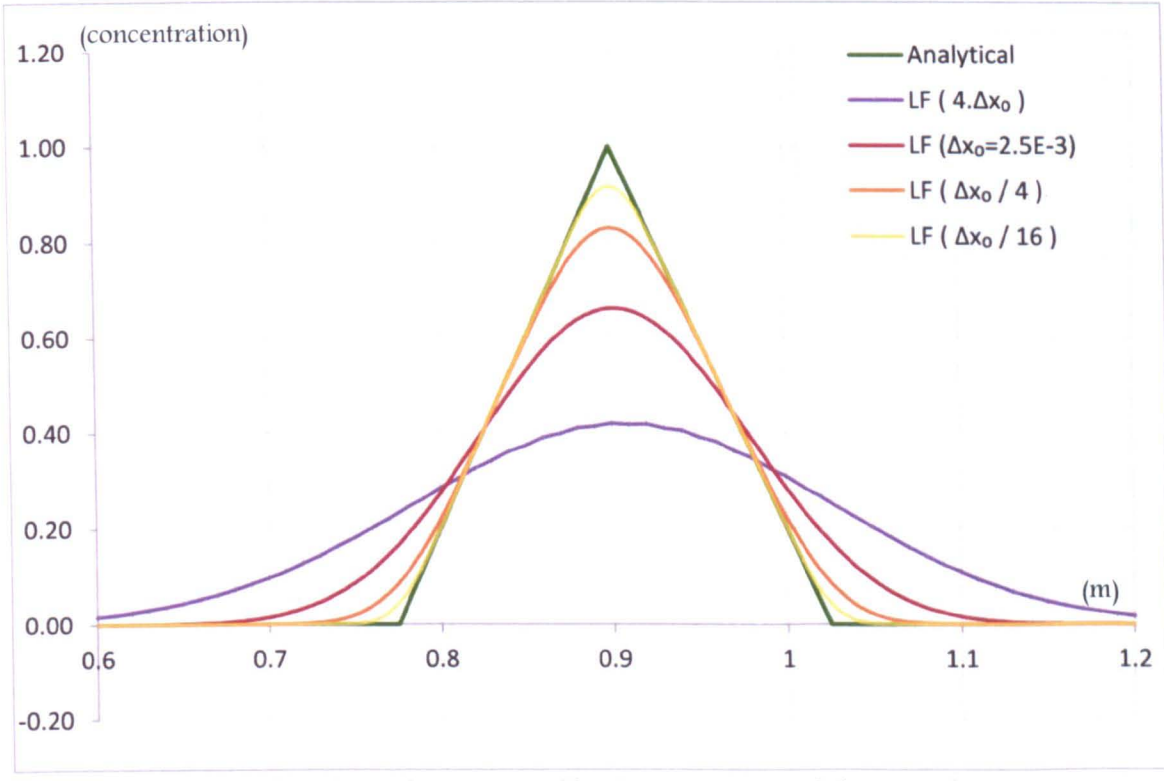

Figure 3.15 – 1D advection of tracer profile, Convergence of the LF-scheme

As for the KP-scheme, the results confirm that the Q2-scheme and the LF-scheme are second-order accurate. Unlike the KP-scheme, the results obtained previously for the Q2- and LF-scheme (highlighted in orange on the middle inset of Figure 3.12 and Figure 3.14 respectively) lie on a parabola but not the results for larger steps. As the principal multiplier of the parabola for the KP-scheme is almost 100 times larger than for the LF-scheme, the KP-scheme converges much faster. The KP-scheme shows grid and time convergence for larger steps, which allows for faster simulation of longer

periods in environmental hydraulics applications.

The same numerical convergence analysis was also carried out with the norm maximum with similar conclusions, where the norm is defined as the maximum of the absolute difference between a given solution and the corresponding analytical solution.

Finally, Figure 3.16 shows the KT-scheme predictions as a function of time step. When applied to environmental hydraulic studies, the time step of the entire model is indeed likely to be driven by the hydrodynamics, which would usually be smaller than for tracer advection in isolation. The time step of the solution shown previously in Figure 3.6 has been successively reduced by more than 2, 10 and 50, while keeping the grid space unchanged.

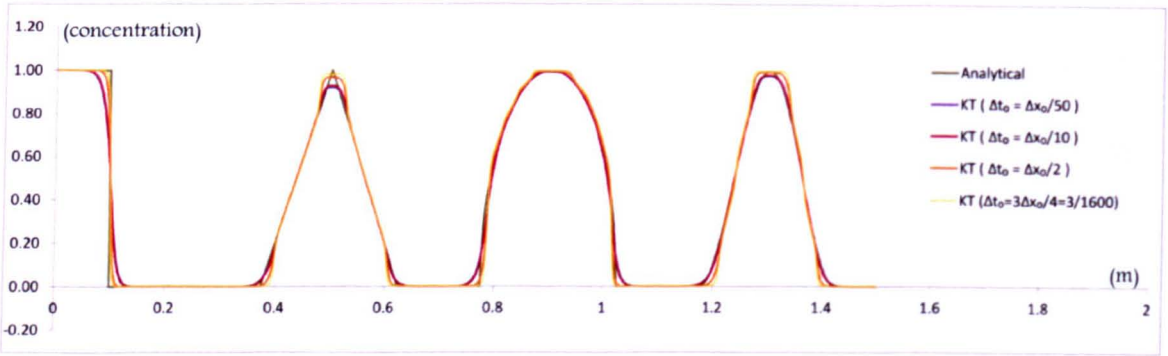

Figure 3.16 – 1D advection of tracer profile, Time step convergence of the KT-scheme

This confirms that the KT-scheme preserves the individual profile form of the solution relatively well without dramatically widening the bases or lowering the crests. For comparison purposes, Figure 3.17 and Figure 3.18 show the same results for the Q2- and the LF-schemes respectively.

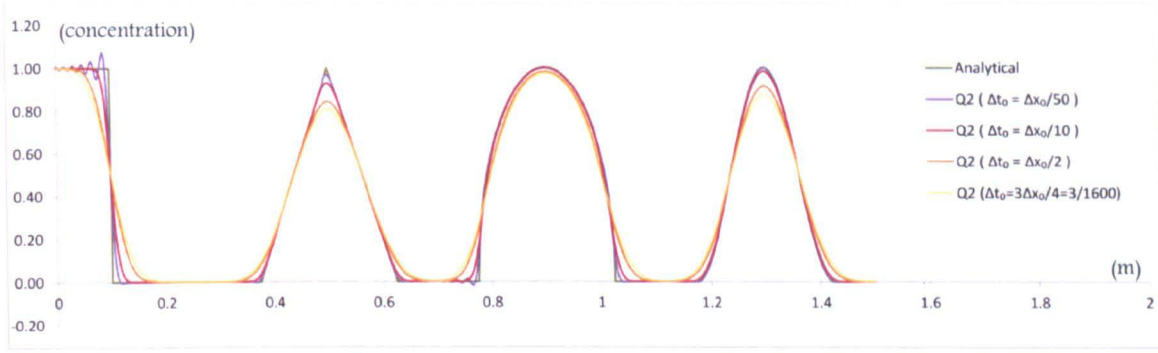

Figure 3.17 – 1D advection of tracer profile, Time step convergence of the Q2-scheme

Unlike the KP-scheme, the Q2-scheme becomes less dissipative as the time step is reduced. However the Q2-scheme also becomes non-monotonic (oscillatory) where the function or the gradients of the function are discontinuous. This is not acceptable in the context of the present work.

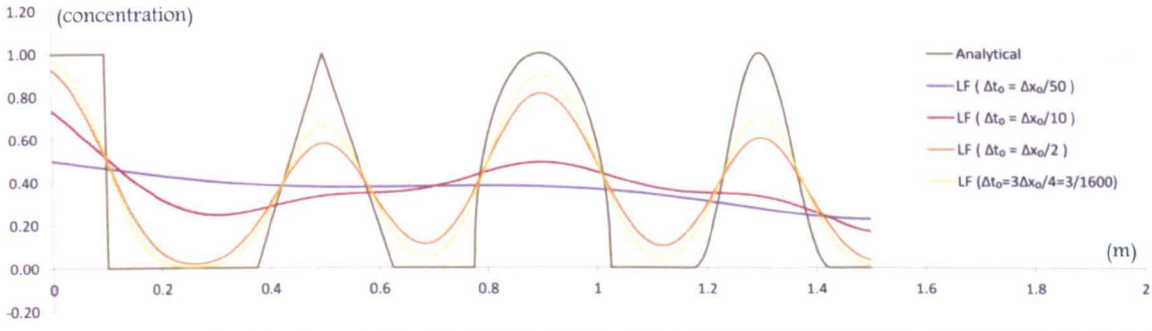

Figure 3.18 – 1D advection of tracer profile, Time step convergence of the LF-scheme

As shown in Figure 3.18, the LF-scheme tends to become infinitely dissipative as the time step reduces.

Ch.3-2.3. Generalisation to unstructured meshes, the BCT-scheme

Kurganov and Petrovna (2004) introduced a generalisation of the KP-scheme to unstructured meshes (see Figure 3.19). The principal assumption was to consider the mesh as an ensemble of triangular elements, where the values of certain dependent variables such as depth and tracer concentrations are averaged over the elements

(light orange) and where the Riemann fan discontinuities are described at the edge between two elements (dark orange). Hence 3 fluxes are defined perpendicularly through the 3 edges of each triangular element. This numerical framework, in its conservative form, is identical to most finite volume solvers such as revisited by Toro in the 3rd edition of his book (2009).

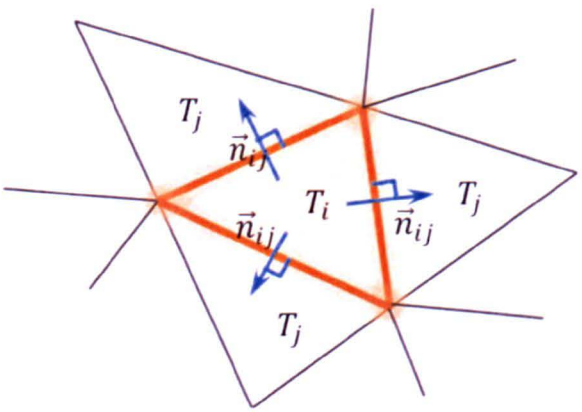

Figure 3.19 – Kurganov and Petrovan (2004), Element and through fluxes definition

It is noted that Scheme C^T is equivalent to the relative locations adopted. It represents naturally the conservative form with fluxes through the sides of elements while keeping track of the volume in the element. This also confirms that finite differences based on Scheme C^T, written in a conservative form are equivalent to finite volumes, albeit the fluxes and the computation of gradients may differ.

A prototype solver of the St Venant equations based on this numerical framework was implemented for gaining understanding and for benchmarking purposes.

One of the goals of the present work is to retain the stencil definition of a finite element solver for implementation with the open source TELEMAC system, the mathematics of which is presented by Hervouet (2007). The reader is referred to the books of Zienkiewicz and Taylor, in particular Volume 1 The Basis (2000) and Volume 3 Fluid Dynamics (2000), for a detail introduction to finite element methods. A novel implementation of the KP-scheme is therefore introduced, where all principal

quantities are retained at the vertices of the unstructured mesh and where all fluxes are exchanged between pairs of nodes along the edges on the mesh. Throughout the remainder of the thesis, this numerical framework is referred to as the BCT-scheme, where "BCT" would appropriately stand for Bounded within Control Triangle for reasons highlighted in the finite element implementation of the scheme. While being prototyped, the scheme was referred to as the BCT-scheme following the convention previously adopted by the authors of the series of schemes considered (Nessyahu, Tadmor, Kurganov, Petrova, Noelle and Lin in various combinations). In the BCT-scheme, "B" stands for the name of its principal author, S.E. Bourban, and "C" and "T" acknowledge C.J. Cawthorn and M.S. Turnbull respectively for their contribution under the principal author's lead.

In its conservative form, the BCT-scheme defines a control volume around an arbitrary node by summing up the contributions of every element connected to that node, element by element, therefore mimicking the finite element assembling methodology. The contribution of one element to the control volume around a node joins the node with the middle of the connecting edges and with the centroid of that element (see orange triangle on Figure 3.20).

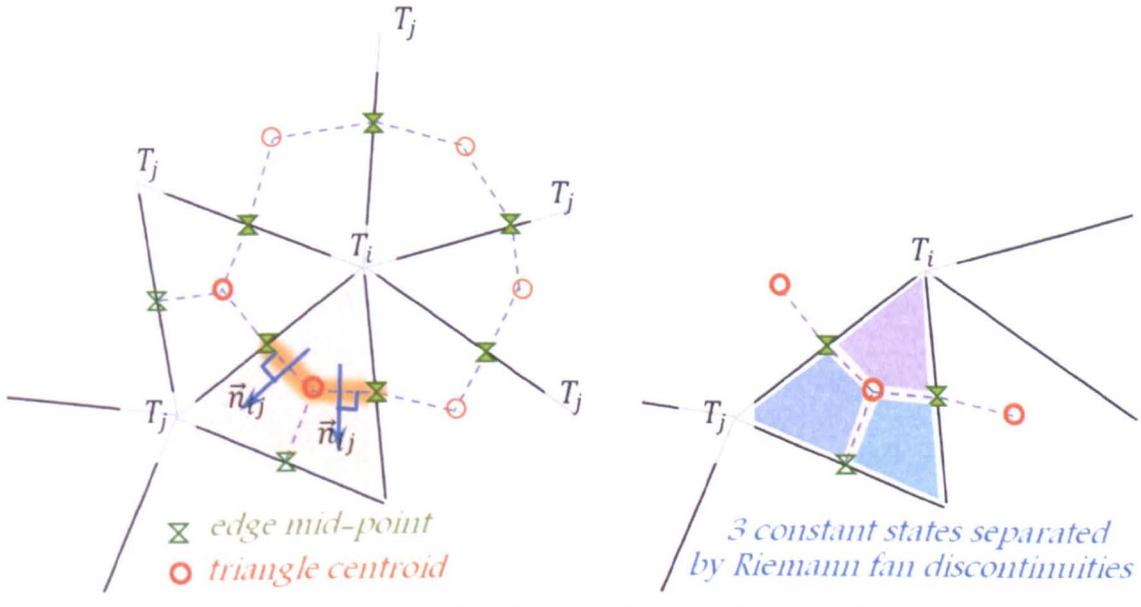

Figure 3.20 – BCT-scheme, Control volume and through fluxes definition

The Riemann fan discontinuities are defined at the mid-edge joining the centroid (in orange) with an edge mid-point (in green). That is defining 3 fluxes perpendicularly through the 3 mid-edges within each triangular element (see Figure 3.20) between 3 constant states within each triangle (in blue, turquoise, purple).

It is worth highlighting that, contrary to the generalisation proposed by Kurganov and Petrovna and also used by others as highlighted above, the BCT-scheme computes fluxes within each element independently of its neighbours. As a consequence, the scheme leads straightforward to parallelism whereby the computation of fluxes connects two nodes within one element rather than two neighbouring elements, which could be done on different processors. Moreover, the exchange of information (inter-processor communication) between neighbouring elements is reduced. The scheme is well suited to wetting and drying interfaces for which elements (as opposed to nodes) are either declared wet (part of the domain) or dry (removed from the domain). Further, the BCT-scheme makes use of the finite element assembling methodology and of its associated algebra regardless of whether or not the product matrix-vector are computed in assembled form. That goal to retain the stencil definition of a finite element solver and all of its features has been achieved.

As a generalisation of the KP- scheme (see Eq. (3.22)) and making use of the Gauss divergence theorem, the BCT-scheme is written as follows:

$$V_i^{n+1}u_i^{n+1} = V_i^n u_i^n - \Delta t.\sum_j H_{ij} \tag{3.24}$$

where the sum Σ_j corresponds to the finite element assembly and the flux is given by:

$$H_{ij} := \frac{\Gamma_{ijc}}{a_{ij}^{>}-a_{ij}^{<}} < \vec{n}_{ij} \mid a_{ij}^{<} f(u_{ij}^{>}) + a_{ij}^{>} f(u_{ij}^{<}) > -\frac{\Gamma_{ijc}.a_{ij}^{>}a_{ij}^{<}}{a_{ij}^{>}-a_{ij}^{<}}(u_{ij}^{>} - u_{ij}^{<}),$$

with $f(.)$ the flux function of the principal variable u, with V_i the volume around the i^{th} vertex, with $\vec{n}_{ij}$ the normal vector to the mid-edge used to project the flux

term perpendicularly to the mid-edge and Γ_{ijc} the surface area of the mid-edge, and all other quantities defined previously.

The BCT-scheme has been implemented in the open TELEMAC system (2007). For comparison purposes, reference to available schemes based on the open TELEMAC system will be prefixed by "oTM", a notation that is used by developers of the system.

Ch.3-2.4. 2D linear laws, comparisons with 1D profiles

For 2D linear laws, the flux function $f(.)$ reduces to $(u_i T_i)$, where u_i represents the advective velocity field and T_i the principal variable replacing the variable u_i in Eq. (3.24). In that case, the BCT-scheme becomes:

$$V_i^{n+1} T_i^{n+1} = V_i^n T_i^n - \Delta t . \sum_j H_{ij} \tag{3.25}$$

where the flux is given by:

$$H_{ij} := \frac{\Gamma_{ij}}{a_{ij}^{>} - a_{ij}^{<}} < \vec{n}_{ij} \mid a_{ij}^{>} (uT)_{ij}^{<} - a_{ij}^{<} (uT)_{ij}^{>} > \; + \; \frac{\Gamma_{ij}}{a_{ij}^{>} - a_{ij}^{<}} a_{ij}^{<} a_{ij}^{>} \left(T_{ij}^{>} - T_{ij}^{<} \right)$$

and where the right and left values are approximated by (for example for the tracer):

$$T_{ij}^{>} = T_j - (T_j)' = T_j - l_{jc}(\Delta T_j) \text{ and } T_{ij}^{<} = T_i + (T_i)' = T_i + l_{ic}(\Delta T_i)$$

with l_{jc} (and l_{ic}) the distances between node j and the centre of the mid-edge joining the centroid with the ij-edge mid-point (see Figure 3.20), and all other quantities defined previously.

In order to conform to the finite element convention, the node-centric formulation of Eq. (3.25) is rewritten to group the contribution one edge (of one element) has on the pair of nodes to which it is connected. The flux is:

$$H_{ij} := \frac{\Gamma_{ij}}{a_{ij}^{>} - a_{ij}^{<}} \left[a_{ij}^{>} (< \vec{n}_{ij} \mid u_{ij}^{<} > - a_{ij}^{<}) \, T_{ij}^{<} \; - \; a_{ij}^{<} (< \vec{n}_{ij} \mid u_{ij}^{<} > - a_{ij}^{>}) \, T_{ij}^{>} \right]$$

Replacing $T_{ij}^{>}$ and $T_{ij}^{<}$, the flux becomes:

$$
\begin{aligned}
H_{ij} := T_i & \left[\frac{\Gamma_{ij}}{a_{ij}^{>}-a_{ij}^{<}} a_{ij}^{>}(<\vec{n}_{ij} \mid u_{ij}^{<}> -a_{ij}^{<})\right] \\
& - T_j \left[\frac{\Gamma_{ij}}{a_{ij}^{>}-a_{ij}^{<}} a_{ij}^{<}(<\vec{n}_{ij} \mid u_{ij}^{<}> -a_{ij}^{>})\right] \\
& + l_{ic}\nabla T_i \left[\frac{\Gamma_{ij}}{a_{ij}^{>}-a_{ij}^{<}} a_{ij}^{>}(<\vec{n}_{ij} \mid u_{ij}^{<}> -a_{ij}^{<})\right] \\
& - l_{jc}\nabla T_j \left[\frac{\Gamma_{ij}}{a_{ij}^{>}-a_{ij}^{<}} a_{ij}^{<}(<\vec{n}_{ij} \mid u_{ij}^{<}> -a_{ij}^{>})\right]
\end{aligned}
\tag{3.26}
$$

For verification purposes, a 2D unstructured triangular mesh was set up to represent a flume under uniform and constant discharge. This follows from the cases developed for the 1D linear laws (see Section Ch.3-2.2).

The graphical user interface and freeware Blue Kenue (2011) was used to generate the mesh and all other meshes used throughout the thesis. The mesh generator within Blue Kenue was developed by the Canadian Hydraulics Centre under the leadership and supervision of the author of this thesis. The mesh generation relies on an advancing front method, starting from known geometrical objects (model boundary, constrained lines, hard points), following an underlying user-defined map of maximum triangle edge lengths. The modelled domain is gradually filled in with nodes (vertices of the triangles) placed according to a sorting algorithm from the location of the smallest edge length to the largest. A user-defined maximum edge length growth criterion caps the variability (smoothness) of the mesh density as the advancing front progresses. A Delaunay triangulation completes the process.

The 2D model is constituted of 70,688 elements covering an area of length 2 m by width 0.1 m. This is equivalent to about 1,200 representative cells in the streamwise direction, which is 50% larger than the number of cells used for the 1D case. Similarly to the 1D case, the transport speed c is set to 0.5 m/s and four types of initial solution profiles are used. Figure 3.21 shows a schematic plan view of the model set up (bottom inset) together with the detail of part of the unstructured mesh (top inset). It is noted

that even though the domain is rectangle, the mesh is not necessarily regular everywhere.

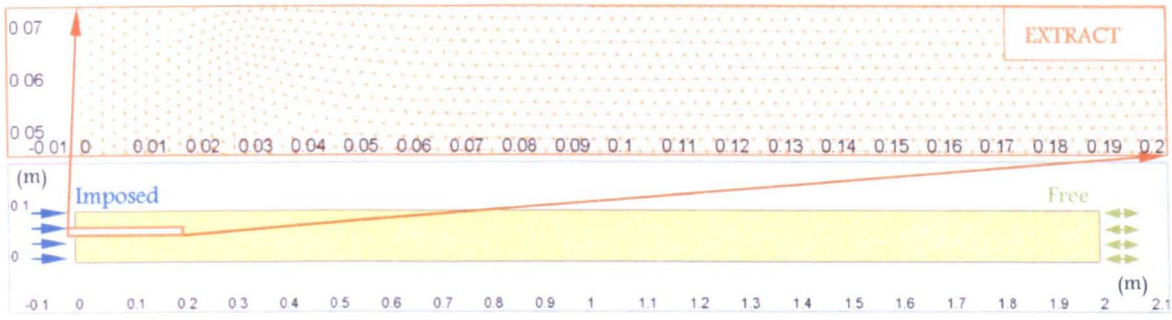

Figure 3.21 – 2D advection of tracer profile, Plan view of model characteristics

The tracer concentration is imposed on the left of the domain (a Dirichlet condition at the inflow) and let free on the right (a Neumann condition at the outflow).

Figure 3.22 shows the numerical solution obtained with the BCT-scheme on the 2D unstructured mesh, compared with its 1D equivalent, the solution of the KP-scheme.

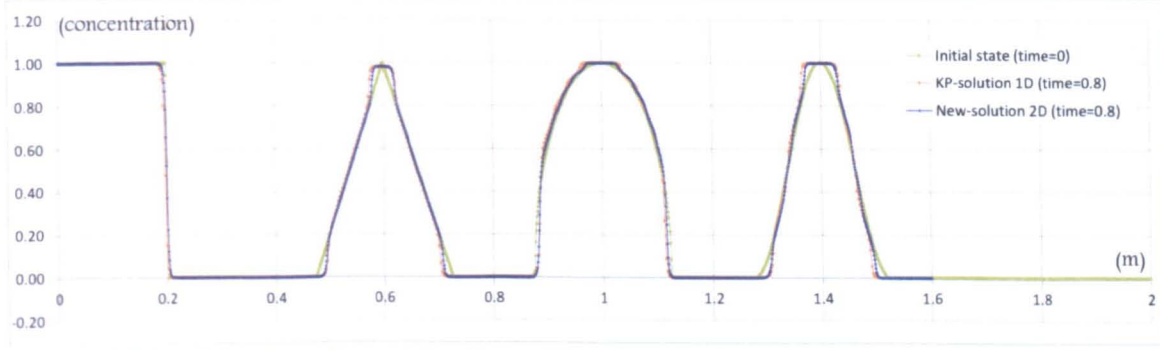

Figure 3.22 – 2D advection of tracer profile, Comparison with 1D equivalent

The results of the 2D solution are very similar to the 1D solution, except that the 2D is only slightly more diffusive. This is to be expected given the nature of the elements of the unstructured mesh as opposed to regular 1D segments. Even so, the BCT-scheme is an appropriate extension of the KP-scheme with similar behaviour.

Figure 3.23 shows a comparison of the BCT-scheme with the available schemes of the open TELEMAC system considered, in particular oTM-schemes 1 and 5 as defined by Hervouet (2007). It is noted that oTM-scheme 2 is highly oscillatory and unstable

under these conditions. It is not presented here for this reason. It is also noted that oTM-scheme 3 and 5 are similar in the case of tracer advection. Therefore only oTM-scheme 5 will be presented.

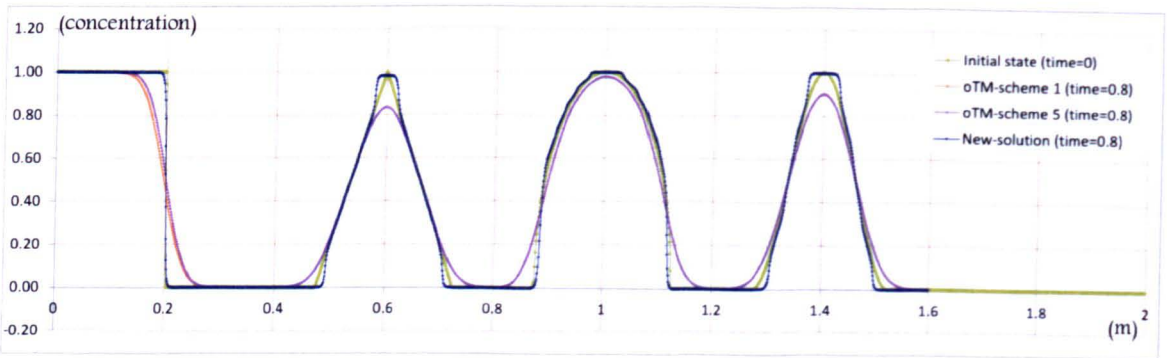

Figure 3.23 – 2D advection of tracer profile, Comparison with TELEMAC schemes

Table 4 summarises the error for each scheme between the computed and the analytical solutions. The norm L2 is here used for the error computed over the whole length of the model; L2 is defined as the sum of the square of the difference between a given solution and the corresponding analytical solution. The error for the 1D solution of the KP-scheme is also presented.

Scheme	Norm L_2 (domain)	Norm L_2 (profile (a))	Norm L_2 (profile (b))	Norm L_2 (profile (c))	Norm L_2 (profile (d))
KP-scheme (1D)	1.51	0.30	0.28	0.57	0.36
BCT-scheme (2D)	2.03	0.43	0.38	0.82	0.41
oTM-scheme 1 (2D)	10.12	6.40	0.75	1.96	1.00
oTM-scheme 5 (2D)	9.40	5.69	0.75	1.96	1.00

Table 4 - 2D advection of tracer profile, Comparison of norm L2 errors

It is clear that the BCT-scheme is less diffusive than the other available schemes considered in the open TELEMAC system, particularly around the discontinuity of profile (a).

Ch.3-2.5. 2D linear laws, implicitness and linear algebra

Having verified the explicit form of the BCT-scheme, an implicitness factor is introduced by replacing the linear term in T_i in the flux term H_{ij} of Eq. (3.26) by its semi-implicit equivalent $\theta T_i^{n+1} + (1-\theta)T_i^n$. As mentioned previously, one of the goals of the present work is to retain the stencil definition of a finite element solver. By extension, the implementation of the BCT-scheme is to conform to the following linear algebra of the open TELEMAC system as described by Hervouet (2007):

$$(I - \Delta t.A) \cdot T^{n+1} = T^n + \Delta t.(b + c) \tag{3.27}$$

where I is the identity matrix the size of the diagonal of which is also the number of point in the domain, A is the matrix representing all implicit terms for a given scheme (advection, diffusion, sinks, outflows and other implicit external forcing), and the vectors b and c represent all explicit terms for a given scheme (advection, diffusion, sources, inflows and other explicit external forcing) with b those terms in T^n and c those terms in ∇T^n, and all other quantities defined previously.

Introducing the implicitness factor θ in Eq. (3.26) , the flux rewrites:

$$\begin{aligned} H_{ij} := & \left(\theta T_i^{n+1} + (1-\theta)T_i^n\right)\left[\frac{\Gamma_{ij}}{a_{ij}^{>}-a_{ij}^{<}} a_{ij}^{>}(<\vec{n}_{ij} \mid u_{ij}^{<}> - a_{ij}^{<})\right] \\ & - \left(\theta T_j^{n+1} + (1-\theta)T_j^n\right)\left[\frac{\Gamma_{ij}}{a_{ij}^{>}-a_{ij}^{<}} a_{ij}^{<}(<\vec{n}_{ij} \mid u_{ij}^{<}> - a_{ij}^{>})\right] \\ & + l_{ic}\,\nabla T_i^n \left[\frac{\Gamma_{ij}}{a_{ij}^{>}-a_{ij}^{<}} a_{ij}^{>}(<\vec{n}_{ij} \mid u_{ij}^{<}> - a_{ij}^{<})\right] \\ & - l_{jc}\,\nabla T_j^n \left[\frac{\Gamma_{ij}}{a_{ij}^{>}-a_{ij}^{<}} a_{ij}^{<}(<\vec{n}_{ij} \mid u_{ij}^{<}> - a_{ij}^{>})\right] \end{aligned}$$

which leads to the details of the terms of Eq. (3.27):

$$\begin{aligned} A_{ii} &= \theta\left[\frac{\Gamma_{ij}}{a_{ij}^{>}-a_{ij}^{<}} a_{ij}^{>}(<\vec{n}_{ij} \mid u_{ij}^{<}> - a_{ij}^{<})\right] \\ A_{ij} &= -\theta\left[\frac{\Gamma_{ij}}{a_{ij}^{>}-a_{ij}^{<}} a_{ij}^{<}(<\vec{n}_{ij} \mid u_{ij}^{<}> - a_{ij}^{>})\right] \\ b_i &= (1-\theta)T_i^n\left[\frac{\Gamma_{ij}}{a_{ij}^{>}-a_{ij}^{<}} a_{ij}^{<}(<\vec{n}_{ij} \mid u_{ij}^{<}> - a_{ij}^{>})\right] \\ b_j &= -(1-\theta)T_j^n\left[\frac{\Gamma_{ij}}{a_{ij}^{>}-a_{ij}^{<}} a_{ij}^{<}(<\vec{n}_{ij} \mid u_{ij}^{<}> - a_{ij}^{>})\right] \end{aligned} \tag{3.28}$$

$$c_i = l_{ic}\,\nabla T_i^n \left[\frac{\Gamma_{ij}}{a_{ij}^{>}-a_{ij}^{<}}\,a_{ij}^{>}(<\vec{n}_{ij}\mid u_{ij}^{<}> - a_{ij}^{<})\right] - l_{jc}\,\nabla T_j^n \left[\frac{\Gamma_{ij}}{a_{ij}^{>}-a_{ij}^{<}}\,a_{ij}^{<}(<\vec{n}_{ij}\mid u_{ij}^{<}> - a_{ij}^{>})\right]$$

where all quantities are defined previously.

For reference, the open TELEMAC system includes a number of linear algebra matrix solvers including various forms of the conjugate gradient (including the double conjugate gradient, the conjugate gradient stabilised) and of the generalised minimum residual method. Hervouet (2013) provides a detailed and exhaustive description of all iterative solvers implemented in the open TELEMAC system. The so-called conjugate gradient with normal equation was used to produce the outputs shown in this thesis.

While the implementation of the numerical fluxes defining the BCT-scheme follows the framework of Eq. (3.27) , it is noted that the resulting terms of Eq. (3.28) are node-centric. They represent contributions that neighbours j would have on an arbitrary node i (see Figure 3.20). However, the algebraic matrix and vector terms are not assembled but rather defined by element (see Section B.2 in Appendix B). The linear algebra of the open TELEMAC system (including its iterative and direct solvers) is implemented on that basis.

The BCT-scheme follows the framework of Eq. (3.27) as well as the implementation by element in a non-assembled form. For an arbitrary triangular element of node numbers i, j, and k, the implementation loops over the 3 pairs of nodes, ij, jk and ki, filling in the non-assembled a 3x3 matrix terms A_{ii}, A_{ij}, A_{ji} and A_{jj} and the permutations with jk and ki. A similar permutation is also used for the vectors b and c.

Ch.3-2.6. Boundary conditions, implicit differentiation

As introduced previously (see Section Ch.3-2.3) the BCT-scheme computes 3 fluxes within each triangular element between each pair of nodes through the mid-edges (orange mid-edges and blue normal vectors on Figure 3.24). Contrary to most finite volume solvers such as revisited by Toro in the 3rd edition of his book (2009), the BCT-scheme does not compute fluxes across the edges of the element.

However, there is one exception. In order to allow for boundary fluxes through the edges of the domain, two additional flux terms are computed, independently of the internal fluxes. Figure 3.24 highlights in orange an arbitrary element ijk for which the edge jk in green (normal vectors $\vec{n}_{jjk}$ and $\vec{n}_{jkk}$ in red) is also an edge of the model domain.

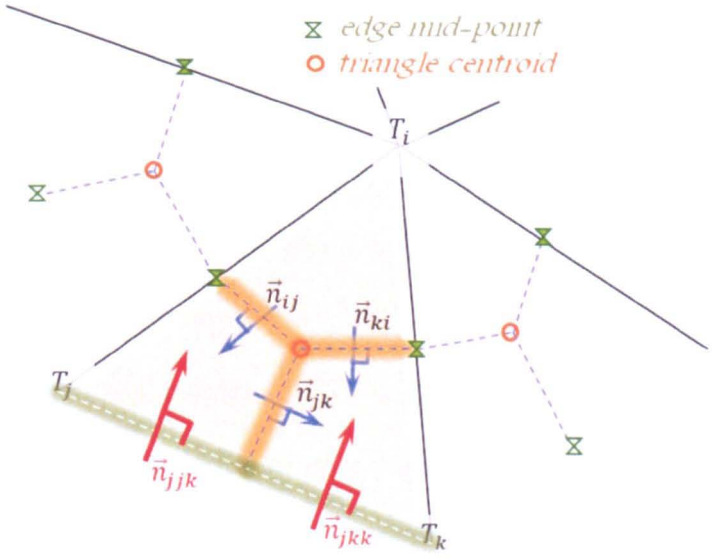

Figure 3.24 – BCT-scheme, Additional boundary flux term

In the context of an implicit framework, boundary fluxes can be categorised in two classes:

(a) When the flow through a boundary edge is incoming, the tracer concentration is imposed. The advective flux terms are explicit and contribute to the vector b of Eq. (3.27); and

(b) When the flow through a boundary edge is outgoing, the tracer concentration leaving the domain is given by the concentration inside the domain, which varies with time. The advective flux terms are therefore implicit and contribute to the diagonal of the matrix term A of Eq. (3.27).

It is noted that in the absence of a linear algebraic system, it is difficult for explicit solvers to remove the correct amount of tracer on outgoing flows.

Ch.3-2.7. Sources and sinks, implicit differentiation

In the context of an implicit framework, sources and sinks are similar to incoming and outgoing boundary fluxes respectively:

(a) When a source is used to discharge water to the domain, the tracer concentration is imposed. The source is explicit and contributes to the vector b of Eq. (3.27), even though it is acting on a node and not computed as an advective flux; and

(b) When a sink is used to withdraw water from the domain, the tracer concentration leaving the domain is given by the concentration inside the domain, which varies with time. The sink is therefore implicit and contributes to the diagonal of the matrix term A of Eq. (3.27), even though it is acting on a node and not computed as an advective flux.

Similarly to outgoing boundary conditions, it is noted that it is difficult for explicit solvers to remove the correct amount of tracer on withdrawn flows.

Ch.3-2.8. Generalisation of the BCT-scheme to layered meshes

Similarly to many 3D solvers such as ELCOM, MICOM, MOM, POM, ROMS, UnTRIM, ELCIRC, etc. (see Chapter 2 and Appendix B), the vertical structure of the 3D domain of the open TELEMAC system is based on a sigma-stretched transformation, where the 2D mesh is extruded vertically into a volume between the surface defining the bottom of the model and the surface defining the water free surface (see Figure 1.1 in Ch.1-1.3). Each surface is supported by 2D unstructured mesh; all surfaces are stacked one above the other and project to the same 2D unstructured mesh; each layer is made of prism elements. It is noted that the 3D element are wedges rather, and that the name only comes from the 3D finite element method computed on a prism.

For reference in the rest of the thesis, $NPOIN2$ is the number of vertices in the 2D mesh and $NELEM2$ is the number of triangular elements. The total number of surfaces is $NPLAN$, including the bottom plan P_1 and the surface plan P_{NPLAN}.

By extension of the work in 2D (see Section Ch.3-2.3), the BCT-scheme defines a control volume around an arbitrary node by summing up the contributions of every element connected to that node, element by element, again mimicking the finite element assembling methodology. The contribution of one element to the control volume around builds on the base of the 2D element and joins vertically the node with the middle of the connecting edges above and below that element (see Figure 3.25).

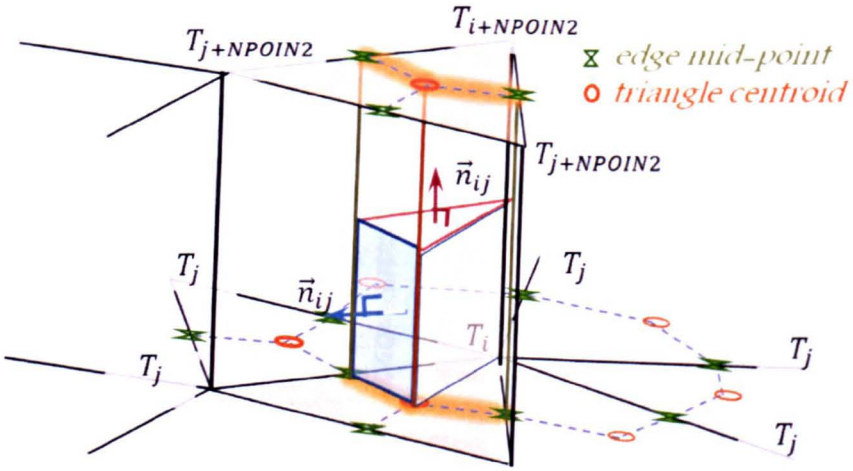

Figure 3.25 – BCT-scheme, Control volume and through fluxes definition

The Riemann fan discontinuities are defined through the vertical trapezoidal surface (in blue) based on the mid-edge joining the centroid (in orange) with an edge mid-point (in green) and through the triangle (in red) midway between the two surfaces. That is defining 9 fluxes perpendicularly through the 6 vertical faces and 3 plan faces within each prism element (see Figure 3.25).

With this, the BCT-scheme in 3D space is computed as a combination of its 2D version for the horizontal fluxes and the KL-scheme for the 1D vertical fluxes. In 2D, the scheme is defined by Eq. (3.24), where the computation of the fluxes through the vertical trapezoidal surface Γ_{ijc} as a function of the water depth is replaced by the same computation but restricted to the half the thickness of a layer (in blue on Figure 3.25). In 1D the scheme is defined by defined by Eq. (3.22), where the computation of the fluxes at the mid-point of the connecting edge is replaced by a computation of fluxes through the triangular element (in red on Figure 3.25) where all vertices are placed on the same verticals. The 2D definition of the scheme through Eq. (3.24) remains valid in 3D.

Again, it is worth highlighting that, contrary to what is being considered by other authors of 3D solvers such as ELCOM, MICOM, MOM, POM, ROMS, UnTRIM, ELCIRC, etc. (see Chapter 2 and Appendix B), the BCT-scheme computes fluxes within each

prism element independently of its neighbours. Similarly to the its 2D version and for the same reasons, the scheme leads straightforward to parallelism while being also well suited to wetting and drying interfaces for which columns of prism elements (as opposed to columns of nodes) are either declared wet (part of the domain) or dry (removed from the domain). Finally, the 3D version of the BCT-scheme also keeps on making use of the finite element assembling methodology and of its associated algebra regardless of whether or not the product matrix-vector are computed in assembled form. The goal to retain the stencil definition of a finite element solver in 3D and all of its features has been achieved.

The BCT-scheme has been implemented for the 3D linear laws in the open TELEMAC system following an extension to 3D prism elements of the algebra described through Eq. (3.27) and Eq. (3.28) in a non-assembled form, to which vertical fluxes are added to the sum of all contributions to a node.

Ch.3-2.9. Generalisation of the BCT-scheme to moving meshes

An important point of the sigma-stretched transformation is that the vertical placement of the surfaces (or the thickness of the layers) is a function of time and of the physical problem. Whether in the form of velocity shear layers or rapid changes in saline or thermal stratifications, thin layers with large gradients form an important part of many hydrodynamic processes. Providing a finer resolution vertically in area of strong tracer gradients is necessary to identify and refine around such gradients.

At this point it is noted that the physical vertical velocity component of the fluid is independent of the vertical movement of the surfaces, although the vertical placement of the top surface plan P_{NPLAN} results of the conservation of the fluid in the water

column.

The principal idea of the generalisation of the BCT-scheme to vertically moving meshes is to consider the advective velocity as the sum of the physical velocity and the local velocity of the mesh. Both the flux function $f(.)$ and the local speeds $a_{ij}^{<}$ and $a_{ij}^{>}$ bounding the Riemann fan on the right and on the left respectively are modified accordingly. With these definitions, the semi-discrete formulation of the KL-scheme Eq. (3.22) remains unchanged.

It is noted that the principles of the developments made to generalise the BCT-scheme to 1D moving meshes are also applicable to 2D unstructured moving meshes. A prototype solver of the rotating profile forms (see Section Ch.4-1) has been implemented for which the tracer profile forms and the hydrodynamics remain still while the unstructured mesh is rotating. Just as is done vertically, there is indeed a duality between fluid passing through a surface and a surface passing through a fluid. The implement of the prototype was carried out to gain additional understanding of the scheme by C.J. Cawthorn under the lead of the author of the present work.

For validation purpose, the following 3 cases illustrate the correctness of the vertical implementation of the BCT-scheme with respect to the relative movement of the surfaces with respect to both physical changes (sources and sinks introduced in the water column, for instance) and surface position changes (arbitrary mesh movement). The principal objective is to validate the computation of the fluxes by looking at the conservation of the mass of an arbitrary tracer.

Figure 3.26 illustrates an example of a 12-meter deep water column, constituted of $NPLAN = 7$ non-equidistant horizontal surfaces, based on a 2D mesh of $NELEM2 = 6$ non-equilateral triangles. While the 2D mesh remains unchanged throughout the series of cases, the property of the surfaces (horizontal or at an angle) their numbers

and their relative positions vary, the position of the top surface resulting from the continuity equation. An arbitrary intermediate plan (in red) is used to drive the movement of the surfaces, assuming standard sigma-stretched transformation above and below that intermediate surface.

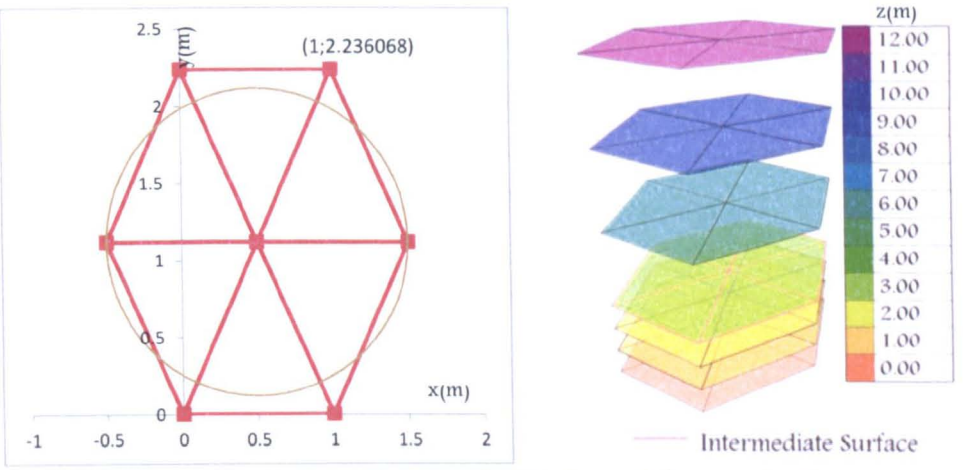

Figure 3.26 – 3D column of water, Validation of the vertically moving mesh

Several other cases were also set up within the same water column to verify further the combination of other physical aspects such as wind, hydrostatic or non-hydrostatics assumptions. These do not bring more to the demonstration for the present work and are not presented but augment the number of validation cases available for the open source distribution of the TELEMAC system.

Case 1: Hydrodynamics at rest, vertical mesh advection

In the first case, the surfaces remain horizontal and the water remains still (no hydrodynamics). The vertical position of the intermediate surface P_4 is set to evolve between 3 m and 9 m following: $z_{P_4} = 3 * (1 + 2\,sin^2(\pi t/100))$, where t is the current time in seconds and z_{P_4} is the elevation of all vertices of the intermediate surface P_4. The model mesh comes back to its original position after 100 seconds. The model time step is 1 second.

Figure 3.27 shows 5 vertical cross sections along the y-axis through the water column, each captured at a different time. The positions of the 7 surfaces at the corresponding time are highlighted in colour and in particular the position of the intermediate surface (dashed line) driving the vertical movement of the mesh.

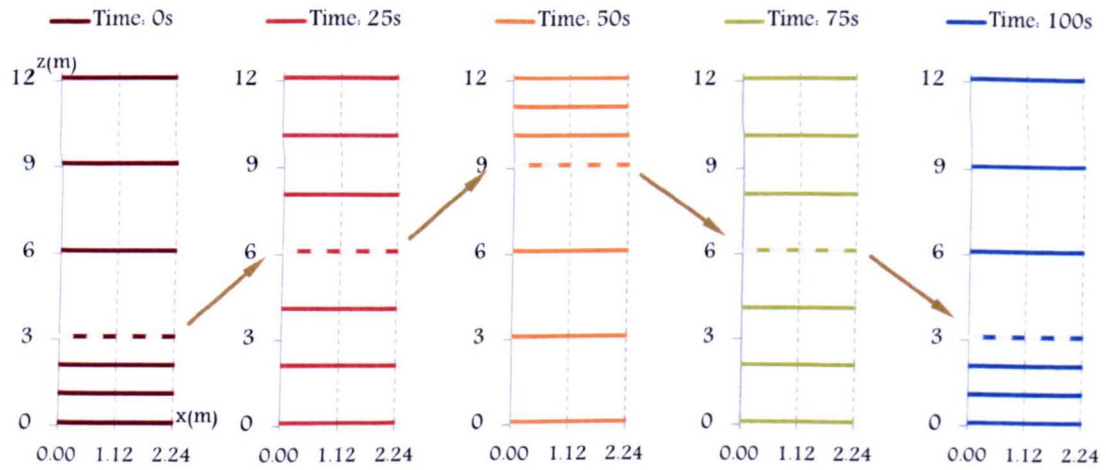

Figure 3.27 – Case 1, hydrodynamics at rest, vertical advection of the mesh

The integration of the mass of tracer within the water column shows that the model conserves mass exactly. The computation of the fluxes as the mesh moves vertically independently of the hydrodynamics is correct.

Case 2: Hydrodynamics at rest, angled mesh advection

In the second case, both the vertical position and the angle of the surfaces evolve with time, while the water remains still (no hydrodynamics). The vertical position of the intermediate surface P_4 is set to follow:

$$z_{P_4} = 3 * (1 + 2\,sin^2(\pi t/100)) + 2 * (x - 0.5) * sin(\pi t/100)$$

where x is the abscissa of the vertices on the intermediate surface P_4, and all other quantities defined previously. The model mesh comes back to its original position after 100 seconds. The model time step is 1 second.

Similarly to the previous case, Figure 3.28 shows 5 vertical cross sections along the y-axis through the water column, each captured at a different time. The position of the intermediate surface (dashed line) highlights the angle driving the vertical movement of the mesh.

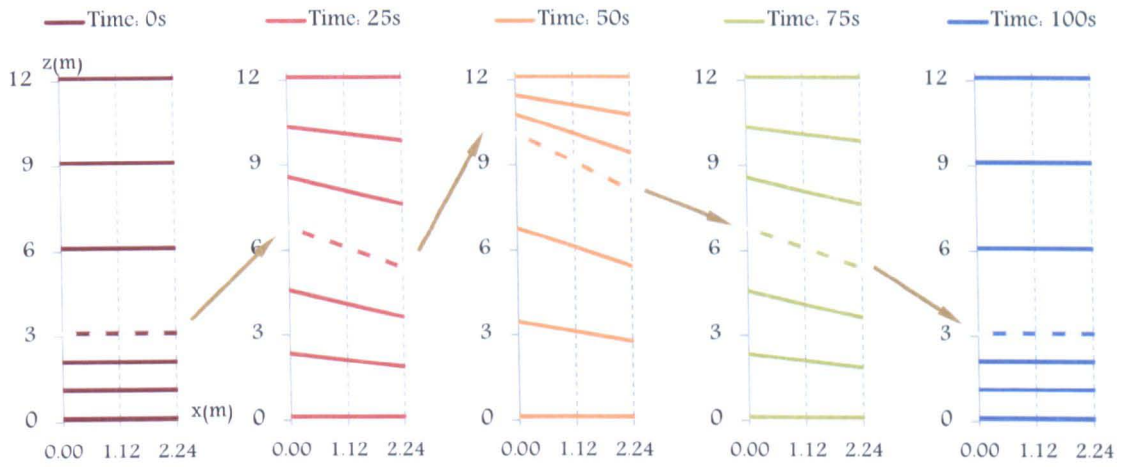

Figure 3.28 – Case 2, hydrodynamics at rest, angled mesh advection

Again, the model conserves mass exactly. The correctness of the computation of the fluxes has been verified even though the fluxes are projected on the non-horizontal mid-way triangles (in red on Figure 3.25) as the mesh moves vertically.

Case 3: Balanced sets of sources and sinks

In the third case, the hydrodynamics is varying within the water column, driven by a balance of sources (at the bottom) and sinks (at the top) in order to prevent movements in the vertical position of the surfaces. The total discharge exchanged between the sources and sinks is 1.8 m^3/s. The model time step is 1 second. The model stabilise around steady state with a few time steps.

Figure 3.29 shows the one cross section along the y-axis through the water column with the fixed positions of the surfaces (in orange).

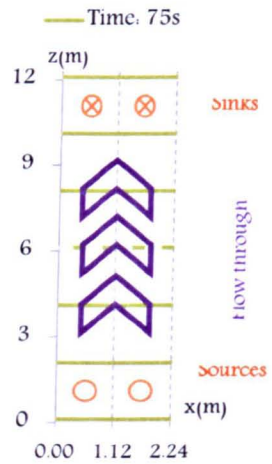

Figure 3.29 – Case 3, Balanced sets of sources and sinks

For this case also, the model conserves mass exactly. The computation of the fluxes as the mesh remains still and the hydrodynamics of the vertical flows through the water column is correct.

Ch.3-2.10. The adaptive mesh displacement method

As discussed previously (see SectionCh.3-2.1), the KL-scheme in 1D, applied to the vertical tracer profile, maintains sharp gradients of tracer and converges rapidly towards the analytical solution when the grid resolution increases. With the generalisation of the BCT-scheme to vertically moving meshes (see Section Ch.3-2.9), it becomes only natural to use the latter feature in an attempt to provide the BCT-scheme with an increased resolution around high gradients without any additional computation cost. The principal idea of the method is here to automate the displacement of nodes within one water column so it adapts to high gradients.

It should be acknowledged that while the following method and its improvements were designed by the author of the present work, it was prototyped in TELEMAC by Dr C.J. Cawthorn under the author's line management at the time. The final verified

version of the code was later completed by the author and parallelised for final release of TELEMAC in collaboration with J.-M. Hervouet at Électricité de France.

The adaptive mesh displacement (AMD) method was designed to move the intermediate surfaces based on certain aspects of the local solution profile, whether the profile relates to a tracer profile or a velocity shear profile, or a combination of several profiles, for instance.

The implementation of the AMD method was eventually refined according to the "variational formulation" of Winslow (1966) further explained by Tang and Tang (2003). The principles of the formulation consist in finding the map $Z(\xi)$ that minimises a function of the form:

$$E[Z(\xi)] = \int \omega(Z(\xi)) \left|\frac{\partial Z(\xi)}{\partial \xi}\right|^2 d\xi, \tag{3.29}$$

where $0 \leq \xi \leq 1$, and the elevation of the bottom and the free surface are $z_1 = Z(0)$ and $z_{NPLAN} = Z(1)$ respectively, and where the *monitor function* $\omega(z)$ is positive definite function that can typically take the form, for instance,

$$\omega(z) = \sqrt{1 + \lambda \frac{(df/dz)^2}{max(df/dz)^2}}$$

where λ is a tuning parameter and f the tracer profile, and where the maximum runs over the nodes on each water column.

It is noted that the normalisation of the function derivative of the monitor function prevent very large solution gradients in one part of the 3D mesh to affect the mesh layering in another region with smaller (yet still significant) gradient. The parameter λ can be tuned globally to increase or decrease the sensitivity of the intermediate surface position to the profile gradient.

From a numerical computation viewpoint, minimising the function $E[Z(\xi)]$ is equivalent to solving the 1D Laplace equation:

$$\frac{\partial}{\partial \xi}\left[\ \omega(Z(\xi))\ \frac{\partial Z}{\partial \xi}(\xi)\ \right], \tag{3.30}$$

where ξ takes $NPLAN$ distinct values for each water column at each time step, independently of its neighbouring water column, and where the resulting mesh placement is given by $Z(\xi)$.

The monitor function varies spatially and depends upon the profile of the conserved quantities. This makes it possible to attract nodes to regions of interest, such as where the profile has large gradients. For illustrative purposes, a 1D prototype of the AMD method was implemented prior to its application in TELEMAC. The prototype reads in a prescribed discretised along a 1D-grid, $(Z_i)^{(0)}_{i=1,NPLAN}$, and a tracer profile f interpolated on that 1D-grid, and displaces each node to produce a varying 1D-grid $(Z_i)^{(1)}_{i=1,NPLAN}$ according to the monitor function $\omega(z)$ of Eq. (3.29). The profile is then iteratively re-interpolated on the modified 1D-grid. Figure 3.30, shows, for instance, the final results of the vertical placement of each node with $\lambda = 50$, depending on the initial profile. The initial profile is here chosen as $T(z) = tanh\left[\alpha\left(z - \frac{1}{2}\right)\right]$ with various values for α shown in purple.

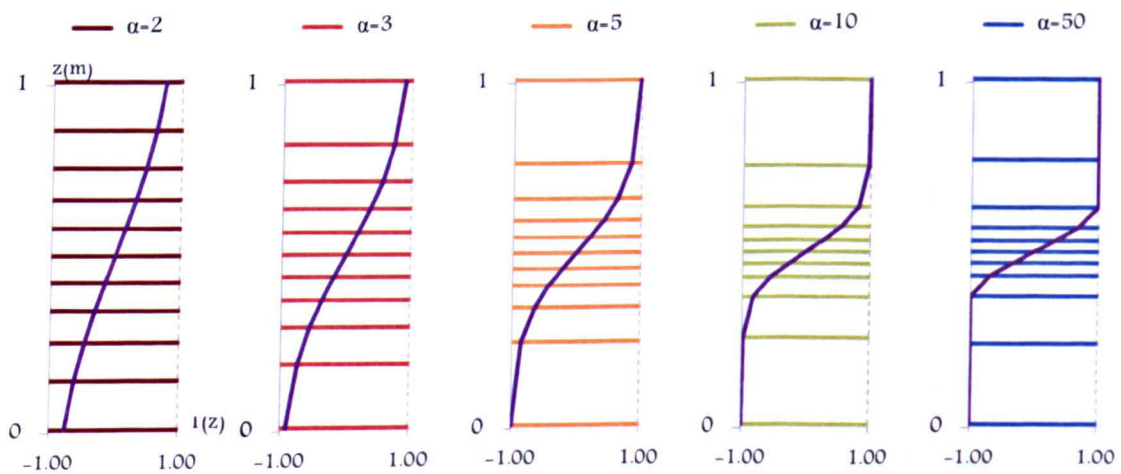

Figure 3.30 – AMD method, refinement around a hyperbolic tangent profile

The test demonstrate that the AMD method is flexible regarding choice of both the tuning parameter and monitor function and can adapt to and track sharp gradients.

It is observed that exaggeration in the variability of the mesh could lower the order of accuracy of the solution. The reader is referred to the analysis of Roache (1998), for a detailed discussion. Similarly the advection of the sharp gradient would also result in a lower order of accuracy in the vicinity of highest gradient. Therefore, the increased resolution produced by the AMD method remains beneficial.

Ch.3-2.11. Additional improvements to the AMD method

The presence of extrema in the profile within the water column (as opposed to at the free surface or at the bottom) locally results in low gradients, which in turn moves the intermediate surfaces away from these positions, which in turn changes the position and magnitude of the extrema resulting in a sort of numerical diffusion. In order to eliminate this problem, the positions of all local extrema are first identified in each water column and retained in the new distribution. As a result, no interpolation takes places at extrema and the solution magnitude there is not diminished.

In addition, the AMD method places nodes along the vertical independently of its horizontal neighbours (see Section Ch.3-2.10). In order to reduce the local steepness of the horizontal variations of intermediate surfaces between two neighbouring verticals, the monitor function is smoothed using a simple low-pass filter in two dimensions before solving the Laplace equation Eq. (3.30). The low pass filter simply consists of averaging the value of one node with half the value of its neighbouring nodes.

For illustrative purposes, consider a point source of tracer located at the bottom of a straight channel with rectangular cross-section with a constant flow in the absence of friction. The channel is 1 km long, 100 m wide and 10 m deep. A depth-averaged

velocity of 1 m/s is applied at the entrance of the channel. At the source, the tracer concentration is arbitrarily set to 215 units, discharged at a rate of 0.5 m^3/s. The steady state results of the following two test cases are considered:

- A standard vertical discretisation based on 21 horizontal surfaces, which in this case of a flat bottom and free surface can be associated either to a sigma-stretched transformation or a fixed horizontal layers.

  The top right inset of Figure 3.31 shows the concentration contours of the tracer in a vertical cross section along the xz-plane, through the middle of the channel. The 21 horizontal lines from the bottom of the channel at $z = -10$ m to the top of the channel at $z = 0$ m highlight the locations of the 21 surfaces in the 3D mesh. The top left inset also shows a vertical cross section but along the yz-plane, at $x = 250$ m. The bottom inset of Figure 3.31 shows a horizontal cross section along the xy-plane, through the bottom plane of the channel.

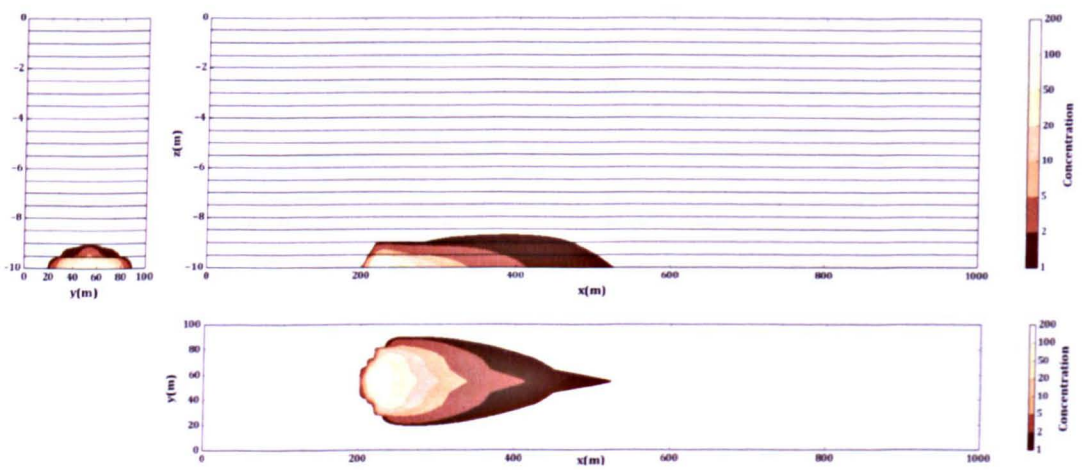

Figure 3.31 – Bottom source case, tracer concentration for 20 fixed layers

- Use of the AMD method based on only 11 surfaces, or half the number of layers

  Again, the top left and right insets of Figure 3.32 show the concentration contours in vertical cross-sections along the xz-plane and yz-plane respectively. The 11 curvatures of the mesh in the vicinity of the highest gradient of the concentration highlight the successful adaptation of the 3D mesh. The bottom inset of

Figure 3.32 shows the concentration contours in a horizontal cross section along the same xy-plane as in Figure 3.31.

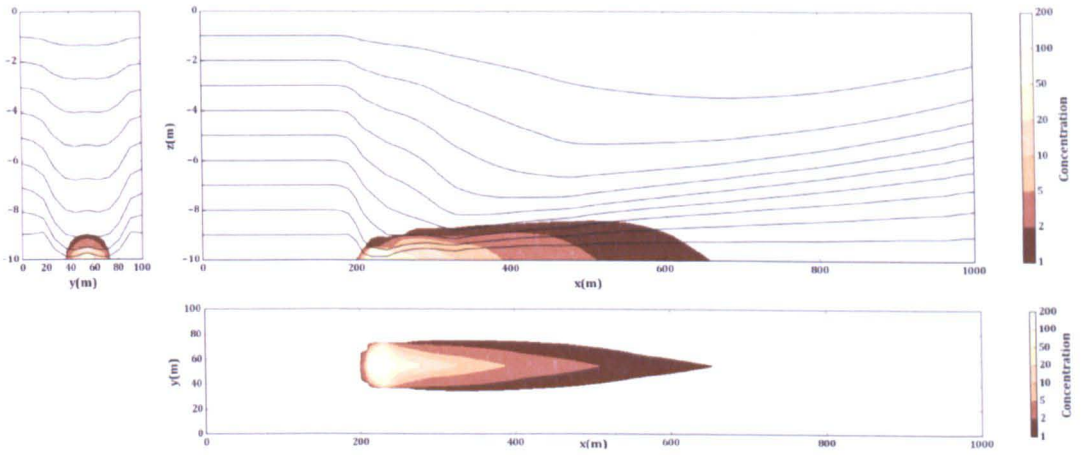

Figure 3.32 – Bottom source case, tracer concentration for AMD, 10 adapted layers

The top insets of Figure 3.32 show the effect of a 2D low-pass filter with a smooth transition between refined resolution near the region of maximum gradient and the coarser resolution used elsewhere.

A comparison of the vertical cross-sections (see top insets of Figure 3.31 and Figure 3.32) shows that the most concentrated part of the plume is resolved by further layers with the AMD method despites the model utilising half the overall number of surfaces. The increased resolution in the source region near the bottom gives the resulting plume a more rounded front than that predicted using a sigma-stretched transformation with 20 fixed layers. The rounded front is similar to that observed in analytical solutions based potential flow theory, as derived by Rutherford (1994), for instance, using the method of images superposing the solution of the equivalent unbounded dispersion problem.

A comparison of the horizontal cross-sections (see bottom insets of Figure 3.31 and Figure 3.32) shows that the horizontal extent of the tracer is strongly affected by the choice of layering strategy. In the case of the standard vertical discretisation (both

fixed horizontal layers or sigma-stretched transform), the volume discharged is vertically extended because of the thicker layering, resulting in a larger obstruction to the ambient flow forcing it around the plume. In the case of AMD, the volume discharge occupies a much smaller vertical extent, thus it has a reduced effect on the ambient flow.

Last but not least, the AMD method uses half the number of layers, and so is twice as fast computationally as the standard fixed grid sigma-stretched transformation. This particular aspect is a welcomed solution to seasonal / annual stratified flows modelling in environmental hydraulics.

Chapter 4 –
Analytical and experimental validation

This Chapter reports the tests used to evaluate the performance of certain numerical schemes against analytical solutions and to validate the models against published data in the scientific literature. Section Ch.4-1 presents the case of the 2D rotation of an initial tracer profile to demonstrate that the BCT-scheme is far less diffusive than the schemes currently available in TELEMAC. Section Ch.4-2 presents the case of the source and sink pair to show that the new approach to compute the dynamic pressure (see Section Ch.3-1.8) is valid. In stratified reservoirs, these source and sink are used to represent, for instance, de-stratification devices, such as bottom outlets, jet-circulations, or bubble diffusers. Finally, Section Ch.4-3 presents the lock exchange case highlighting the developing front of sharp stratification to show that the new method of mesh displacement produces far better results than current sigma stretched transformation method.

Ch.4-1. Tracer advection, 2D rotating profile forms

In Section Ch.3-2, the BCT-scheme has been applied to a problem that is essentially one dimensional for comparison with solutions of the KP-scheme. For further validation purposes, a similar problem of the advection of a tracer profile is presented, for which the BCT-scheme is applied to a rotating flow field and the results compared with available scheme in the open TELEMAC system (2007).

The 2D model is constituted of 67904 elements covering a circle of radius 20 m. Figure 4.1 shows a schematic plan view of the model set up (left inset) together with the detail of part of the unstructured mesh (right inset). It is noted that even though the domain is a circle, the mesh is not necessarily regular everywhere.

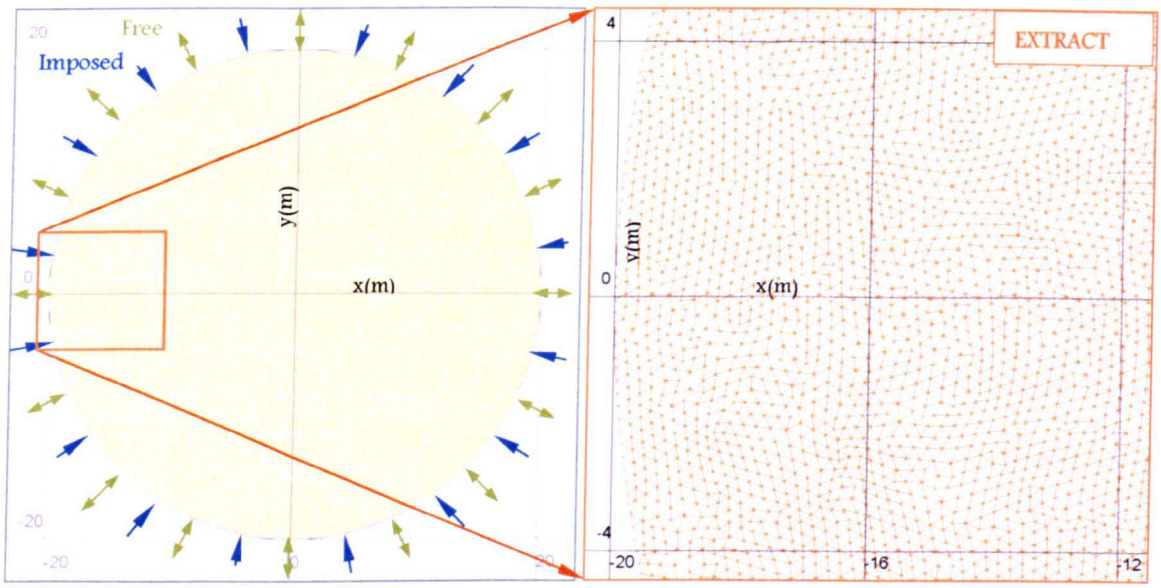

Figure 4.1 – Rotation of tracer profiles, Plan view of model characteristics

At the perimeter of the circle, the tracer concentration is either imposed explicitly (a Dirichlet condition) or let free implicitly (a Neumann condition) depending on whether the projection of the velocity vector on the mesh segment representing the circle (see Section Ch.3-2.6) is entering or exiting the circle. In this instance, the hydrodynamic rotational flow field was imposed stationary.

Two initial profiles are considered, a cone (linear variation of concentration) and a cylinder (discontinuous variation of concentration), each associated with a given tracer (Tracer 1 and 2 respectively). Figure 4.2 shows 2D plan views of the initial values for Tracer 1 (left) and Tracer 2 (right). The profiles are centred at 8 m from the centre of the disk.

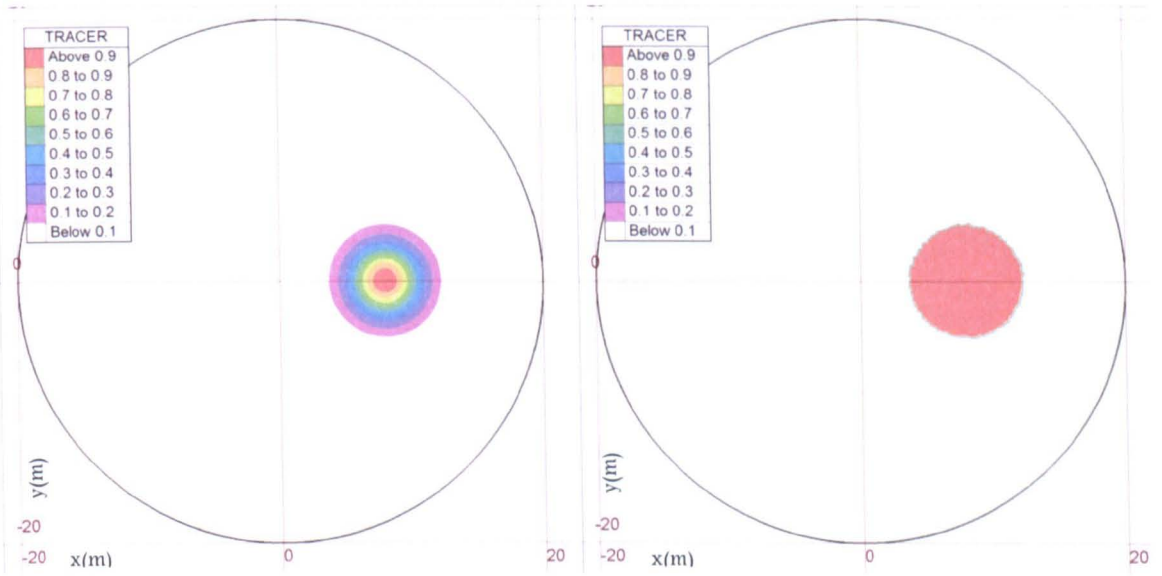

Figure 4.2 – Rotation of tracer profiles, Initial solution for Tracer 1 and 2

Cross sections transverses to the advection (along the radius) are used to evaluate the evolution of the tracer profile. Figure 4.3 and Figure 4.4 show Tracer 1 and Tracer 2 respectively, for a rotation of ¼ of the flow field, ½, ¾ and a full rotation of the flow field.

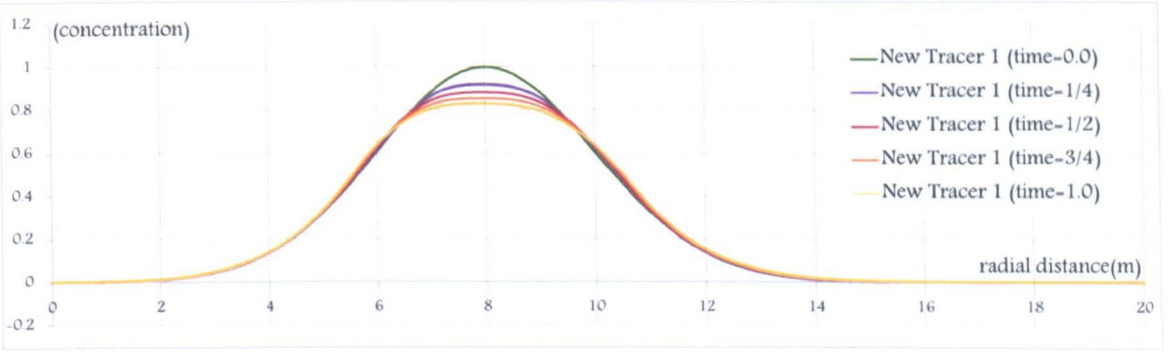

Figure 4.3 – Rotation of Tracer 1 profile, Evolution of the BCT-scheme

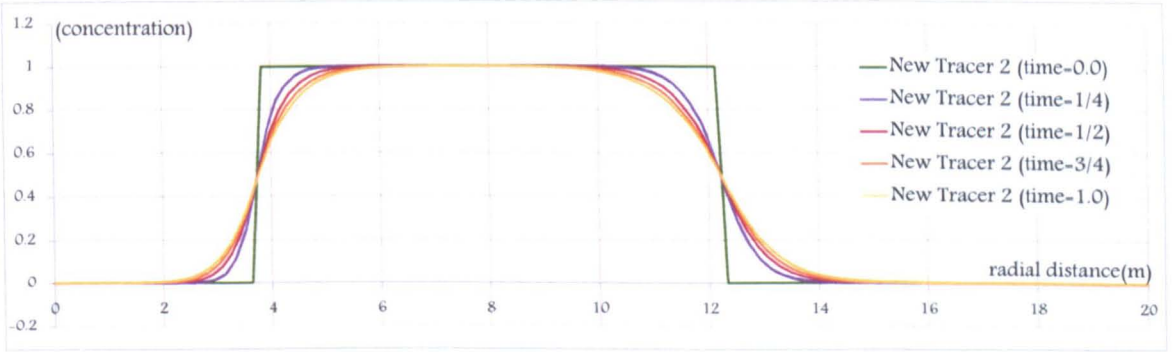

Figure 4.4 – Rotating of Tracer 2 profile, Evolution of the BCT-scheme

Figure 4.5 show the 2D plan views of the final values for Tracer 1 (left) and Tracer 2

(right). After a full rotation, the tracer profiles have been reasonably well preserved. This confirms that the BCT-scheme is correctly implemented in 2D.

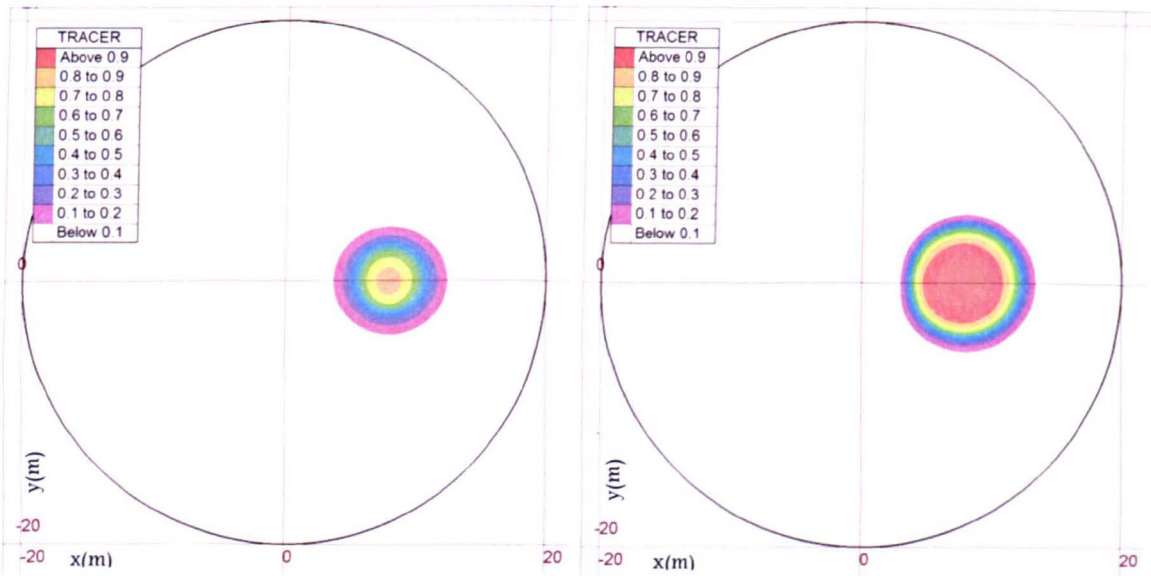

Figure 4.5 – Rotation of tracer profiles, BCT-scheme 2D solutions

For comparison and reference purposes, Figure 4.6 and Figure 4.7 show a comparison of the BCT-scheme with one of the other available schemes considered within the open TELEMAC system, in particular oTM-scheme 5 as defined by Hervouet (2007).

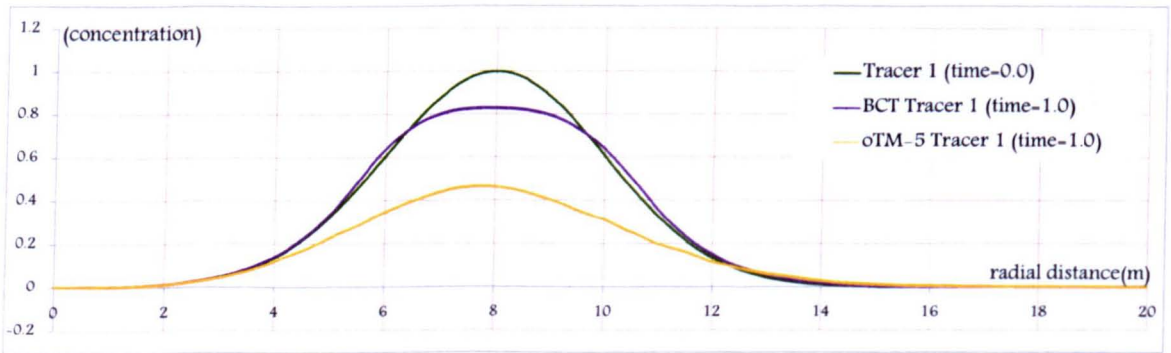

Figure 4.6 – Rotation of Tracer 1 profile, Comparison with oTM-scheme 5

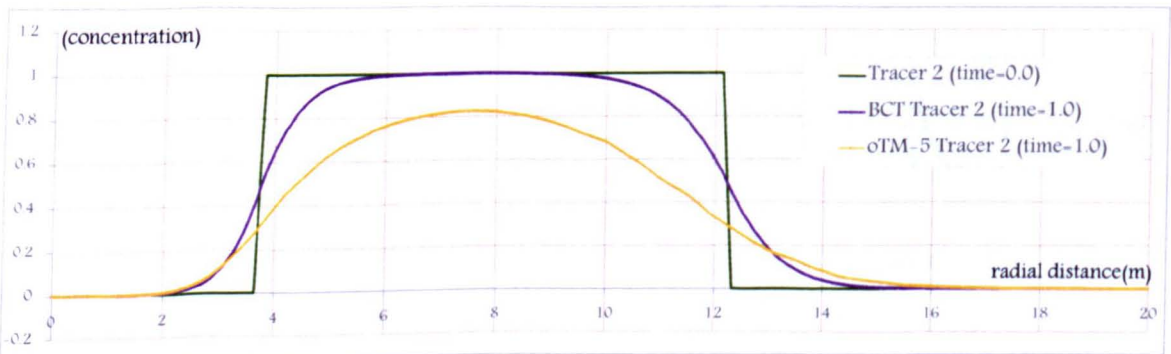

Figure 4.7 – Rotation of Tracer 2 profile, Comparison with oTM-scheme 5

Finally, Figure 4.8 shows the 2D plan views of the final values for Tracer 1 (left) and Tracer 2 (right) for the oTM-scheme 5.

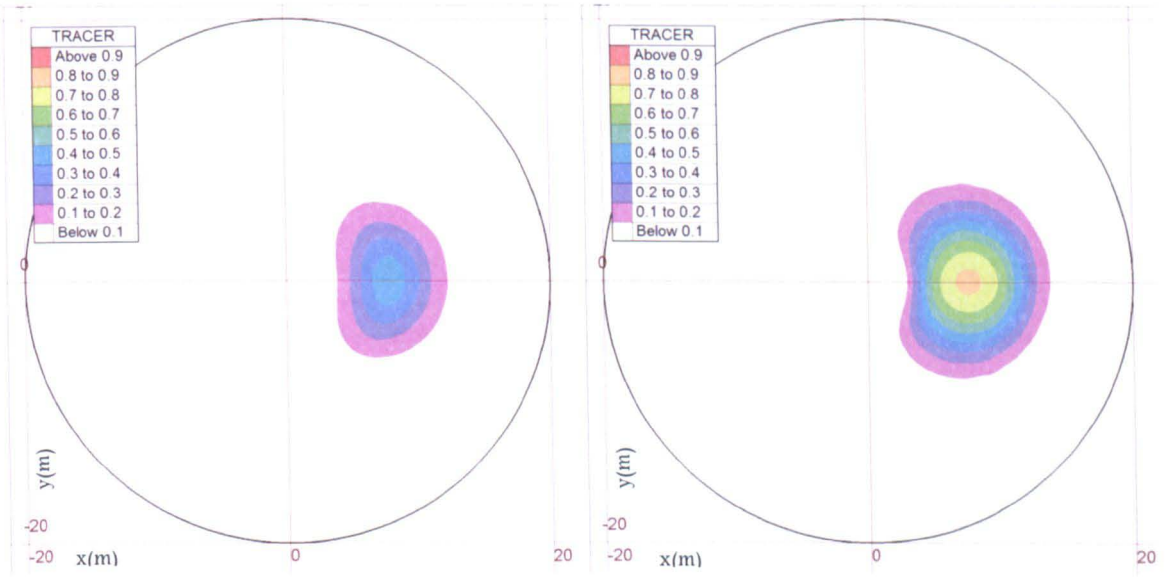

Figure 4.8 – Rotating advection of tracer profile, oTM-scheme 5 2D solutions

The distortion of the profile towards the inside of the circle shows a greater dependency of the solutions with grid size. Given a constant mesh resolution, the outside track is longer than the inside track for the same angular velocity. Table 5 summarises the error for the BCT-scheme between the computed and the analytical solutions. The norm L2 is here used for the error computed over the whole domain; L2 is defined as the sum of the square of the difference between a given solution at nodes and the corresponding analytical solution.

Scheme (rotation)	Norm L_2 Tracer 1	Norm L_2 Tracer 2
BCT-scheme (1/4)	0.77	15.34
BCT-scheme (2/4)	1.90	21.68
BCT-scheme (3/4)	3.16	26.03
BCT-scheme (4/4)	4.64	29.75
oTM-scheme 5 (4/4)	90.12	127.05

Table 5 – Rotation of tracer profiles, Comparison of norm L2 errors

It is clear that the BCT-scheme is much less diffusive than the other available schemes in the open TELEMAC system presently considered.

Ch.4-2. Dynamic pressure: the source-sink pair

As introduced in Chapter 1, it is important to model the entrainment and dilution around intakes, outfalls and de-stratification devices in environmental hydraulics studies of reservoirs and lakes, particularly when assessing water quality, mixing or thermal or saline outfalls. In addition, as discussed in Section Ch 3-1 8, inclusion of non-hydrostatic pressure is necessary for numerical schemes to model recirculation devices, particularly when these are within the same water column. Modelling the correct streamlines and pressure contours around sources and sinks is therefore one of the goals of the work presented here. Validation of the new approach to compute the non-hydrostatic pressure will also be tested through this example.

For validation against an analytical solution, consider a source-sink pair, one above the other in otherwise still water in a flat-bottomed closed 2D vertical tank. The analytical solution is introduced here for both the 3D case (axisymmetric coordinates) and its associated vertical 2D case (polar coordinates). The analysis is based on potential flow theory and inspired by the development of electromagnetic field around a dipole, although the dipole formulation assumes the distance between the source and sink to reduce to zero. Contrarily, the representation of bubbles rising through the water column as a mean to de-stratify stagnant waters, for instance, requires multiple sources and sinks through the water column, at distinct locations. The dipole assumption is not valid in this case.

Of interest here, a parameter study of a line sink in 2D has previously been reported by Stokes et al. (2007), who examined the impact on the free surface profile of possible variations in the intensity of a line sink and induced the effect of surface tension

Analytical formulation for one sink

A sink induces a radial inflow. Where the flow is assumed incompressible and irrotational, both a scalar and vector velocity potential can be defined from the radial inflow itself (see Section C.1 in Appendix C).

- In 2D polar coordinates, if the source is placed at the origin, the angular velocity $\vec{u}_\theta$ is zero. The radial velocity $\vec{u}_r$ is defined through the discharge of the source q_{Srce}, which is unchanged across any circle of radius r and perimeter $(2\pi r)$: $\vec{u}_r = -q_{Srce}/(2\pi r)$.

  (a) The velocity potential φ is defined by its gradient, $\vec{u} = \vec{\nabla}\varphi = \left(\frac{\partial\varphi}{\partial r}; \left(\frac{1}{r}\right)\frac{\partial\varphi}{\partial\theta} = 0\right)$, which leads to

  $$\varphi = -q_{Srce} ln\, r/2\pi$$

  (b) The vector velocity potential reduces to a stream function ψ also defined by its gradient $\vec{u} = \vec{\nabla}\psi = \left(\left(\frac{1}{r}\right)\frac{\partial\psi}{\partial\theta}; -\frac{\partial\psi}{\partial r} = 0\right)$, which leads to

  $$\psi = -q_{Srce}\theta/2\pi$$

- Similarly in 3D axisymmetric coordinates, the discharge is the same across any sphere of radius r and surface $(4\pi r^2)$. The (tangential) zenithal and azimuthal velocities $\vec{u}_\theta$ and $\vec{u}_\phi$ are zero while the radial velocity $\vec{u}_r = -q_{Srce}/(4\pi r^2)$.

  (a) The potential velocity φ is defined by its gradient with , $\vec{u}_r = \partial\varphi/\partial r$, which leads to

  $$\varphi = +q_{Srce}/(4\pi r)$$

  (b) The vector velocity potential reduces to a stream function ψ also defined by its gradient with $\vec{u}_r = (1/r^2 sin\phi)\partial\psi/\partial\phi$, which leads to

  $$\psi = +q_{Srce} cos\phi/4\pi$$

The same solutions are found for a source, replacing q_{Srce} by its opposite.

Analytical solution for a pair of source and sink

Now consider both a source and a sink of same intensity separated by a finite distance. The pair could influence the liquid free surface depending on the strength and distance of the source and sink from the free surface (Stokes, et al., 2007). It is here assumed that this is not the case and that the strength remains small.

The source is placed on the vertical axis at $-z_0$ below the origin and the sink placed at $+z_0$ above the origin (see Figure 4.9). Since the Laplace operator is a linear operator, potential velocity fields can be added or superimposed.

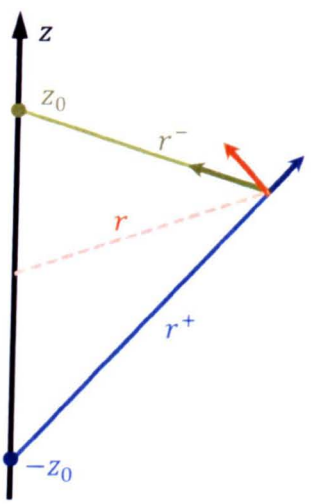

Figure 4.9 – Forces form a balanced sets of cources and sinks

In 2D polar coordinates, the resulting velocity potential, stream function and velocity components are as follows:

$$\text{(a)} \quad \varphi = -(q_{Srce}/2\pi) ln\left(\frac{r^-}{r^+}\right) = -\frac{q_{Srce}}{4\pi} ln\left(\frac{r^2+z_0^2+2z_0 r\, sin\theta}{r^2+z_0^2-2z_0 r\, sin\theta}\right) \tag{4.1}$$

$$\text{(b)} \quad \psi = -(q_{Srce}/2\pi)[\,\theta^- - \theta^+\,]$$

with distances defined as: $(r^{\pm})^2 = r^2 + z_0^2 \mp 2z_0 r\, sin\theta = x^2 + z^2 + z_0^2 \mp 2z_0 z$

and angles as $r^{\pm} sin\theta^{\pm} = r sin\theta \mp z_0 = z \mp z_0$

$$\text{(c)} \quad u_r = -\frac{q_{Srce}}{4\pi}\left[\frac{2r+2z_0 sin\theta}{r^2+z_0^2+2z_0 r\, sin\theta} - \frac{2r-2z_0 sin\theta}{r^2+z_0^2-2z_0 r\, sin\theta}\right] = \frac{q_{Srce}}{4\pi}\left[\frac{4z_0 sin\theta(r^2-z_0^2)}{(r^2+z_0^2)^2-4r^2 z_0^2 sin^2\theta}\right] \tag{4.2}$$

$$\text{(d)} \quad u_\theta = -\frac{q_{Srce}}{4\pi}\left[\frac{2z_0 cos\theta}{r^2+z_0^2+2z_0 r\, sin\theta} + \frac{2z_0 cos\theta}{r^2+z_0^2-2z_0 r\, sin\theta}\right] = -\frac{q_{Srce}}{4\pi}\left[\frac{4z_0 cos\theta(r^2+z_0^2)}{(r^2+z_0^2)^2-4r^2 z_0^2 sin^2\theta}\right]$$

For a comparison with the predicted numerical results in Cartesian coordinates, algebraic manipulation leads to:

$$u_x = \frac{q_{Srce}}{4\pi}\left[\frac{8\,x\,z\,z_0}{\left(r^2+z_0^2\right)^2-4z^2z_0^2}\right]$$
$$u_z = \frac{q_{Srce}}{4\pi}\left[\frac{4z_0\left(z^2-x^2-z_0^2\right)}{\left(r^2+z_0^2\right)^2-4z^2z_0^2}\right] \tag{4.3}$$

In 3D axisymmetric coordinates, the resulting velocity potential, stream function and velocity components are as follows:

$$\text{(a)}\quad \varphi = +(q_{Srce}/4\pi)\left[\frac{1}{r^-}-\frac{1}{r^+}\right] \tag{4.4}$$
$$\text{(b)}\quad \psi = +(q_{Srce}/4\pi)[\,cos\phi^- - cos\phi^+\,]$$

with distances defined as: $(r^{\pm})^2 = r^2 + z_0^2 \mp 2z_0 r\,cos\phi = x^2 + y^2 + z^2 + z_0^2 \mp 2zz_0$

and angles as $r^{\pm}cos\phi^{\pm} = z \mp z_0$

$$\text{(c)}\quad u_r = -\frac{q_{Srce}}{4\pi}\left[\frac{2r+2z_0cos\phi}{r^2+z_0^2+2z_0rcos\phi}-\frac{2r-2z_0cos\phi}{r^2+z_0^2-2z_0rcos\phi}\right] = \frac{q_{Srce}}{4\pi}\left[\frac{4z_0cos\phi(r^2-z_0^2)}{\left(r^2+z_0^2\right)^2-4r^2z_0^2cos^2\phi}\right] \tag{4.5}$$
$$\text{(d)}\quad u_\phi = -\frac{q_{Srce}}{4\pi}\left[\frac{-2z_0sin\phi}{r^2+z_0^2+2z_0rcos\phi}+\frac{-2z_0sin\phi}{r^2+z_0^2-2z_0rcos\phi}\right] = \frac{q_{Srce}}{4\pi}\left[\frac{4z_0sin\phi(r^2+z_0^2)}{\left(r^2+z_0^2\right)^2-4r^2z_0^2cos^2\phi}\right]$$

The potential velocity and stream functions are particular forms of the general solutions to the Laplace equation for both the 2D polar and 3D axisymmetric coordinate system (see Appendix C.2.4).

Analytical solution for a pair of source and sink in a bounded box

In deriving the above, the analytical solution for a source and sink pair, it has been assumed that the domain is unbounded. In practice, a reservoir has finite dimensions, the boundaries of which are impermeable including at the free surface (fixed lid assumed in the analytical solution). In order to account for the finite domain, the method of mirror images is considered. Just as was done when adding the scalar velocity potential (and the stream function) of a single source and sink together, the scalar functions of all virtual pairs of sources and sinks are added to produce the final

analytical solution.

The following layout of virtual pairs of sources and sinks is envisaged (see Figure 4.10). In theory, the symmetry axis is such only if the pattern is repeated indefinitely. In practice only a few source-sink couples are relevant for comparison with the predicted numerical solution.

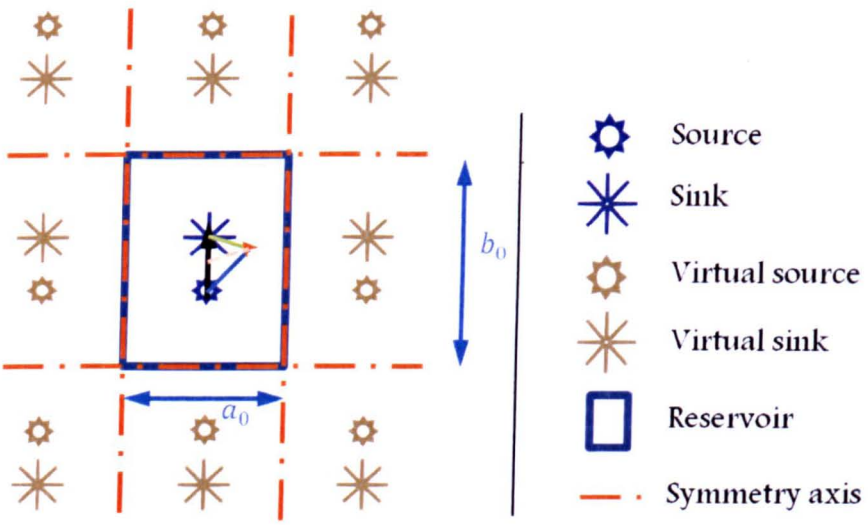

Figure 4.10 – Mirror images for a pair of cources and sinks within a box

In 2D polar coordinates, the resulting potential, stream function and velocity components are as follows:

$$\text{(a)}\quad \varphi = -\frac{q_{Srce}}{2\pi}\cdot\sum_{i=-\infty}^{+\infty}\sum_{j=-\infty}^{+\infty} ln\left(\frac{r_{ij}^{-}}{r_{ij}^{+}}\right) \tag{4.6}$$

$$\text{(b)}\quad \psi = -\frac{q_{Srce}}{2\pi}\cdot\sum_{i=-\infty}^{+\infty}\sum_{j=-\infty}^{+\infty}\left[\theta_{ij}^{-} - \theta_{ij}^{+}\right]$$

with distances defined as:

$$(r_{ij}^{\pm})^2 = r^2 + z_0^2 + (ja_0)^2 + (ib_0)^2 - 2ja_0 rcos\theta - 2ib_0 rsin\theta \mp 2s_i z_0(rsin\theta - ib_0)$$

and angles as $r_{ij}^{\pm} sin\theta_{ij}^{\pm} = rsin\theta - ib_0 \pm s_i z_0$ where $s_i = +1$ if i even or -1 otherwise.

$$\text{(c)}\ u_r = -\frac{q_{Srce}}{4\pi}\cdot\sum_{i=-\infty}^{+\infty}\sum_{j=-\infty}^{+\infty}\left[\frac{2r-2ja_0cos\theta-2ib_0sin\theta+2s_iz_0sin\theta}{(r_{ij}^{-})^2} - \frac{2r-2ja_0cos\theta-2ib_0sin\theta-2s_iz_0sin\theta}{(r_{ij}^{+})^2}\right] \tag{4.7}$$

$$\text{(d)}\ u_\theta = -\frac{q_{Srce}}{4\pi}\cdot\sum_{i=-\infty}^{+\infty}\sum_{j=-\infty}^{+\infty}\left[\frac{2ja_0sin\theta-2ib_0cos\theta+2s_iz_0cos\theta}{(r_{ij}^{-})^2} - \frac{2ja_0sin\theta-2ib_0cos\theta-2s_iz_0cos\theta}{(r_{ij}^{+})^2}\right]$$

The same approach applies to the 3D axisymmetric coordinates but with three indices instead of two. For instance:

$$\varphi = +\frac{q_{Srce}}{4\pi} \cdot \sum_{i=-\infty}^{+\infty} \sum_{j=-\infty}^{+\infty} \sum_{k=-\infty}^{+\infty} \left[\frac{1}{r_{ijk}^{-}} - \frac{1}{r_{ijk}^{+}} \right]$$

with the distances computed as: $(r_{ijk}^{\pm})^2 = r^2 + z_0^2 + (ja_0)^2 + (ib_0)^2 - 2ja_0 r cos\phi - 2ib_0 r sin\phi \mp 2s_i z_0 (r sin\phi - ib_0) + (ka_0)^2 - 2ka_0 r cos\theta$.

Model setup

The 3D solver SULIS is the basis of the test case. A 2D vertical tank was set up for comparison with the analytical solution developed under 2D polar coordinate system. The width of the tank a_0 is set to 99 m, where the odd distance is to accommodate the parity on either side of the central column containing the pair. The mean depth of the tank b_0 is set 120 m with a distance between the source and the sink $2z_0$ set at 19 m. The grid spacing is chosen to be 1 m in all direction. Finally, the strength of the pair, or the discharge q_{Srce} is set to 10^{-3}. Figure 4.11 shows a sketch of the model setup.

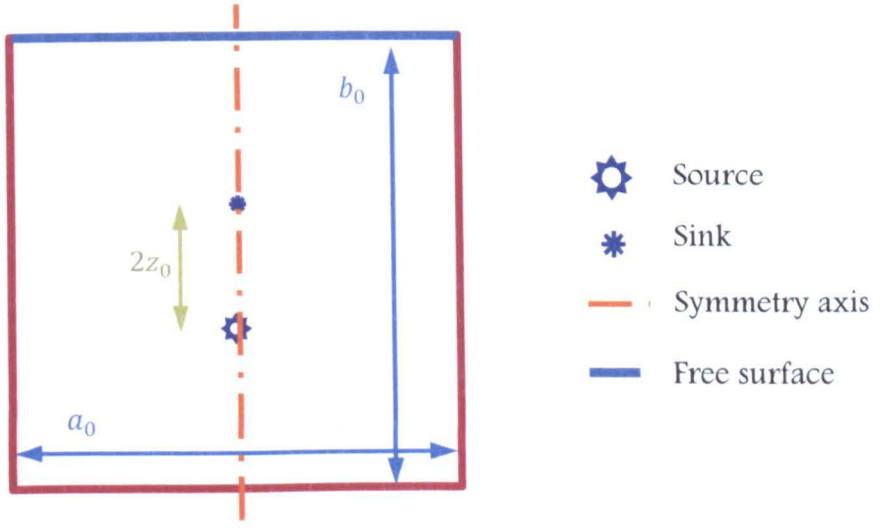

Figure 4.11 – Sketch of the source and sink pair model setup

In order to converge to the steady state, the initial conditions are set to still water where the following ramping curve (infinite derivative) is used to gradually increase the discharge from 0 to q_{Srce} within 120 seconds: $q(t) = q_{Srce} \frac{1}{2}\left(1 - cos\left(\frac{\pi t}{120}\right)\right)$.

Model comparison

Figure 4.12 shows a vertical slice through the iso-contours of the velocity potential φ for both the analytical solution (left inset, Eq. (4.6)and Eq. (4.1)) compared to the velocity potential computed by the 3D solver SULIS, as a re-integration of the predicted flow field.

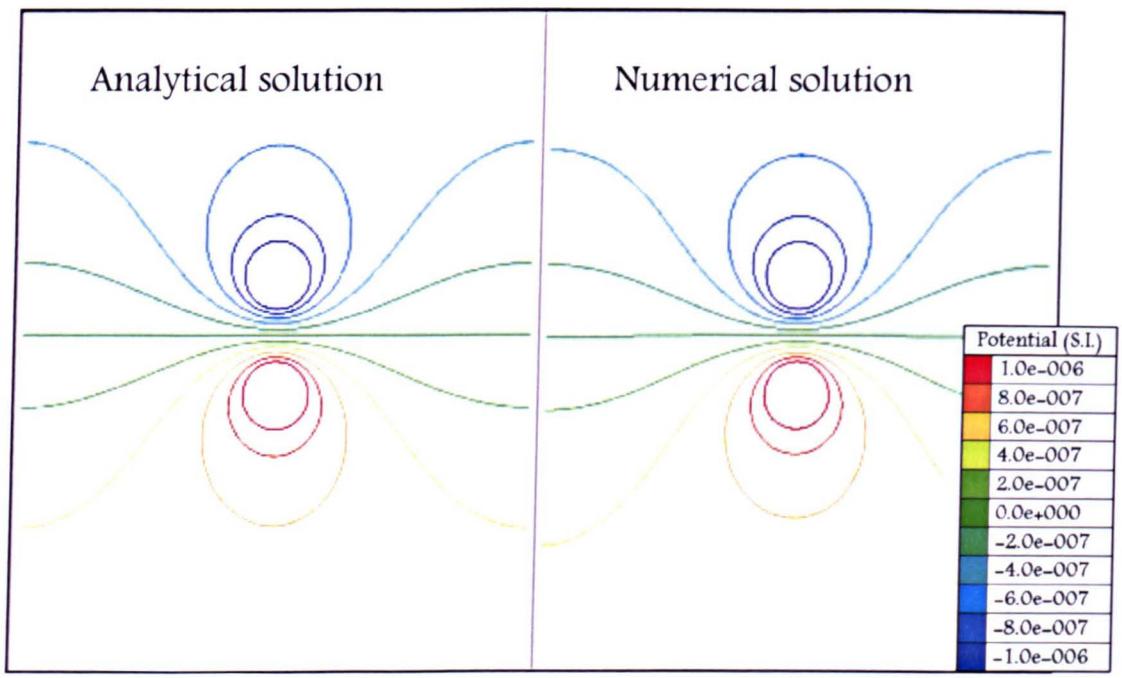

Figure 4.12 – Model results comparison with analytical solution

The comparison shows that the new approach to the direct calculation of the dynamic pressure term is adequate. From this it can be concluded that:

- All 3D solvers assembling and solving a Laplace equation through the projection method could save a significant amount of time by implementing the new approach.
- Because the new approach does not add much to the computation cost (and can be implemented explicitly, based on a vertical integration starting from the free surface), there is no need for any 3D hydrodynamic solver to be based on the non-hydrostatic assumption.
- Applications to long term simulations of water quality processes in deep reservoirs

and lakes, for instances, is possible with the new approach.

Ch.4-3. Stratification: the lock exchange case

As introduced in Chapter 1, it is important to model the interaction between fluids of different density in environmental hydraulics studies, be it either the interaction between fresh (landward) and salt (seaward) waters in an estuary, or the positive or negative buoyancy of a thermal or saline outfall respectively in coastal waters. Also, as discussed in Section Ch.2-3, the monotonic representation of the sharp gradients of conserved quantities is necessary to model the opposite gravity-driven movement of one layer (plume of lower density) above another (plume of higher density). Identifying and refining the interface between the two layers of different density is therefore one of the goals of the work presented here. Validation of the new approach to automatically displace the mesh will also be tested through this example.

It should be highlighted that the density difference observed in environmental hydraulics studies is very small (within 2 to 5% at most), except for highly concentrated sediment-laden flows. As a result, the Boussinesq approximation is used in virtually all 3D solvers listed (see Appendix B), where gradient of density is neglected in the inertia term, but retained in the buoyancy term where it is multiplied by the gravitational constant (see the Navier-Stokes equations in Section Ch.3-1.2).

Experimental results

The work of Shin, et al., (2004) forms the basis of the present test case. In the lock exchange experiment, immiscible fluids of different densities initially at rest in a tank are separated by a vertical lock gate. The right half contains the less dense fluid while

the left half contains a denser fluid. For reference and comparison, Figure 4.13 is extracted from Shin, et al.'s description (2004) of the experiment.

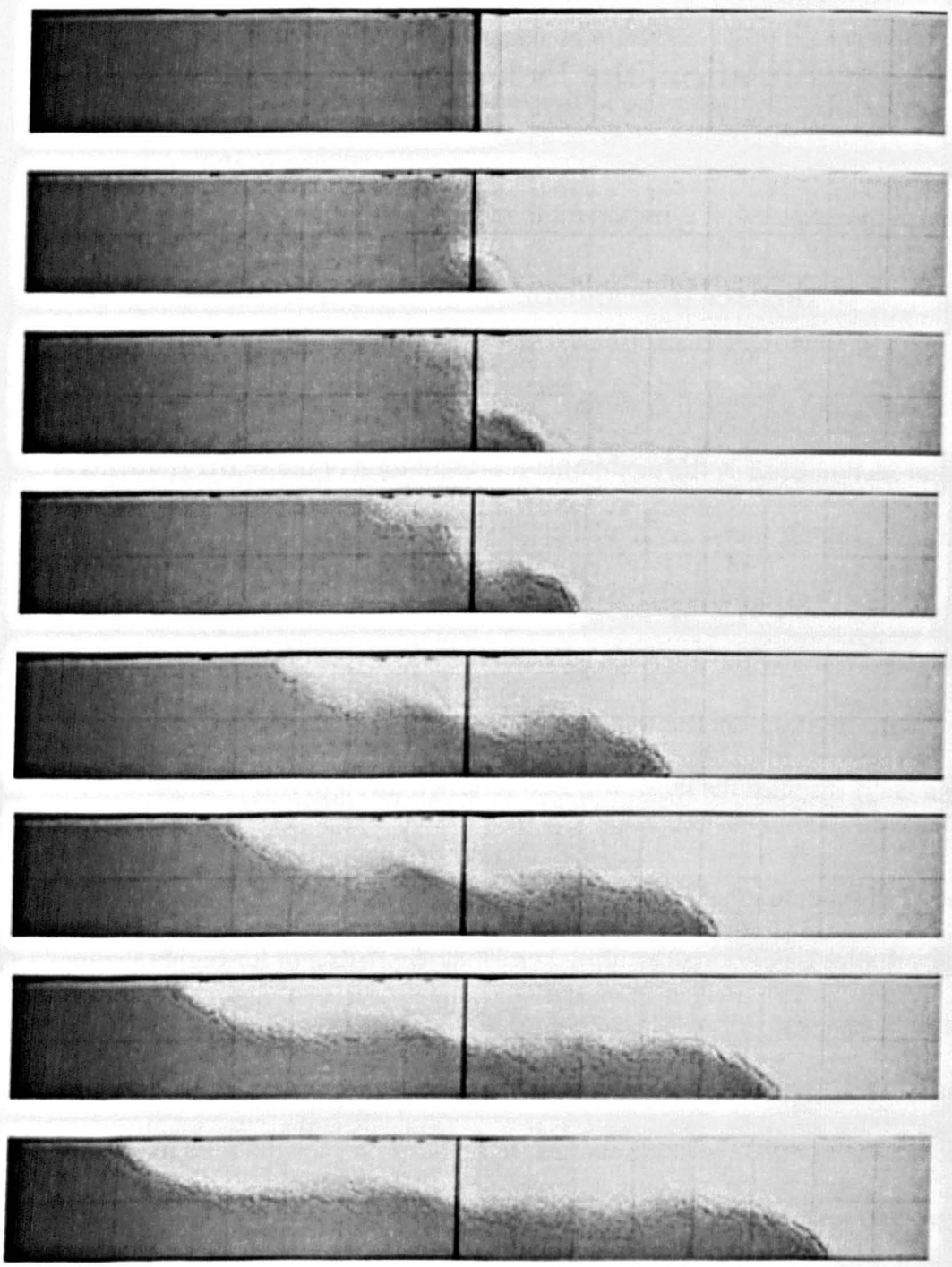

Figure 4.13 – Lock exchange experiment (Shin, et al., 2004)

When the gate is instantaneously removed, differences in the hydrostatic pressure cause the lighter density (ρ_l, positively buoyant) fluid to flow over the denser fluid along the surface of the tank, while the heavier density (ρ_h, negatively buoyant) fluid

flows underneath along the bottom of the tank ($\rho_h > \rho_l$). In this case the densities on the two sides of the lock gate are very similar (the density ratio $\gamma = \rho_h/\rho_l$ is close to unity). The strongly sheared flow at the interface between the two fluids leads to Kelvin-Helmoltz instabilities.

Interestingly, Shin, et al., (2004) demonstrates that, contrary to early publications, the dynamics of gravity currents are not influenced by dissipation due to turbulence and mixing when the Reynolds number is sufficiently high (the Reynolds number being defined as the dimensionless ratio of the product of the fluid front velocity and the tank depth by the kinematic viscosity). Instead, Shin, et al., (2004) provide an alternative theory that predicts the current speed and depth based on energy-conserving flow that is in good agreement with experiments. That work was followed one year later by the Part 1 – Theory and experiments of Lowe, et al., (2005) and the Part 2 – High-resolution simulations of Birman, et al., (2005).

For illustration and comparison purposes, Figure 4.14 is an extract of the latter article by Birman, et al., (2005). It shows the numerical results of a high resolution simulation of the formation of a Boussinesq gravity current at a Reynolds number of 4,000.

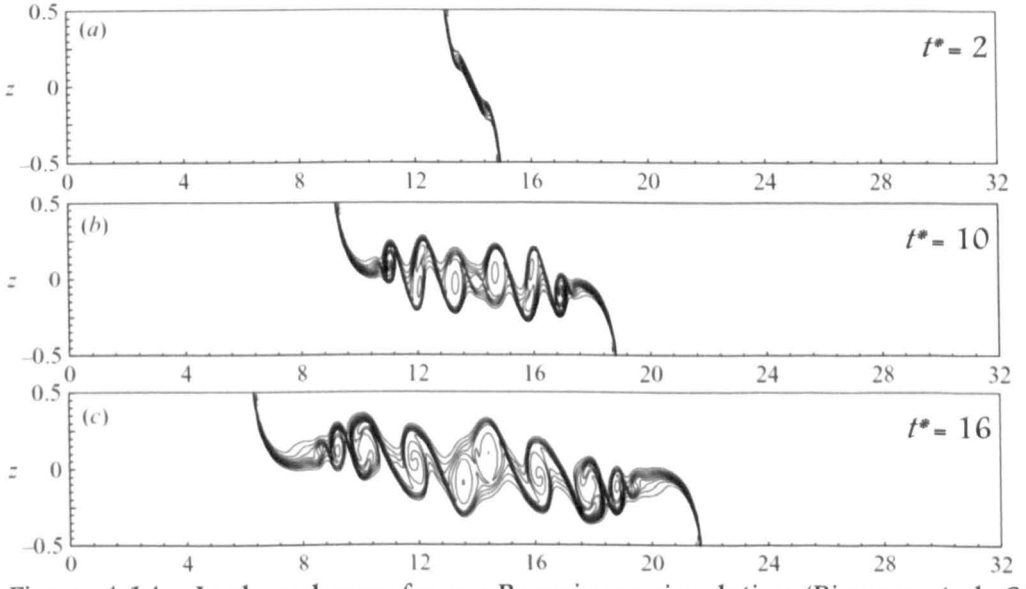

Figure 4.14 – Lock exchange from a Boussinesq simulation (Birman, et al., 2005)

The mesh resolution is based on a regular grid, for which each vertical contains 200 points regularly spaced and fixed throughout the simulation. The time t^* is dimensionless and defined as $t^* = t\sqrt{g(1-\gamma)/H}$.

It can be visually observed from both the experiment and the high resolution solution that the Boussinesq flows are virtually symmetric, that the dense and light fronts travel at almost the same speeds, and that the currents of either fronts occupy about half the channel depth, although they may be shallower immediately behind the head where Kelvin-Helmoltz instabilities are.

Analytical characteristics

In their theoretical demonstration, Shin, et al., (2004) use the following diagram (see Figure 4.15) to define the principal quantities and write the hydrostatic pressure along the lines BE and CD and the Bernoulli's equation along the BO, OC resulting in

$$\frac{U^2}{gH} = \frac{(1-\gamma)}{\gamma}\frac{h(2H-h)(H-h)}{H^2(H+h)}$$

followed by the Bernoulli's equation along the interface leading to:

$$\frac{U^2}{gH} = 2\frac{(1-\gamma)}{\gamma}\frac{h(H-h)^2}{H^3}$$

which in turn defines the solution $h = H/2$.

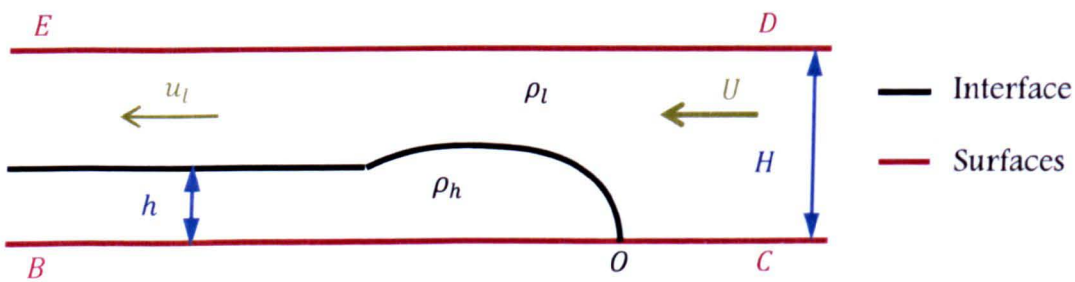

Figure 4.15 – Idealised gravity currents in the rest frame of the heavier current

Therefore, an energy-conserving current occupies one half the depth of the channel and travels with a non-dimensional speed of $\frac{U^2}{gH} = \frac{1}{4}\frac{(1-\gamma)}{\gamma}$.

Results from other 3D solvers

Because of the importance of this type of density driven exchanges in environmental hydraulics, in estuaries for instance, some 3D solvers present that test case as a mean to verify applicability to modelling stratified flows. For instance, the following two 3D solvers were selected for that they are often compared to the capabilities of the open TELEMAC system.

The solver FVCOM from the University of Massachusetts (see Section B.3.9 in Appendix B), is a 3D solver using a sigma-stretched transformation combining both finite element method and finite-difference methods. Figure 4.16 shows results for the lock exchange case, for similar times / displacements.

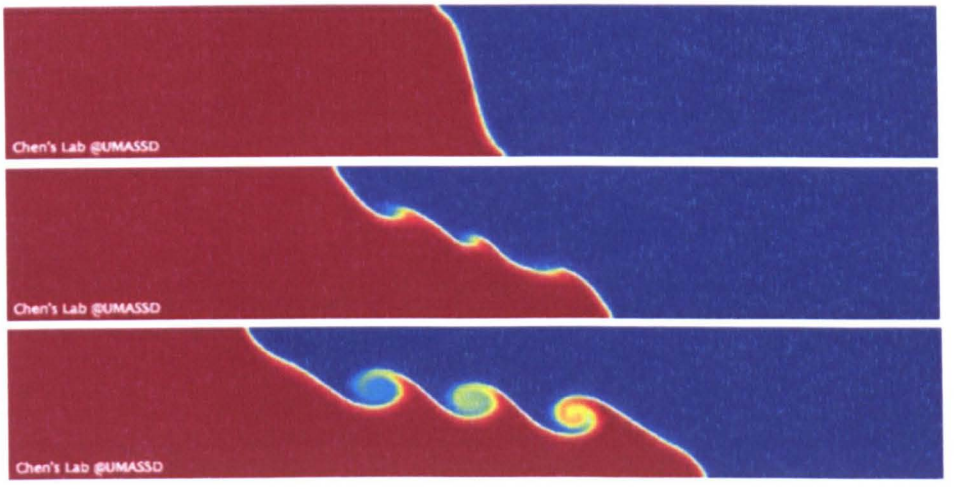

Figure 4.16 – Lock exchange case applied to solver FVCOM

While the resolution of the model is sufficiently fine to resolve the Kelvin-Helmholtz instabilities at the interface of the two fluids, some of the analytical characteristics identified previously do not seem to apply here. The solution is not entirely symmetrical and the front does not appear to travel with half the depth. The distinctive curve at both propagation fronts with a virtually horizontal plateau seems absent.

The solver FLUIDITY from Imperial College, London (see Section B.3.12 in Appendix B),

is a 3D solver using a complete unstructured mesh (vertically and horizontally) that automatically adapt to the physics of the problem by refining its mesh close to sharp gradients. Figure 4.17 shows results for the lock exchange case, for similar times / displacements together with the adaptive mesh resulting refinement.

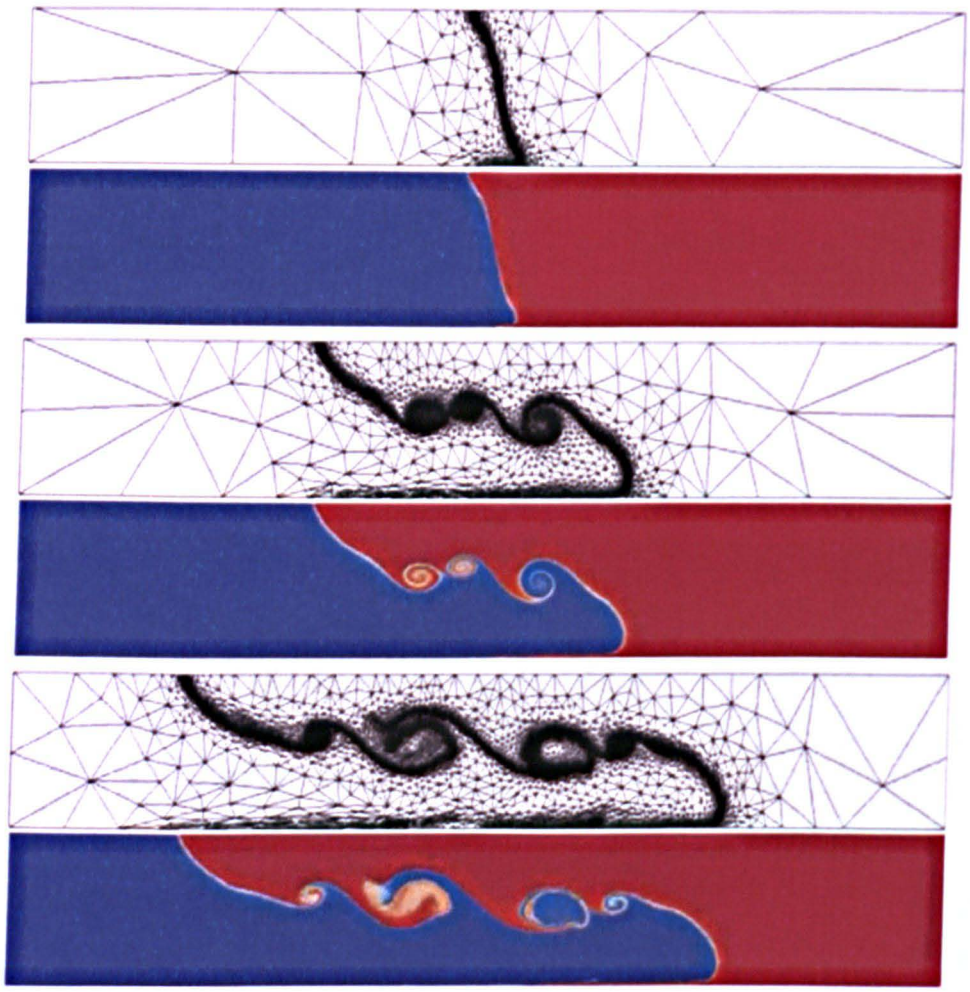

Figure 4.17 – Lock exchange case applied to solver FLUIDITY

The increased resolution at the interface between the two fluids is well resolved (with no visible light colours). However, the solution is not entirely symmetrical with a refinement of the bottom of the flume not observed at the surface. Also, the front does appear to travel with half the depth but only for the denser (blue) fluid and a lighter (red) fluid travelling faster.

Model setup

The 3D solver TELEMAC-3D is the basis of the test case. A 2D vertical tank was set up for comparison with the experimental solution (Shin, et al., 2004) and its high resolution simulations (Birman, et al., 2005). The length of the tank L is set to 32 m. The mean depth of the upper free surface in the tank H is set 1 m. Again, the graphical user interface and freeware Blue Kenue (2011) was used to generate the mesh. The unstructured mesh is formed of triangles of similar sizes, with an average edge length of the 0.05 m. The 2D model is constituted of 9,632 elements covering an area of length 32 m by width 0.4 m. This is equivalent to about 3,850 representative cells in the streamwise direction. Figure 4.18 shows a schematic plan view of the model set up (bottom inset) together with the detail of part of the unstructured mesh (top inset).

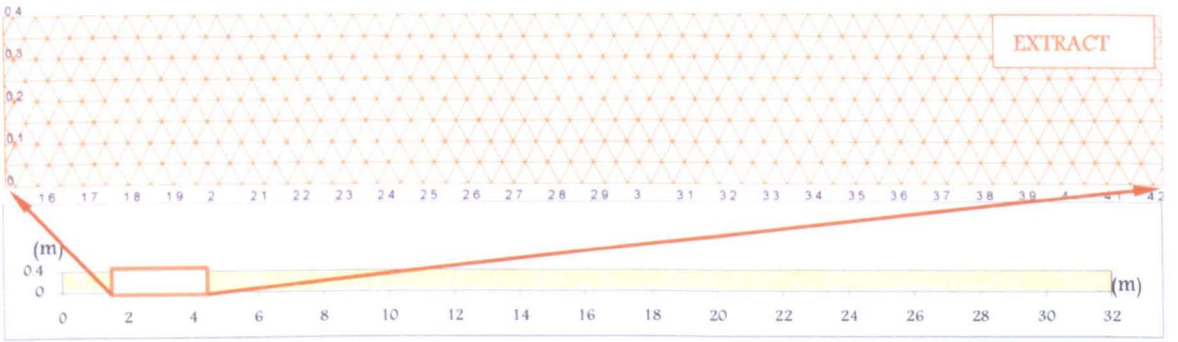

Figure 4.18 – Lock exchange case, Plan view of model characteristics

The tank is split in two regions, where the tracer concentration on the right is zero, and the tracer on the left has a concentration of 1 units for visualisation purposes. The density ratio γ is set to 0.9995, the reference density is set to 1,000 kg/m^3. The hydrodynamics is at rest at the start of the simulation. With these, the theoretical velocity of the front is $u_l = u_h = \sqrt{g(1-\gamma)/\gamma} = 0.07$ m/s and we note with $H = 1$ m that t^* is also the travelled distance of the front.

Model comparison

For comparison purpose, the results of three simulations are presented here for

different time t^*. The first two simulations are based on the standard sigma-stretched transformation (10 horizontal layers in the first simulation; twice as many layers in the second). The third simulation is based on 10 layers (11 surfaces) but combined with the AMD method developed through the present work (see Ch.3-2.10). The simulations were conducted in the absence of any other forces except gravity.

Overall, the symmetry of the heavier and lighter propagating fronts is seen for all times and all simulations. This is a result of the symmetry of the governing equations under the Boussinesq approximation.

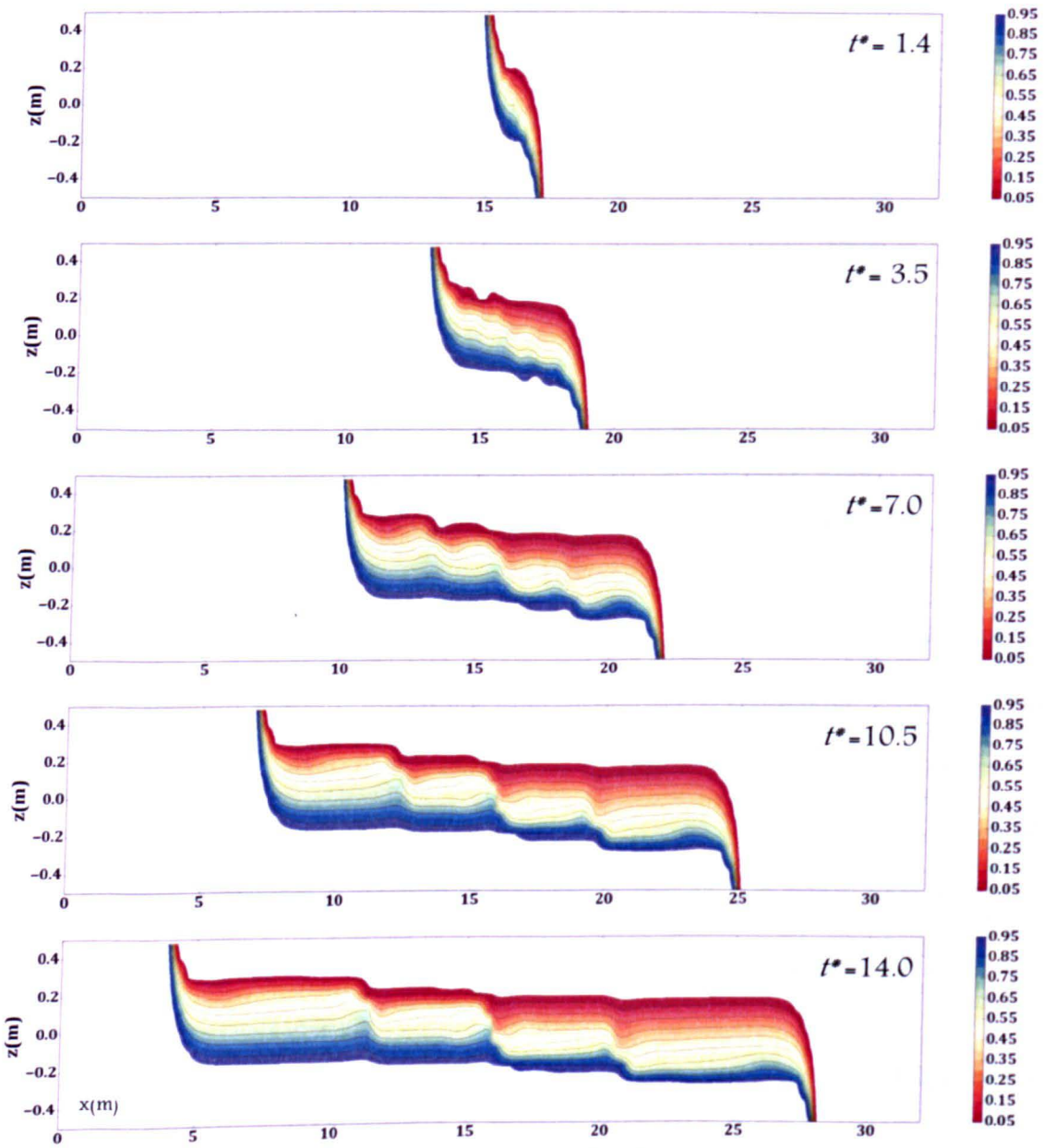

Figure 4.19 – Model results comparison, 11 σ-levels

Specifically for the first case, Figure 4.19 shows the results of the lock exchange based on 11 surfaces of the standard sigma-stretched transformation. It is observed that the horizontal interface is varying gradually between the lighter and heavier fluids and that what seems to be three steps in the central part of the interface is in fact the result of the positions of the horizontal surfaces, defining the vertical resolution of the model and supporting the interpolation of the solutions.

Specifically for the second case, Figure 4.20 shows the equivalent results but based on 21 surfaces of the standard sigma-stretched transformation (twice as many layers).

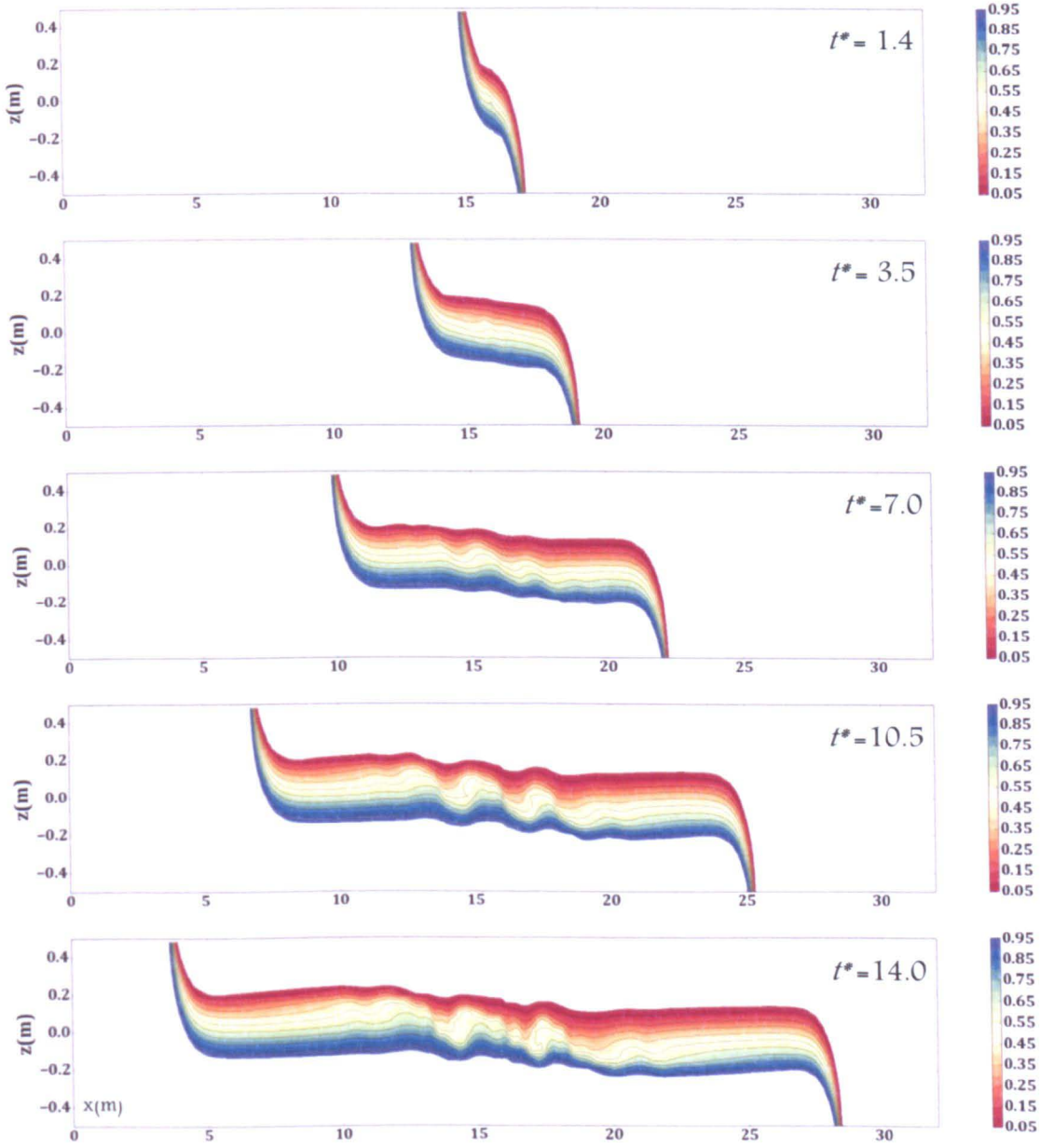

Figure 4.20 – Model results comparison, 21 σ-levels

It is observed that the horizontal interface remains large and is still varying smoothly (linearly) between the lighter and heavier fluid. It is also observed that the influence of the positions of the horizontal surfaces is less significant with the increased resolution.

Finally the oscillations forming at a later stage in the central part of the interface could be interpreted as genuine Kelvin-Helmholtz instability and related to the stronger eddies seen in the reference simulation (see Figure 4.14). However, these instabilities appear much earlier in the experiment (see Figure 4.13) and in the high resolution simulation (see Figure 4.14).

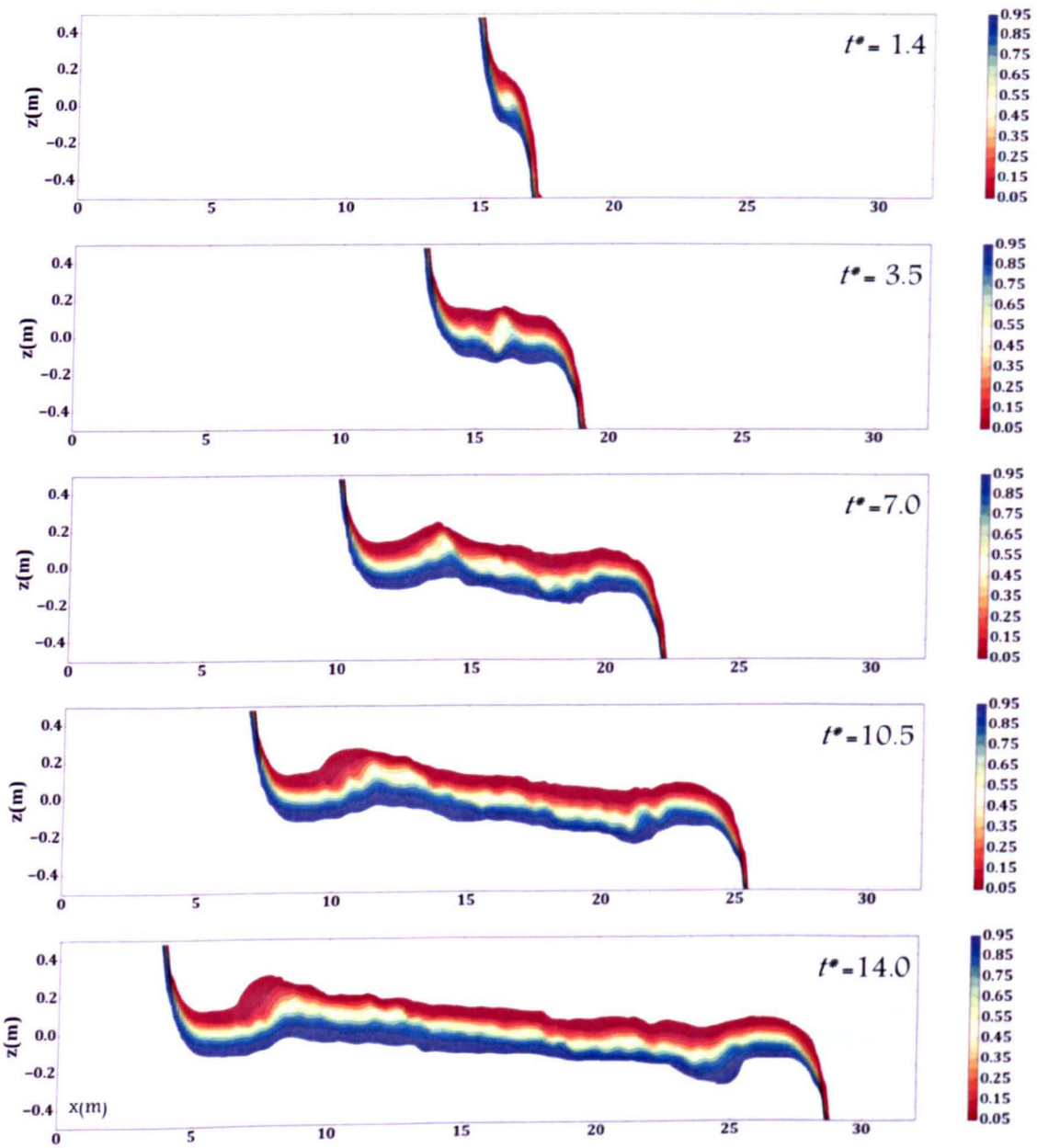

Figure 4.21 – Model results comparison, 11 automatically displaced levels

Specifically for the third case, Figure 4.21 shows the results of the lock exchange based on 11 surfaces combined with the AMD method. As anticipated, the high gradients at the interface are better refined and tracked with a central band (light colours) virtually absent when compared to the gradual variations highlighted in the case of sigma-stretched transformations.

From a hydrodynamics viewpoint, some eddy structures are observed and the shape of the envelope of the interface is close to the reference simulation, particularly the distinctive curve at both propagation fronts. The height of these fronts also remains in agreement with the theoretical value, i.e. half the total depth throughout the simulation. The increased resolution around the high gradients of tracer is indirectly increasing the resolution of the hydrodynamics quantities in the same region and as a result, dramatically improves the overall hydrodynamics, even with a fewer number of layers.

Nonetheless, the velocity of the fronts is a little slow, even though they are slightly faster with the AMD method than with the sigma-stretched transformation. For instance, at $t^* = 10.5$, the front should have travelled 10.5 m starting from a position $x_{t^*=0} = 16$ m on the x-axis, therefore be at $x_{t^*=10.5} = 26.5$ m. It has only reached 25.5 m approximately thus travelled 9.5 m.

BLANK PAGE IN ORIGINAL

Chapter 5 –
Conclusions and recommendations

Ch.5-1. Conclusions

Environmental hydraulics covers a very wide range of activities, including but not only physical and numerical modelling of free surface flows in rivers, coastal waters and estuaries and lakes. This thesis focused on numerical modelling within a subset of environmental hydraulics activities: stratified shallow flow modelling. The presence of at least two layers of different densities leads to 3D processes, the prediction of which is critical to mitigate the environmental impact on water and its quality of population growth, industrialisation, climate change, development of riverine and coastal areas, etc.

A relatively extensive review of existing 3D free surface solvers known to the author to date was produced to define the state-of-the-art of stratified shallow water modelling. The review concluded that there were at least three areas where significant advances could be made, in relation to which three objectives were set out.

First, virtually all 3D free surface solvers could be grouped in two mutually exclusive categories, depending on the vertical discretisation: (a) those with fixed horizontal layers; and (b) those with sigma-stretched transformation. The first of the three research objectives was therefore to develop a novel numerical method allowing a

greater flexibility of the vertical representation within 3D solvers to automatically adapt to the evolving physics of the model, specifically to stratified flows.

Second, only a handful of 3D solvers implement a numerical scheme that is monotonic, at least second order accurate, capable of capturing strong gradients present in stratified waters and implicit to perform long term simulations. The second of the three research objectives was therefore to investigate a series of numerical schemes for their application to stratified flows, particularly to multi-dimensional hydrodynamics and tracer advection over long periods of time.

Third, many 3D free surface shallow water solvers do not compute a non-hydrostatic pressure term, and those that do do so via a computationally intensive resolution of a Laplace equation. Because of the importance of dynamic pressure in long term modelling of stratified waters subject to, for instance, the influence of natural forces (winds, tides, etc.) or artificial forces (recirculation devices, thermal outlets, etc.), The third of the three research objectives was therefore to develop a novel method to calculate dynamic presume without resolving to the solution to the Laplace equation.

In response, three major developments were carried out and validated through the present research work. All three developments have direct applicability to practical environmental hydraulics applications.

First, the herein called AMD method was implemented and validated within the numerical framework of the open TELEMAC system. The AMD automatically focuses vertical mesh resolution in key portions of the water column depending on a monitor function of the gradient of a tracer profile, for instance, or of its curvature etc. It is important to note that this adaptive mesh displacement does not change the number of nodes or elements in the mesh. Rather it allows the model to concentrate refinements only in places of interest, thus significantly decreasing computational costs compared

to other types of fixed or terrain following layering while reducing numerical diffusion around sharp gradients. The lock exchange case was used to validate the AMD method. Its use produced an area representative of the Kelvin-Helmoltz instabilities at the interface between the exchanged fluids with only a few layers.

Second, following a literature review of numerical monotonic and non-diffusive advection schemes, one particular series of schemes was selected for its order of accuracy, semi-discrete form, while being applicable to both the advection and diffusion terms of the Navier Stokes equations. The so-called BCT-scheme was developed to fit to the finite element framework of TELEMAC and its parallelisation element-by-element. The main advantage is its simplicity averaging over Riemann problems without solving them, while excessive numerical viscosity is compensated for by using high-resolution MUSCL type reconstruction. The development of the scheme was here focused on non-diffusive tracer advection. The 2D case of a tracer profile rotating within a closed basin was used to validate the new scheme. Its use highlighted a significant decrease of numerical diffusion when compared to existing schemes implemented in the open TELEMAC system.

Third, a new direct method to compute dynamic pressure was implemented and validated in the finite difference framework of SULIS. Rather than using the computationally intensive projection method, whether computed or simplified as described in the vast majority of 3D hydrodynamic solvers, a novel approach was introduced where the third equation of momentum is used to solve for the vertical gradient of the pressure. The method can either be implicit or explicit and requires no additional cost to the rest of the 3D solver. The case of a source-sink pair within a water column was used to validate the direct pressure computation within the Navier-Stokes equations against an analytical solution derived from potential flow theory.

In the context of stratified shallow flow modelling within the field of environmental hydraulics, the aim of this thesis was to improve the applicability of existing 3D solvers to a wider spectrum of problems in order to model both short and long term evolution of stratified flows. The author believes that the work produced here significantly advances research in three distinct areas towards that aim.

Ch.5-2. Recommendations

The author believes that some of the novel approaches presented in this thesis could open new axis of research within and beyond stratified shallow flow modelling, free surface flows and more generally numerical modelling within environmental hydraulics. For each of the three objectives, a number of recommendations are made.

First, the AMD method could be extended to focus resolution at multiple locations within the water column. For instance, the strongly sheared flow at the interface between two fluids of different density leads to Kelvin-Helmoltz instabilities, resulting in the formation of eddies. An extended AMD method would be able to capture the full circle of each eddies without requiring much additional computing.

Second, it is recommended that the BCT scheme developed in the context of tracer advection, be extended to the momentum of the 3D non-linear shallow water equations. Several articles exist on these types of equations in the context of finite volumes, including various methods to solve the source terms for wetting and drying applications. The principal goal would be to retain the same formulation for a direct implementation within the finite element framework in order to benefit from existing desirable properties of the open TELEMAC system such as finite element assembly and domain decomposition parallelism. Additionally, it is also recommended that the new

advection schemes be generalised to the diffusion terms and to other equations such as turbulence closure methods.

Finally third, it is recommended that the direct implicit method to compute the dynamic pressure by vertically integrating the third equation of momentum, implemented in the finite difference framework SULIS, be implemented in the finite element framework of the open TELEMAC system. Had the TELEMAC system be an open source solver at the start of this research work, the author might have opted for it from the start.

BLANK PAGE IN ORIGINAL

Chapter 6 – References

Abbott, M. & Basco, D., April 1997. *Computational Fluid Dynamics: An Introduction for Engineers.* 1 ed. Harlow: Longman Pub Group.

Aboiyar, T., Georgoulis, E. H. & Iske, A., 2006. *High Order WENO Finite Volume Schemes using Polyharmonic Spline Reconstruction.* Cluj-Napoca, Proceedings of the International Conference on Numerical Analysis and Approximation Theory, pp. 1-14.

Ahmad, N., Boybeyi, Z., Löhner, R. & Sarma, A., 2007. A Godunov-Type Scheme for Atmospheric Flows on unstructured Grids, Euler and Navier Stokes Equations. *Journal of Pure and Applied Geophysics,* Volume 164, pp. 217-244.

Arakawa, A. & Lamb, V., 1977. Computational design of the basic dynamical process of the UCLA general circulation model. *Methods in Comutational Physics,* pp. 173-265.

Batten, P., Clarke, N., Lambert, C. & Causon, D. M., 1997. On the Choice of Wavespeeds for the HLLC Riemann Solver. *SIAM,* 18(6), pp. 1553-1570.

Beckmann, A. & Haidvogel, D., 1993. Numerical simulation of flow around a tall isolated seamount: Part I: Problem formulation and model accuracy. *Journal of Physical Oceanography,* Volume 23, pp. 1736-1753.

Birman, V. K., Martin, J. E. & Meiburg, E., 2005. The non-Boussinesq lock-exchange problem. Part 2. High-resolution simulations. *Journal of Fluid Mechanics,* Volume 537, pp. 125-144.

Birman, V. K. & Meiburg, E., 2006. High-Resolution Simulations of Gravity Currents. *Journal of the Brazilian Society of Mechanical Sciences & Engineering,* XXVIII(2), pp. 169-173.

Blumberg, A. & Mellor, G., 1987. A description of a three-dimensional coastal ocean circulation model. In: N. Heaps, ed. *Coastal and Estuarine Studies.* Washington D.C.: s.n., pp. 1-16.

Boris, J. P., 1971. *A fluid transport algorithm that works.* Trieste, Italy, in Seminar Course on Computing as a Language of Physics.

Boris, J. P. & Book, D. L., 1973. Flux-Corrected Transport, I. SHASTA, A fluid transport algorithm that works. *Journal of Computational Physics,* Volume 11, pp. 38-69.

Boris, J. P. & Book, D. L., 1997. Flux-Corrected Transport, I. SHASTA, A fluid transport algorithm that works. *Journal of Computational Physics,* Volume 135, pp. 172-186.

Bouchut, F., Bourdarias, C. H. & Perthame, B., 1996. A MUSCL Method Satisfying all the Numerical Entropy Inequalities. *Mathematics of Computation,* 65(216), pp. 1439-1461.

Bourban, S., 1997. *3DSL (SULIS), A fully implicit solution of 3D hydrodyanmics,* Toulon: Institut des Sciences de Toulon et du Var.

Bowles, R., 2007. *MATHM242 Lecture Notes - first half.* [Online] Available at: http://www.ucl.ac.uk/~ucahdrb/MATHM242/M242.pdf [Accessed 25 November 2007].

Brown, D., Cortez, R. & Minion, M., 2001. Accurate Projection Methods for the Incompressible Navier Stokes Equations. *Journal of Computational Physics,* Volume 168, pp. 464-499.

Burgers, J., 1948. A mathematical model illustrating the theory of turbulence. *Advanced Applied Mechanics,* Volume 1, pp. 171-199.

Canadian Hydraulics Centre, 2011. *Blue Kenue Reference Manual.* [Online] Available at: ftp://kenueftp.chc.nrc.ca/BlueKenue/BlueKenue.pdf [Accessed 1 october 2013].

Cawthorn, C. J. et al., 2011. *Adaptive vertical layering in TELEMAC-3D.* Chatou, France, The TELEMAC-MASCARET User Conference, pp. 137-141.

Chen, X., 2002. *Responses of a Hybrid z-Level Model to Various Topography Treatment Methods for a boundary value Problem and an Initial Value Problem.* Reston (VA.), ASCE Press, pp. 614-627.

Cornelissen, S., 2004. *Numerical Modelling of Stratified Flows, Comparison of the and z coordinate systems,* Delft: TU Delft.

Curington, I. & Bourban, S., 2009. *HR Wallingford 2D/3D Flow Modelling Strategy,* (internal): IT560, HR Wallingford.

Falconer, R. A., 1976. *Mathematical modelling of jet-forced circulation in reservoir and harbours,* Thesis submitted to: The University of London and the Imperial College of Science and Technology.

Falconer, R. A. & Owens, P. H., 1987. Numerical simulation of flooding and drying in a depth-averaged tidal model. *Proceedings of Institution of Civil Engineers,* vol 83(Part 2), pp. 161-180.

Ferracina, L. & Spijker, M. N., 2005. An extension and analysis of the Shu-Osher representation of Runge-Kutta Methods. *Mathematics and Computing,*

Volume 249, pp. 201-219.

Fortunato, A. B. & Baptista, A. M., 1996. Vertical Discretization in tidal Flow Simulations. *International Journal for numerical Methods in Fluids,* Volume 22, pp. 815-834.

Friedrichs, K., 1954. Symmetric hyperbolic linear differential equations. *Communications in Pure Applied Mathematics,* Volume 7, p. 345.

Godunov, S. K., 1959. A Difference Method for Numerical Calculation of Discontinuitous Solutions of the Equation of Hydrodynamics. *Matematicheskii Sbornik,* 47(89), pp. 271-306.

Gottlieb, S., 2005. On High Order Strong Stability Preserving Runge-Kutta and Multi Step Time Discretisation. *Journal of Scientific Computing,* 25(1/2), pp. 105-128.

Gottlieb, S. & Shu, C.-W., 1998. Total Variation Diminishing Runge-Kutta Schemes. *Mathematics of Computation,* 221(67), pp. 73-85.

Gottlieb, S., Shu, C.-W. & Tadmor, E., 2001. Strong Stability Preserving High Order Time Discretisation Methods. *SIAM,* 43(1), pp. 89-112.

Griffiths, G. W., 2007. *Wikipedia.* [Online] Available at: https://en.wikipedia.org/wiki/File:LimiterPlots1.png [Accessed 6 February 2014].

Guy, R. & Forgelson, A., 2005. Stability of approximate projection methods on cell-centered grids. *Journal of Computational Physics,* 203(2), pp. 517-538.

Hairer, E., Nørsett, S. P. & Wanner, G., 1987. *Solving Ordinary Differential Equations I - Non-Stiff Problems.* Springer-Verlag: ISBN-3 540-17145-2.

Hairer, E. & Wanner, G., 1991. *Solving Ordinary Differential Equations I --Stiff and Differential-Algebraic Problems.* Springer-Verlag: ISBN-3-875-37759.

Haney, R. L., 1991. Notes and Correspondance, On the Pressure Gradient Force over Steep Topography in Sigma Coordinate Ocean Models. *Journal of Physical Oceanography,* Volume 21, pp. 61-619.

Harlow, F. H. & Welch, J. E., 1965. Numerical Calculations of Time Dependent Viscous Incompressible Flow of Fluid with a Free Surface. *Phys. Fluid.,* Volume 8, pp. 2182-2189.

Harten, A., Lax, P. D. & van Leer, B., 1983. On upstream differencing and Godunov-type schemes for hyperbolic conservation laws. *SIAM Review,* 25(1), pp. 35-61.

Hervouet, J.-M., 2007. *Hydrodynamics of Free Surface Flows, modelling with the finite element method.* Chichester: Wiley.

Hervouet, J.-M., 2013. *Solving linear systems with iterative techniques.* [Online] Available at: http://www.opentelemac.org/downloads/TRAINING AND TUTORIALS/course_on__linear_systems-en.pdf [Accessed 21 August 2013].

Hofmeister, R., Burchard, H. & Beckers, J.-M., 2010. Non-uniform adaptive vertical grids for 3D numerical ocean models. *Ocean Modelling,* Volume 33, pp. 70-86.

Hughes, W. & Brighton, J., 1999. *Outline of Fluid Dynamics (Schaum's).* 3rd ed. New York: McGraw-Hill.

Kantha, L. & Carniel, S., 2003. Comments on < A generic length-scale equation for gephysical turbulence models > by L. Umlauf and H. Burchard. *Journal of Marine Research,* Volume 61, pp. 693-702.

Koçyigit, B., Falconer, R. & Lin, B., 2002. Three-dimensional numerical modelling of free surface flows with non-hydrostatic pressure. *International Journal for numerical Methods in Fluids,* Volume 40, pp. 1145-1162.

Krauss, E. & Turner, J., 1967. A one-dimensional model of the seasonal thermocline II. The general theory and its consequences. *Tellus*, 19(1), pp. 98-106.

Kurganov, A. & Lin, C., 2007. On the reduction of numerical dissipation in central-upwind schemes. *Communications in Computational Physics*, Volume 2, pp. 141-163.

Kurganov, A., Noelle, S. & Petrova, G., 2001. Semi-discrete central-upwind schemes for hyperbolic conservation laws and Hamilton-Jacobi equations. *SIAM Journal of Scientific Computing*, Volume 23, pp. 707-740.

Kurganov, A. & Petrova, G., 2004. Central-Upwind Schemes on Triangular Grids for Hyperbolic Systems of Conservation Laws. *Wiley InterScience*, 1 September, pp. 536-552.

Kurganov, A. & Tadmor, E., 2000. New High-Resolution Central Schemes for Nonlinear Conservation Laws and Convection-Diffusion Equations. *Computational Physics*, Volume 160, pp. 214-282.

Lamb, H., 1945. *Hydrodynamics*. 6 ed. Dover publications; Dover Books on Physics.

Large, W. G. & Gent, P. R., 1999. Validation of vertical mixing in an equatorial ocean model using large eddy simulations with observations. *Journal of Physical Oceanography*, Volume 29, pp. 449-464.

Lax, P., 1954. Weak solution of nonlinear hyperbolic equations and their numerical computations. *Communications in Pure Applied Mathemtics*, Volume 7, p. 159.

Leonard, B., 1979. A stable accurate convective modelling procedure based on quadratic upstream interpolation. *Computer Methods in Applied Mechanics and Engineering*, Volume 19, pp. 59-98.

Leonard, B., 1991. The ULTIMATE conservative difference scheme applied to

unsteady one-dimensional advection. *Computer Methods in Applied Mechanics and Engineering,* Volume 88, pp. 17-74.

Levy, D., Puppo, G. & Russo, G., 2000. On the behaviour of the total variation in CWENO methods for conservation laws. *Applied Numerical Mathematics, Elsevier,* Volume 33, pp. 407-414.

Lilly, D., 1964. Numerical Solution for the Shape-Preserving 2D Thermal Convection Element. *Journal of Atmospheric Sciences,* Volume 21, pp. 83-98.

Lin, B. & Falconer, R. A., 1997. Tidal Flow and Transport Modelling Using ULTIMATE QUICKEST Scheme. *Journal of Hydraulic Enginering,* pp. 303-314.

Lowe, R. J., Rottman, J. W. & Linden, P. F., 2005. The non-Boussinesq lock-exchange problem. Part 1. Theory and experiments. *Journal of Fluid Mechanics,* Volume 537, pp. 101-124.

McDonough, J. M., 2004. *Lecture on Turbulence – Physics, Mathematics and Modelling.* 144 pages, Department of Mechanical and Mathematics of university of Kentucky.

Mellor, G. L., Ezer, T. & Oey, L. Y., 1994. The Pressure Gradient Conundrum of Ocean Circulation Models. *Journal of Atmospheric and Oceanic Technology,* Volume 11, pp. 1126-1134.

Mellor, G. & Yamada, T., 1982. Development of a Turbulence Closure Model for geophysical Fluid Problems. *Reviews of Geophysics and Space Physcis,* Volume 20, pp. 851-875.

Morton, K. & Mayers, D., 1994. *Numerical Solution of Partial Differential Equations.* Cambridege: Cambridge University Press.

Namin, M., Lin, B. & Falconer, R., 2001. An implicit numerical algorithm for solving non-hydrostatic free-surface flow problems. *International Journal for*

Numerical Methods in Fluids, Volume 35, pp. 341-356.

Nessyahu, H. & Tadmor, E., 1990. Non-oscillatory central differencing for hyperbolic conservation laws. *Computational Physics,* Volume 87, pp. 408-463.

Perot, B., 2000. Conservation Properties of Unstructured Mesh Schemes. *Journal of Computational Physics,* Volume 159, p. 58–89.

Rauch, J., 1986. BV Estimates Fail for Most Quasilienar Hyperbolic Systems in Dimensions Greater Than One. In: *Communications in Mathematical Physics.* s.l.:Springer-Verlag, pp. 481-484.

Rawat, P. S. & Zhong, X., 2009. *High-Order Shock-Fitting and front-tracking Methods for Numerical Simulation of Shock-Disturbance Interactions.* Orlando, Florida, American Institute of Aeronautics and Astronautics.

Roache, P. J., 1998. *Verification and Validation in Computational Science and Engineering.* Albuquerque: Hermosa Publishers.

Roe, P. L., 1981. Approximate Riemann Solvers, Parameter Vectors, and Difference Schemes. *Journal of Computational Physics,* Volume 43, pp. 357-372.

Rutherford, J. C., 1994. *River Mixing.* Chischester, UK: John Wiley & Sons.

Sheu, T., Chiang, T. & Liou, S., 2000. A compact monotonic discretization scheme for solving second-order vorticity-velocity equations. *Comput. Methods Appl. Mech. Engrg.,* Volume 190, pp. 1407-1424.

Shin, J. O., Dalziel, S. B. & Linden, P. F., 2004. Gravity currents produced by lock exchange. *Journal of Fluid Mechanics,* Volume 521, pp. 1-34.

Shu, C.-W. & Osher, S., 1988. Efficient Implementation of Essentially Non-Oscillatory Schok-Capturing Schemes. *Journal of Computational Physics,* Volume 77, pp. 439-471.

Shu, C.-W. & Osher, S., 1989. Efficient Implementation of Essentially Non-oscillatory

Shock-Capturing Scheme, II. *Journal of Computation Physics,* Volume 83, pp. 32-78.

Song, Y. & Haidvogel, D., 1994. A semi-implicit ocean circulation model using a generalized topography-following coordinate system. *Journal of Computational Physics,* Volume 115, pp. 228-244.

Stelling, G. S. & van Kester, J., 1994. On the approximation of horizontal gradients in sigma co-ordinates for bathymetry with steep bottom slopes. *International Journal for Numerical Methods in Fluids,* Volume 18, pp. 915-935.

Stoker, J., 1957. Water waves. *Wiley Intersciences Publishers,* pp. 333-341.

Stokes, T. E., Hocking, G. C. & Forbes, L. K., 2007. Unsteady free surface flow induced by a line sink in a fluid of finite depth. *Computers & Fluids.*

Sweby, P. K., 1984. High resolution schemes using flux limiters for hyperbolic conservation laws. *SIAM Journal of Numerical Analysis,* Volume 21, pp. 995-1011.

Tang, H. & Tang, T., 2003. Adaptive mesh methods for one- and twodimensional hyperbolic conservation laws. *SIAM Journal of Numerical Abalysis,* Volume 41, pp. 487-515.

Toro, E., 1999. *Riemann Solvers and numerical methods for fluid dynamics.* 2nd ed. Berlin: Springer-Verlag.

Toro, E., 2009. *Riemann Solvers and Numerical Methods for Fluid Dynamics.* 3rd ed. Milton Keynes: Springer.

Toro, E. F., Spruce, M. & Speares, W., 1994. Restoration of the contact surface in the HLL Riemann solver. *Shock Waves,* Volume 4, pp. 25-34.

US Bureau of Reclamation, 1966. *Hydraulics of Stratified Flow -- First Progress Report -- An Analysis of the State of the Art and a Definition of Research*

Needs, Denver, Colorado: Office of Chief Engineer.

van Leer, B., 1979. Towards the Ultimate Conservative Difference Scheme V, A Second-Order Sequel to Godunov's Method. *Journal of Computational Physics*, Volume 32, pp. 101-136.

Weinan, E. & Jian, G., 1996. Vorticity Boundary Condition and Related Issues for Finite Difference Schemes. *Journal of Computational Physics*, Volume 124, pp. 368-382.

Winslow, A. M., 1966. Numerical solution of the quasilinear Poisson equation in a nonuniform triangle mesh. *Journal of Computational Physics*, Volume 1, pp. 149-172.

Zhang, X., Schmidt, D. & Perot, B., 2004. Accuracy and Conservaion Properties of a Three-Dimensional Unstructured Staggered Mesh Scheme for Fluid Dynamics. *Continental Shelf Research*, Volume 24, pp. 2187-2214.

Zienkiewicz, O. C. & Taylor, R. L., 2000. *The Finite Element Method, Volume 1: The Basis*. 5th ed. Oxford: Butterworth-Heinemann.

Zienkiewicz, O. C. & Taylor, R. L., 2000. *The Finite Element Method, Volume 3: Fluid Dynamics*. 5th ed. Oxford: Butterworth-Heinemann.

Appendix A
List of symbols

x, y, z Cartesian space coordinates with x and y distances in the horizontal plane along the x–axis and y-axis respectively, and z distance along the vertical z-axis. Distances are in metres.

Δx Spatial step in metres

r, θ and ϕ Polar and spherical coordinates in the mathematics notation, where the radial distance, r is such that $r^2 = x^2 + y^2 + z^2$, the azimuthal angle, θ is such that $tan\theta = y/x$, and the polar angle ϕ is such that $cos\phi = z/r$.

t Time in seconds.

Δt Temporal step in seconds.

$\vec{u}$ Velocity vector in m/s

u, v Conponents of the horizontal velocity vector $\vec{u}$ along the x-axis and y-axis respectively.

h or H Water depth, function of t time and of the location (x, y), in particular.

η Free surface elevation, function of t time and of the location (x, y), in particular

p The pressure in kg/(ms^2), also Pascal.

g Gravitational constant in m/s^2

ρ Fluid density in kg/m^3

μ_{xy} and μ_z Respectively the horizontal and vertical dynamic viscosity coefficients.

κ_{xy} and κ_z Respectively the horizontal and vertical turbulent (or eddy) diffusivities.

F_x, F_y and F_z Represent the three components of the body forces.

S_w and S_T Source or sink terms of water and trcaer respectively.

w Depending on context, the vertical velocity component or an arbitrary vector or conserved dependent quantity.

T Depending on context, tracer concentration, temperature, or conserved dependent scalar quantity, function of t time and of the location (x, y, z), in particular.

F Depending on context, a flux of a dependent quantity through an area within a numerical framework, or a body force within a mathematical framework.

i, j and k Indices at for representative nodes on a grid or mesh.

n Depending on context, either the index of the planar surface between the bottom and the free surface (subscript), or the time level (superscript).

$\vec{n}_{ij}$ Normal vector to the edge or the face between two cells, cell i and j.

l_{jc} The distance between node j and the centre of the mid-edge joining the centroid with the ij-edge mid-point.

Γ_{ij} The area of a face at the interface between two cells, cell i and j.

$()_j^n$ Quantity located at the cell index j in a mesh, at a time n.

$()_{j+\frac{1}{2}}^n$ Quantity located at the interface between cells index j and $j+1$ in a mesh, at a time n.

$H_{j+\frac{1}{2}}$ The fluxes of a dependent quantity through an area, located at the interface between cells index j and $j+1$ in a mesh.

The notation is based on the work of Kurganov & Tadmor (2000).

$a^n_{j+\frac{1}{2}}$ The maximum local wave speed at the discontinuity $x_{j+\frac{1}{2}}$ at time n
The notation is based on the work of Kurganov & Tadmor (2000).

γ, ξ and θ Arbitrary parameters, varying between 0 and 1.

λ_i Eigen values of a matrix.

$()^{\prec}$, $()^{\succ}$ Superscript symbols $\prec$ and $\succ$ define the assumed right and left values respectively of a quantity about an interface or a dicontinuity.

$|\ |$ Absolute value of a quanty.

$\|\ \|$ Norm of a vector function.

$\langle\ .|.\ \rangle$ or $\overrightarrow{\ .\ }\cdot\overrightarrow{\ .\ }$ Define the scalar product between two vector functions

$\forall j$ For all indices j in the list of possible indices.

φ The scalar velocity potential (where the flow is irrotational) such that $\vec{u} = \vec{\nabla}\varphi$.

$\vec{\Lambda}$ and ψ The vector velocity potential (where the flow is incompressible) such that $\vec{u} = \vec{\nabla} \times \vec{\Lambda}$.
In the particular case of axis symetry (or in 2D plane), the vector velocity potential is replaced by the stream function ψ, where the lines of constant φ intersect lines of constant ψ perpendicularly.

BLANK PAGE IN ORIGINAL

Appendix B
3D free surface solvers

A list of twenty four 3D free surface solvers has been assembled and where possible the source code downloaded. Although incomplete, the list illustrates differences and commonalities of the principal features between solvers and provides an overview of the present state of the art. In addition, two separate sections have been added, prior to the list, to provide more details about SULIS (see Section B.1) and TELEMAC (see Section B.2), which were used as modelling frameworks in the present research work.

Separately from the work presented here, it should be highlighted that the list and its associated analysis was in part used by HR Wallingford in an internal research and development strategy document (Curington & Bourban, 2009).

B.1. Particular case of SULIS

The author of the present work wrote the finite difference 3D solver SULIS (Bourban, 1997) on the basis that it had to be a fully implicit solver where all equations are coupled within one linear algebra system.

SULIS splits the geometrical domain with cells that are each defined by a single vertical segment (or water column) and one horizontal layer. Each cell has 6 independent sides not necessarily arranged in parallel pairs. It should be noted that

this generic definition provides flexibility in the shape of each segment (hence of the cell contained) and of its connections to the neighbouring segments. The continuity and tracer mass conservation equations are written within cells, using the fluxes through all sides. The momentum equations are written at all connecting sides. The discretisation of the primary variables follows the Arakawa-C scheme (Arakawa & Lamb, 1977).

Unlike other models, SULIS solves its linear matrix system using a cascade of iterative solvers, most of which are based on the conjugate gradient concept. Although it has never been proven, the author believes that the use of a cascade accelerates the overall process for SULIS. This is supported by the following observations:

- Certain iterative solvers are faster at finding rough solutions from an inadequate initialisation, whereas other iterative solvers are efficient at finding precise solutions but only when starting from a good initialisation. A cascade of solvers, in an appropriate order, therefore optimises the combination of behaviours.

- Conjugate gradient methods vary in their choice of a downhill path to find a solution, with the most obvious downhill directions and displacements used first. A cascade of solvers therefore shakes and mixes the approaches.

A "Morse" or sparse storage is used for all solvers, where 3 arrays (a single array of double precision numbers A, and two arrays of integer numbers I and J) are used solely to store the non-zero coefficients terms of the matrix A_{IJ}.

B.1.1. Original assumptions

Prior to 2006, SULIS solved the advective form of the continuity and Navier-Stokes equations (see Section Ch.3-1.1in Chapter 3) under the following assumptions: (a) the density variations were ignored except in the pressure terms; (b) the third equation of momentum was reduced to the hydrostatic assumption, where the pressure gradient term is the result of two actions, the water surface slope and the density gradient; and (c) turbulent fluctuations were ignored. Further, SULIS solved the continuity equation under the following assumptions: (a) the fluid was incompressible; and (b) the variation of density with the space coordinates is negligible relative to other variations. In addition, a simplification was used at the free surface, in that a direct correspondence was made between the vertical velocity of the free surface and the variation of the water level in time.

From a temporal viewpoint, SULIS was based on the fully implicit, first order backward Euler time integrator. Although the implicitness of the scheme would suggest use of larger time steps, the ability of the scheme to maintain sharp gradients prevented from doing so. From a spatial viewpoint, SULIS implemented a symmetrical centred difference scheme, even though monotonicity of the solution could not be guaranteed.

B.1.2. Improvements to SULIS

One of the first tasks of the work on SULIS was to re-write all equations in their divergence (or conservative) form (see Section Ch.3-1.2). A first order upwind advection scheme was also added to prevent oscillatory behaviour. Finally, the non-hydrostatic terms were also included based on the direct pressure computation

through the vertical momentum equation (see Section Ch.3-1.8). The validity of the latter approach is demonstrated by comparison against an analytical solution (see Section Ch.4-2).

B.2. Particular case of TELEMAC-3D

TELEMAC-3D is the 3D hydrodynamic module of the open TELEMAC-MASCARET system of the Laboratoire National d'Hydraulique et Environnement of Electricité de France (EDF-LNHE).It is distributed as open source software by HR Wallingford and is available at: *http://www.opentelemac.org/*. Other developers of the open TELEMAC system include the Bundes Anstalt für Wasserbau in Germany and the STFC's Daresbury Laboratory (Science & Technology Facilities Council) in the UK.

TELEMAC-3D is a three-dimensional hydrodynamic solver based on a generalised sigma-stretched transformation, where the 2D mesh is extruded vertically into a volume between the surface defining the bottom of the model and the surface defining the water free surface. A constant number of intermediate surfaces further discretises the vertical columns, resulting in a layered mesh, where each layer is defined as the volume between two adjacent surfaces. Each surface is supported by 2D unstructured mesh; all surfaces are stacked one above the other and project to the same 2D unstructured mesh; each layer is made of prism elements. It is noted that the 3D elements are wedges, and that the name only comes from the 3D finite element method computed on a prism.

TELEMAC-3D offers the user a choice between a hydrostatic pressure and a non-hydrostatic pressure formulation, for which the dynamic pressure is the result of the projection method (solving for a Poisson equation). Turbulent closure models include

constant eddy viscosity, Smagorinsky and k-ε models (where k is the turbulent kinetic energy and ε is the turbulent dissipation).

The open TELMAC system undertakes parallel computations based on domain decomposition, whereby the computational domain is split into sub-domains grouping sets of triangles. In order to optimise parallel performance, i.e. limit the communications between sub-domains and triangles, the EBE (element-by-element) formulation is used, for which the majority of finite element implementation is compounded within triangles before being assembled globally. It is important to note that the EBE formulation was first developed in the open TELEMAC system as a technique to optimise storage to make matrix-vector products as efficient as possible on the assumption that it is not necessary to assemble a matrix (in a finite element manner) in order to multiply it by a vector. Its parallel framework is based on the Message Passing Interface (MPI).

The numerical framework in open TELEMAC uses a semi implicit time integrator. Its finite element formulation is based on SUPG (Streamline upwind Petrov-Galerkin).

It should be highlighted that the author of the present work is currently the President of the TELEMAC-MASCARET Consortium and responsible at HR Wallingford for its continuous maintenance and international distribution. Since 1997, the author has developed and used various modules of the open TELEMAC system through many commercial consultancy studies.

B.2.1. Original assumptions

In order to refine the resolution in the vicinity of stratification interfaces in estuaries

and lakes, the spacing between intermediate surfaces can be reduced in two ways:

- Increasing the number of intermediate surfaces (for the whole domain by definition). This, in turn, increases the computation cost while being wasteful in those areas where capturing the fine detail of the dynamics is unnecessary.

- Carefully choosing the placement of the intermediate surfaces at the start of the simulation based on the expected solution. However, prior knowledge of the flow structure could require an iterative process gradually adjusting the plane positions and re-running the simulation for convergence on an 'optimal' configuration.

B.2.2. Improvements to TELEMAC-3D

Two major improvements implemented recently in TELEMAC-3D are detailed in this thesis.

First a new advection scheme has been implemented for the tracer transport equation within the existing finite element and parallel framework. The same numerical scheme was chosen because it could be extended to the Saint Venant and the Navier-Stokes equations as well as turbulence closure. Although not presented here, a new numerical scheme of the horizontal diffusion terms was similarly prototyped in TELEMAC-3D by M.S. Turnbull under the leadership of the author of the present work, based on the advection schemes investigated and developed herein.

Second, an adaptive mesh displacement method was implemented to further refine the vertical resolution in the vicinity of high gradients of conservation quantities, such as found in stratified waters. Although designed by the author, the method was implemented in TELEMAC-3D by C.J. Cawthorn with the help of J.-M. Hervouet at

EDF-LNHE, under the supervision of the author.

B.3. Existing 3D free surface solvers

The following list is in alphabetical order. Each item of the list is accompanied by a summary text usually derived from the relevant website cited.

B.3.1. ADCIRC

ADCIRC is available for academic use as an open source code from the University of North Carolina. It is being developed by teams at the University of Notre Dame, the University of Oklahoma, the University of Texas, and others. Commercial license distribution is non-exclusively available through AQUAVEO for instance (*http://www.aquaveo.com/software/sms-surface-water-modeling-system-introduction*).

ADCIRC is a 3D finite element system using the traditional hydrostatic pressure assumption. The free surface elevation is obtained from the solution of the depth-integrated continuity equation in a generalized wave-continuity equation form. Velocity is obtained from the solution of 3D momentum equations. The parallel capabilities of ADCIRC are based on a domain decomposition strategy with information at sub-domain interfaces being passed using the MPI library. Performance is linearly proportional to the number of nodes, time steps, and processors. ADCIRC includes a transport model and has an implicit time scheme. ADCIRC is the closest relative to the open TELEMAC system. The theoretical report can be accessed from:

http://www.unc.edu/ims/adcirc/adcirc_theory_2004_12_08.pdf

The computational engine in ADCIRC is currently being upgraded from a Continuous Galerkin (CG) based solution to a new h-p adaptive Discontinuous Galerkin (DG) based algorithm.

B.3.2. CH3D-WES and CH3D-SED

CH3D-WES and CH3D-SED (Curvilinear Hydrodynamics in 3-Dimensions) are available from the Coastal and Hydraulics Laboratory (CHL, *http://chl.erdc.usace.army.mil/*) of the US Army Corps of Engineers (USACE).

The solvers are time varying three-dimensional numerical hydrodynamic, salinity, and temperature models. The horizontal grid is a general non-orthogonal curvilinear grid; the vertical grid is a sigma-stretched grid. The solvers are based on the hydrostatic assumption and solve a two-equation $k - \epsilon$ turbulence model. The principal user manual is available through:

http://chl.erdc.usace.army.mil/%5CMedia%5C7%5C7%5C5%5CHL-TR-96-21.pdf

B.3.3. COHERENS

COHERENS (COupled Hydrodynamical-Ecological model for REgioNal Shelf seas) is available from the Management Unit of the North Sea Mathematical Models (MUNSMM, *http://www2.mumm.ac.be/coherens/*) of the Royal Belgian Institute of Natural Sciences.

The solver is a mathematical three-dimensional hydrodynamic multi-purpose model for coastal and shelf seas, which resolves mesoscale to seasonal scale processes. The

solver is available as a free source code for the scientific community. The model equations are discretised on an Arakawa C-grid (1977) using either a rectangular or a curvilinear grid in the horizontal directions. The program uses sigma-stretched coordinates in the vertical. The principal user manual is available through:

ftp://ftp.mumm.ac.be/coherens/V2.0/manualV2.0.pdf

Several further updates with improvements and additional features are due to be released in the near future, including an implicit scheme which removes the mode splitting scheme.

B.3.4. D-FLOW of the Delft3D suite

The Delft3D suite (and its hydrodynamic module D-FLOW) can be purchased from Deltares Systems, formerly WL | Delft hydraulics (*http://www.deltaressystems.com/hydro*).

Delft3D is a flexible integrated modelling suite, which simulates two-dimensional (in either the horizontal or a vertical plane) and three-dimensional flow, sediment transport and morphology, waves, water quality and ecological proceses, and is capable of handling the interactions between these processes. Its D-Flow module simulates non-steady 2D hydrostatic flows in relatively shallow water on curvilinear and rectilinear grids. D-Flow covers salinity, temperature and species transport, density driven flows, float (drogue) tracking, meteorological influences, and wave-current interaction. D-Flow also includes 3D flow and turbulence modelling, spherical grids, domain decomposition, and horizontal large eddy simulations (sub-grid turbulence in the horizontal plane). Vertical representation is based on a sigma-stretched transformation.

Current developments in the Delft3D suite include: unstructured mesh support (an integrated engine based on 1D networks and 3D/2D layered mesh of mixed triangles, quadrilaterals, and more complex cells), a non-hydrostatic and a z-layer option, and parallel computing.

B.3.5. DieCAST

DieCAST (Dietrich Center for Air Sea Technology) is available from the National Taiwan University (*http://efdl.as.ntu.edu.tw/research/diecast/*).

DieCAST is a primitive equation, z-level ocean and lake model patterned after the Sandia Ocean Modeling System (SOMS). The original DieCAST model is hydrostatic, incompressible, rigid-lid, partially implicit, and uses an "Arakawa A" grid (1977). DieCAST uses a higher order treatment of the dominant terms in ocean dynamics, i.e. pressure gradient and Coriolis. This leads to accurate and robust (stable with realistically small dissipation) models. In the latest version, the model includes the non-hydrostatic, free surface, immersed boundary method and two-way coupling capabilities. The principal user manual is available through:

http://efdl.as.ntu.edu.tw/research/diecast/publication/users_manual.pdf

B.3.6. EFDC

The Environmental Fluid Dynamics Code (EFDC) is available from Dynamic Solutions-International, LLC (DS-INTL, *http://www.ds-intl.biz*) as open source. EFDC was originally developed at the Virginia Institute of Marine Science.

EFDC is a general-purpose modelling package for simulating three dimensional flow,

transport, and biogeochemical processes in surface water systems including, rivers, lakes, estuaries, reservoirs, wetlands, and near-shore to shelf-scale coastal regions. In addition to hydrodynamic and salinity and temperature transport simulation capabilities, EFDC is capable of simulating cohesive and non-cohesive sediment transport, near-field and far-field discharge dilution from multiple sources, the transport and fate of toxic contaminants in the water and sediment phases, and the dissolved oxygen/nutrient process (i.e. eutrophication). Special enhancements to the hydrodynamics of the code, including treatment of vegetation resistance, drying and wetting, hydraulic structure representation, wave current boundary layer interaction, and wave-induced currents, allow refined modelling of wetland and marsh systems, controlled-flow systems, and near-shore wave-induced currents and sediment transport. The solver solves the hydrostatic, turbulent-averaged equations on an orthogonal curvilinear horizontal grid and a sigma-stretched vertical grid. A Mellor-Yamada (1982) level 2.5 turbulence closure scheme is implemented.

B.3.7. ELCOM

ELCOM (Estuary and Lake Computer Model) can be purchased from the Centre of Water Research of the University of Western Australia (*http://www.cwr.uwa.edu.au/software1/models1.php?mdid=5*).

ELCOM is a three-dimensional solver of the Reynolds-averaged Navier-Stokes equations (see Section Ch.3-1.1 in Chapter 3) offering both hydrostatic pressure and non-hydrostatic pressure calculation. The equations are represented on an orthogonal z-layered mesh. The numerical discretisation is based on a second-order accurate Crank-Nicolson scheme. The scalar transport uses a conservative 3rd order scheme expanding similar concepts adopted in TRIM. The Cartesian grid solver uses a

traditional staggered-grid approach. ELCOM has been developed over an extended period and has a unique formulation of vertical stratification, where consecutive layers may be grouped according to stable, unstable, or mixed stratifications. Heat transfer, and density stratification are computed through the water column on a layer-by-layer basis, by computing the available mixing energy at each time step. The principal scientific documentation is available through:

http://www.cwr.uwa.edu.au/software1/CWRDownloads/modelDocs/ELCOM_Science.pdf

B.3.8. FEOM

FEOM (Finite Element Ozean Model) is available from the Alfred Wegener Institute (AWI), in Germany (*http://www.awi.de//en/home/*).

FEOM uses a vertical coordinate scheme which supports z-level and sigma-stretched coordinates as well as any possible combinations of these. On z-level meshes, FEOM supports full cells, shaved cells and partly shaved cells, on an unstructured plan mesh. Vertical prismatic cells are used for the Galerkin Finite Element numerical computations. FEOM utilises the Boussinesq approximation in hydrostatic cases. Advection schemes: FEOM permits selection between Taylor-Galerkin, Crank-Nickolson and Flux-Corrected-Transport advection schemes. The time stepping is based on a variant of the implicit free surface method, which simultaneously serves to stabilize the pressure modes allowed by the chosen discretization.

B.3.9. FVCOM

FVCOM is available as open source from the School of Marine Science and Technology of the University of Massachusetts (*http://fvcom.smast.umassd.edu/FVCOM/index.html*).

The solver is a three-dimensional solver using a sigma-stretched transformation vertically and an unstructured triangular cell grid horizontally. The finite-volume method used in FVCOM combines the advantages of a finite element method for geometric flexibility and a finite-difference method for simple discrete computation. It is closed physically and mathematically using the Mellor and Yamada (1982) level 2.5 turbulence closure scheme. FVCOM supports both local and global momentum, mass, salt, heat, and tracer conservation. The principal user manual is available through:

http://woodshole.er.usgs.gov/staffpages/rsignell/rps/share/FVCOM_Manual.pdf

Recent additions include non-hydrostatic and spherical coordinate schemes to resolve vertical convection, internal waves, and small scale baroclinic instability. Recent efforts to improve parallel computational efficiency are based on mesh partitioning with METIS, and MPI communication layers.

B.3.10. HEMAT

HEMAT (Hydro-Environmental Modelling and Analysis Tool) is a 3D research system developed by M.M. Namin of the Water Research Centre, Tehran, Iran in collaboration with R.A. Falconer at Cardiff University, UK. It is, however, not generally available except to students of Cardiff University.

HEMAT solves the Reynolds-averaged Navier-Stokes equations and the kinematic free

surface boundary condition simultaneously, so that the water surface elevation can be integrated into the solution together with the velocity and pressure fields. An efficient numerical algorithm has been developed, deploying implicit parameters similar to those used in the Crank–Nicholson method, and generating a block tri-diagonal algebraic system of equations. The model has been applied to simulate a range of unsteady flow problems involving relatively strong vertical accelerations. HEMAT includes both hydrostatic and non-hydrostatic modes, on triangular meshes.

B.3.11. hpGEM / DG-FEM

hpGEM / DG-FEM is a research system available at the University of Twente (*http://cinder.cwi.utwente.nl/hpGEM/*).

The solver was developed by Ambati and Bokhove. It uses 2D and 3D finite-element discretisations of the shallow water equations, based $h-p$ Discontinuous Galerkin (DG) methods. The hpGEN / DG-FEM is second-order accurate in both space and time for linear polynomials, is able to follow irregular bathymetry, and can model discontinuities such as bores and hydraulic jumps. It has been applied to intermediate scale ocean waves, coastal currents and breaking waves. The linear algebra solver uses LAPACK.

B.3.12. ICOM - FLUIDITY

ICOM and FLUIDITY are research hydrodynamics solvers from the Applied Modelling and Computation Group at Imperial College, London. They are available as open

source software from

http://www3.imperial.ac.uk/earthscienceandengineering/research/amcg/fluidity

The ICOM solver is non-hydrostatic, using an unstructured 3D tetrahedral Finite Element grid to conform to coastlines and steep beds with adaptive re-meshing to track flow and bathymetry gradients, with application to tsunami, and coastal ocean modelling. FLUIDITY is a closely related generalised CFD model with application to fine scale eddy, vortex formation and complex boundary geometry. ICOM and FLUIDITY are particularly suited to fully 3D problems with significant transient flow features such as tsunami and flow-structure dynamic interaction. Arbitrary vertical flow is addressed over a range of large to local scales. Applications to tidal, tsunami, and ocean thermohaline circulation are emphasised by the authors on the website serving the solver. ICOM also has research extensions for internal wave breaking, LES, salt fingering, spherical coordinates, wetting & drying. A Mellor-Yamada (1982) level 2.5 turbulence closure scheme is implemented. FLUIDITY employs an SUPG equation solver.

The principal user manual is available through:

http://launchpad.net/fluidity/4.1/4.1.9/+download/fluidity-manual-4.1.10.pdf

B.3.13. MICOM, HYCOM and HIM

These solvers are available from the Rosenstiel School of Marine and Atmospheric Science (RSMAS) of the University of Miami (*http://hycom.org/*) HYCOM and HIM are based on MICOM.

These are based on the primitive equations horizontally discretized on an "Arakawa C"

grid (1977). Vertical turbulence is implemented through the mixed layer depth approach by Krauss Turner (1967). HIM includes Smagorinsky's biharmonic viscosity, with parallel versions on MPI libraries. The hybrid coordinate is one that is isopycnal in the open, stratified ocean, but smoothly reverts to a terrain-following coordinate in shallow coastal regions, and to z-level coordinates in the mixed layer and/or unstratified seas. The hybrid coordinate extends the geographic range of applicability of traditional isopycnic coordinate circulation models (the basis of the present hybrid code), such as the Miami Isopycnic Coordinate Ocean Model (MICOM) and the Navy Layered Ocean Model (NLOM), toward shallow coastal seas and unstratified parts of the world ocean. The principal scientific documentation is available through:

http://hycom.org/attachments/063_hycom_users_manual.pdf

B.3.14. MIKE 3

MIKE3 can be purchased from The Danish Hydraulics Institute (DHI), Denmark

(*http://www.mikebydhi.com/Products/CoastAndSea/MIKE3.aspx*)

It is a three-dimensional hydrodynamic solver of the Reynolds-averaged Navier-Stokes equations (see Section Ch.3-1.1 in Chapter 3). It offers a choice between a hydrostatic pressure assumption combined with a generalised sigma transformation and a non-hydrostatic pressure formulation combined with a z-level coordinate formulation. A total of five different turbulent closures can be employed: constant eddy viscosity, Smagorinsky subgrid scale model, k model, $k-\epsilon$ model, or a mixed Smagorinsky / $k-\epsilon$ model. Using "FM" flexible mesh, MIKE 3 offers a triangulated plan grid scheme. A parallel multi-core version is available. The FM version is currently restricted to hydrostatic, but is able to model shocks as it solves hydrodynamics using a Roe approximate Riemann solver, with 2^{nd} order accuracy

using a linear gradient reconstruction. The structured (non-FM) version uses an ADI finite difference scheme with selective upwinding to model hydraulic jumps.

B.3.15. MOM

MOM (Modular Ocean Model) is available at the Geophysical Fluid Dynamics Laboratory of the National Oceanic and Atmospheric Administration (NOAA), USA (*http://www.mom-ocean.org/web*).

It is a hydrostatic three-dimensional solver of the primitive equations using generalised orthogonal horizontal coordinates, with spherical curvilinear coordinates for special cases. Bottom topography is represented using a partial cell approach. Vertical mixing schemes include various mixing length turbulence closure model. MOM is one of the oldest and established models still in use. The principal scientific documentation is available through:

http://www.mom-ocean.org/web/docs/project/user_guide

Current developments include integrating features from HIM (Isopycnal Z) and MITcgm (Coupled Ocean-Climate models).

B.3.16. POM

POM (Princeton Ocean Model) is co-developed at the Atmospheric and Oceanic Sciences Program of Princeton University, at the Geophysical Fluid Dynamics Laboratory of the National Oceanic and Atmospheric Administration (NOAA), and The Dynalysis of Princeton, USA (*http://www.aos.princeton.edu/WWWPUBLIC/htdocs.pom/*)

POM is a three-dimensional solver based on the "Arakawa C" differencing scheme with a vertical sigma transform and a horizontal curvilinear orthogonal coordinates. The turbulence closure sub-model is the Mellor and Yamada (1982) level 2.5 turbulence model. The principal list of scientific documentation is available through:

http://www.aos.princeton.edu/WWWPUBLIC/htdocs.pom/PubOnLine/POL.html

B.3.17. QUODDY

QUODDY is available from the Dartmouth College in New Hampshire, USA (*http://www-nml.dartmouth.edu/Software/quoddy/documentation.html*).

QUODDY is a three-dimensional solver of the shallow water hydrodynamics with implicit linear triangular finite elements. The turbulence closure scheme can either be set to a mixing length model or to the Mellor and Yamada (1982) level 2.5 turbulence model. The principal scientific documentation is available through:

http://www-nml.dartmouth.edu/Software/quoddy/quoddy3/quoddy3.3/documentation/Q3_3.ps

B.3.18. RMA10

RMA10 is available from Resource Management Associates, California, (*http://chl.erdc.usace.army.mil/rma10*) with modifications made by the US Army Corps of Engineers (USACE) Waterways Experiment Station (WES).

RMA10 is a three-dimensional finite element hydrodynamic model of the Reynolds averaged form of the Navier-Stokes equations (see Section Ch.3-1.1 in Chapter 3). It assumes hydrostatic pressure. Vertical turbulence is estimated with either a quadratic

parameterisation of turbulent exchange or a Mellor and Yamada (1982) level 2.5 turbulence model. RMA10 is only available commercially, and uses an unstructured mesh.

B.3.19. ROMS and TOMS

ROMS (Regional Ocean Modeling System) and TOMS (Terrain-following Ocean Modeling System) are available from the Office of Naval Research (ONR), of the US Navy (*http://chl.erdc.usace.army.mil/rma10*) and several universities including Rutgers University, Stanford University, Princeton University and the University of California.

ROMS and TOMS are identical, although ROMS remains the scientific community model while TOMS is the operational community model. They are split-explicit, free surface, hydrostatic primitive equation ocean models with horizontal orthogonal curvilinear coordinates and stretched terrain-following vertical coordinates. The algorithms include a computational non-linear kernel and a tangent linear and adjoin kernels. The closure schemes are based on the Mellor and Yamada (1982) level 2.5 turbulence sub-model. These models are widely used, spawning other derived research codes such as SYMPHONIE, and CHIMP.

Currently, the data exchange between nodes is done with MPI. However, other protocols like MPI2, SHMEM, and others can be coded without much effort.

B.3.20. SCRUM

SCRUM (S-Coordinates Rutgers University Model) is available from Rutgers University (*http://marine.rutgers.edu/po/models/scrum.html*)

SCRUM solves the free surface, hydrostatic, primitive equations over variable topography using stretched terrain-following coordinates in the vertical and orthogonal curvilinear coordinates in the horizontal. Earlier versions of SCRUM are described by Song and Haidvogel (1994). The model equations are solved separately for total momentum and vertically integrated momentum and then coupled. The total momentum and tracer equations are time discretized using a 3rd Adams-Bashforth scheme; the vertical viscosity/diffusion terms are treated implicitly using a Crank-Nicolson scheme. The free surface and vertically integrated momentum equations are time discretized using a trapezoidal Leapfrog scheme. Horizontal and vertical derivatives are evaluated using finite differences on a staggered horizontal Arakawa C-grid (1977) and a staggered vertical grid.

New features will include vertical staggered grid, replacing vertical finite elements by finite differences, an option for horizontal and vertical Smolarkiewicz advection, rotated mixing tensors to mix on constant z-surfaces and constant "in situ" density surfaces several turbulence closures including Mellor and Yamada (1982) level-2.5 closure.

B.3.21. SHELFE and ELCIRC

SHELFE and ELCIRC is a closely-related pair of codes available from the School of Science & Engineering of the Oregon Heath & Science University, USA (*http://www.stccmop.org/knowledge_transfer/software/selfe* and *http://www.ccalmr.ogi.edu/CORIE/modeling/elcirc/* respectively)

SHELFE and ELCIRC are three-dimensional solvers, greatly inspired by UnTRIM, combining horizontally unstructured grids with vertical z-coordinates. ELCIRC is an

unstructured-grid model designed for the effective simulation of 3D baroclinic circulation across river-to-ocean scales. It uses a finite-volume/finite-difference Eulerian-Lagrangian algorithm to solve the shallow water equations, written to address a wide range of physical processes and of atmospheric, ocean and river forcing. SELFE uses a semi-implicit finite-element/volume Eulerian-Lagrangian algorithm to solve the continuity and Navier-Stokes equations (in either hydrostatic or non-hydrostatic form). The numerical algorithm is low-order for ELCIRC and high-order for SELFE. SELFE is able to follow bed slopes with a hybrid SZ vertical mesh scheme whereas ELCIRC uses a stair-step discretisation on bed depth. Geophysical turbulence closure is based on a generic length-scale equation. The principal user documentation is available through:

http://www.stccmop.org/knowledge_transfer/software/selfe/v3manual and

http://www.stccmop.org/knowledge_transfer/software/selfe/elcirc_54c_user_manual

Higher order and non-hydrostatic enhancements are in development. The parallel version uses the mesh decomposition package ParMetis, with MPI.

B.3.22. SUNTANS

SUNTANS is available from Stanford University (*http://www.stanford.edu/group/suntans/cgi-bin/index.php*)

SUNTANS is a non-hydrostatic, unstructured-grid, parallel, coastal ocean simulation tool that solves the Navier-Stokes equations (see Section Ch.3-1.1 in Chapter 3) under the Boussinesq approximation with a large-eddy simulation of the resolved motions. The formulation is based on the method by Casulli at the University of Trento, where the free surface and vertical diffusion are discretized with the theta-method, which

eliminates the Courant condition associated with fast free surface waves and the friction term associated with small vertical grid spacing at the free surface and bottom boundaries. The grid employs z-levels in the vertical and triangular cells in the horizontal plane. Advection of momentum is accomplished with the 2nd order accurate unstructured-grid scheme of Perot (2000), and scalar advection is accomplished semi-implicitly using the method of Gross (1999), in which continuity of volume and mass are guaranteed when wetting and drying is employed. The theta-method for the free surface yields a two-dimensional Poisson equation, and the non-hydrostatic pressure is governed by a three-dimensional Poisson equation. The message-passing interface (MPI) is employed for use in a distributed memory parallel computing environment. Load balancing and grid-partitioning are managed using the ParMETIS package.

B.3.23. TriVAST (and its 2D related cousin DIVAST)

TriVAST and its 2D related cousin DIVAST (Depth-Integrated Velocities and Solute Transport) are developed at Cardiff University, sponsored by the Halcrow Group (*http://hrc.engineering.cf.ac.uk/*). The solvers are exclusively available to students at Cardiff University and close collaborators.

The solvers are used to predict a range of water quality indicators, including salinity, temperature, coliforms, biochemical oxygen demand and nitrogen and phosphorous cycles, phytoplanktonic algae, non-cohesive and cohesive sediments and heavy metals. The 2D hydrodynamic module is based on the solution of the depth integrated Navier-Stokes equations (see Section Ch.3-1.1 in Chapter 3) solved using the alternating direction implicit (ADI) finite difference technique. The advective accelerations are written in a time centred form for stability, with these terms and the turbulent diffusion terms being centred by iteration. The finite difference equations are

formulated on a space staggered grid scheme, with the water surface elevations and the x-direction velocity components being initially solved for during the first half time step by using Gaussian elimination and back substitution before proceeding to the second half time step and repeating the process for the implicit description of the y-direction derivatives and velocity components. The advective terms are treated using a higher order accurate ULTIMATE QUICKEST formulation.

B.3.24. UnTRIM and TRIM

UnTRIM and TRIM are developed by the University of Trento, Italy and have been the starting point of many other solvers such as ELCOM or SHELFE and ELCIRC or SUNTANS. At the time of writing of the present thesis, these codes are not available for download through a website.

UnTRIM and TRIM are semi-implicit finite difference (-volume) models based on the three-dimensional shallow water equations. UnTRIM is able to work on unstructured orthogonal grids, where the line joining the centres of two adjacent cells is orthogonal to the edge common to the two cells, whereas TRIM is the structured grid predecessor. UnTRIM supports both hydrostatic, and non-hydrostatic modes, with Reynolds-averaged Navier-Stokes equations (RANS), vertical turbulent viscosity influenced by density stratification, and both barotropic and baroclinic vertical pressure gradients. The parallel version uses shared-memory OpenMP, suitable for multi-core PCs but not clusters.

BLANK PAGE IN ORIGINAL

Appendix C–
Tools for the development of analytical solutions

Appendix C introduces a summary of the general concepts and notations behind analytical solutions of the Laplace and Poisson equations in various coordinate systems, following Bowles (2007). American notation (or mathematics notation) is chosen for the spherical coordinates because of its compatibility with polar coordinates.

Therefore the following are defined: the radial distance, r such that $r^2 = x^2 + y^2 + z^2$, the azimuthal angle, θ such that $tan\theta = y/x$, and the polar angle ϕ such that $cos\phi = z/r$, where x, y, and z are the three axis of the Cartesian space.

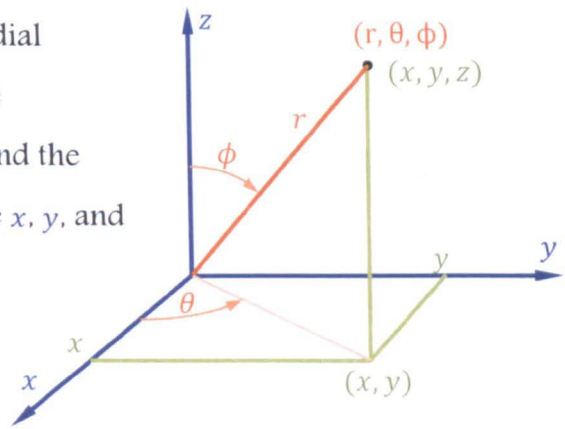

C.1.Notions from potential flow theory

C.1.1. Scalar and vector potentials

In potential flow theory, it is customary to derive the velocity vector $\vec{u}$ from a scalar velocity potential φ and / or a vector velocity potential $\vec{\Lambda}$:

- Where the flow is irrotational ($\vec{\nabla} \times \vec{u} = 0$) there exists a scalar velocity potential φ such that $\vec{u} = \vec{\nabla}\varphi$, in which case the continuity condition $\vec{\nabla}.\vec{u} = q_{Srce}$ leads to a Poisson equation for φ, $\vec{\nabla}.\vec{\nabla}\varphi = \Delta\varphi = q_{Srce}$, or a Laplace equation $q_{Srce} = 0$; and

- Where the flow is incompressible ($\vec{\nabla}.\vec{u} = 0$) there exists a vector velocity potential $\vec{\Lambda}$ such that $\vec{u} = \vec{\nabla} \times \vec{\Lambda}$, in which case the rotational condition $\vec{\nabla} \times \vec{u} = \vec{\omega}$ leads to three Poisson equations, $\vec{\nabla} \times \vec{\nabla} \times \vec{\Lambda} = \vec{\Delta}\vec{\Lambda} = \vec{\omega}$, one for each component of $\vec{\Lambda}$ (hence the vector notation of the Laplace operator) or three Laplace equations where $\vec{\omega} = 0$.

C.1.2. Change of coordinates

When restricting potential flow theory to a 2D plane, the potential velocity vector becomes perpendicular to the 2D plane and reduces to its third component, noted ψ, the stream function. As a result, where the flow is both irrotational and incompressible:

- In 2D Cartesian coordinates, $u_x = \frac{\partial\varphi}{\partial x} = \frac{\partial\psi}{\partial y}$ and $u_y = \frac{\partial\varphi}{\partial y} = -\frac{\partial\psi}{\partial x}$
- In 2D polar coordinates, $u_r = \frac{\partial\varphi}{\partial r} = \frac{1}{r}\frac{\partial\psi}{\partial\theta}$ and $u_\theta = \frac{1}{r}\frac{\partial\varphi}{\partial\theta} = -\frac{\partial\psi}{\partial r}$

Further, since $\vec{\nabla}\psi.\vec{\nabla}\varphi = 0$ everywhere on the 2D plane, the lines of constant φ intersect lines of constant ψ perpendicularly.

Similarly, developing potential flow theory in 3D cylindrical coordinates, the potential velocity vector is invariant in θ and $\vec{u}_\theta = 0$ (American notations). Again, where the flow is both irrotational and incompressible:

- In 3D cylindrical coordinates, $u_r = \frac{\partial\varphi}{\partial r} = \frac{1}{r^2 sin\phi}\frac{\partial\psi}{\partial\phi}$ and $u_\phi = \frac{1}{r}\frac{\partial\varphi}{\partial\phi} = -\frac{1}{rsin\phi}\frac{\partial\psi}{\partial r}$

C.1.3. The unsteady Bernoulli equation

As seen in Section Ch.3-1.4, the Navier-Stokes equations can be modified to highlight vorticity $\vec{\omega}$ (or the curl of the velocity $\vec{\omega} = \vec{\nabla} \times \vec{u}$) where the flow is incompressible:

$$\rho \frac{\partial \vec{u}}{\partial t} + \rho(\vec{\omega} \times \vec{u}) = -\vec{\nabla}\left(p + \frac{1}{2}\rho \vec{u} \cdot \vec{u}\right) - \vec{\nabla} \times (\mu \vec{\omega}) + \vec{F}$$

Where the flow is also irrotational ($\vec{\omega} = \vec{0}$), the modified Navier-Stokes equations can be written as:

$\rho \frac{\partial \vec{u}}{\partial t} = -\vec{\nabla}\left(p + \frac{1}{2}\rho \vec{u} \cdot \vec{u}\right) + \vec{F}$, where $\vec{F}$ is the sum of the body forces and is here assumed to reduce to the sole gravity (the Coriolis forces are ignored in this instance). As seen in Section C.1, where the flow is irrotational and incompressible there exists a scalar velocity potential φ solution of the Laplace equation such that $\vec{u} = \vec{\nabla}\varphi$. Replacing the velocity by the velocity potential and switching the spatial and temporal gradients, gives:

$\vec{\nabla}\left(\rho \frac{\partial \varphi}{\partial t} + p + \frac{1}{2}\rho\left|\vec{\nabla}\varphi\right|^2 + \rho g z\right) = 0$, which leads to the pressure equation:

$\rho \frac{\partial \varphi}{\partial t} + p + \frac{1}{2}\rho\left|\vec{\nabla}\varphi\right|^2 + \rho g z = p_0(t)$, where $p_0(t)$ is a function of time.

The pressure equation, also known as the *unsteady Bernoulli equation*, gives pressure everywhere the scalar velocity potential can be solved.

C.1.4. The kinematic and dynamic free surface boundary conditions

Theoretically, finding a solution to the Laplace equation for the scalar velocity potential requires that all boundary conditions be known at all times. For the free surface (or the interface between two fluids of different densities) the unknown position of the interface introduces an additional dependent variable h. Two conditions are therefore used:

- First, the kinematic free surface boundary conditions result from defining the free surface as a material surface (no flow through the surface), therefore expanding the material derivative as follows $\frac{\partial \eta}{\partial t} + u_\eta \frac{\partial \eta}{\partial x} + v_\eta \frac{\partial \eta}{\partial y} - w = 0$, where η is the free elevation, or replacing the velocity field:

$$\frac{\partial \eta}{\partial t} + \frac{\partial \varphi}{\partial x}\frac{\partial \eta}{\partial x} + \frac{\partial \varphi}{\partial y}\frac{\partial \eta}{\partial y} - \frac{\partial \varphi}{\partial z} = 0$$

- Second, the dynamic free surface boundary condition is given by the *unsteady Bernoulli equation* (see Section C.1.3) assuming the pressure is constant along the free surface ($p_0(t) = 0$):

$$\rho \frac{\partial \varphi}{\partial t} + \frac{1}{2}\rho\left|\vec{\nabla}\varphi\right|^2 + \rho g \eta = 0$$

It is noted that the set of equations are non-linear due to the products of dependent variables. In addition, they lead to an unsteady problem where the velocity potential is a function of space and time.

C.1.5. Other boundary conditions

Again, finding a solution to the Laplace equation for the scalar velocity potential requires that all boundary conditions be known at all times. For solid boundary conditions, the normal velocity is zero, which is written as follows:

$\vec{u} \cdot \vec{n} = 0$, where $\vec{n}$ is a normal vector to the boundary, therefore

$\partial \varphi / \partial n = 0$.

C.2.Solutions to the Laplace equation

C.2.1. The Laplace equation

The Laplace equation for the spatial variable φ can be written as follows, depending on the coordinate system:

- In 3D Cartesian coordinates: $\frac{\partial^2\varphi}{\partial x^2} + \frac{\partial^2\varphi}{\partial y^2} + \frac{\partial^2\varphi}{\partial z^2} = 0$
- In 2D polar coordinates: $\frac{1}{r}\frac{\partial}{\partial r}\left(r\frac{\partial\varphi}{\partial r}\right) + \frac{1}{r^2}\frac{\partial^2\varphi}{\partial\theta^2} = 0$
- In spherical coordinates: $\frac{1}{r^2}\frac{\partial}{\partial r}\left(r^2\frac{\partial\varphi}{\partial r}\right) + \frac{1}{r^2 sin\phi}\frac{\partial}{\partial\phi}\left(sin\phi\frac{\partial\varphi}{\partial\phi}\right) + \frac{1}{r^2 sin^2\phi}\frac{\partial^2\varphi}{\partial\theta^2} = 0$

It is noted that if $\frac{\partial\varphi}{\partial z} = 0$, the 3D Cartesian formulation leads to the 2D Cartesian formulation. Similarly, that if $\frac{\partial\varphi}{\partial\phi} = 0$, the 3D spherical formulation leads to the 3D cylindrical formulation.

C.2.2. Separation of variables

To solve the Laplace equation the method of separation of variables is utilised, i.e. a solution φ of the form $X(x).Y(y).Z(z)$ in 3D Cartesian coordinates or the form $R(r).\Theta(\theta)$ in 2D polar coordinates or of the form $R(r).\Phi(\phi).\Theta(\theta)$ in 3D spherical coordinates. Replacing φ by its assumed form and using simplified ordinary derivative notations the following relationship are established:

- In 3D Cartesian coordinates:

$$YZ.X'' + XZ.Y'' + XY.Z'' = 0$$

leading to:

$(X''/X) + (Y''/Y) + (Z''/Z) = 0$, and in turn to the system:

(a) A *simple harmonic motion equations* $X'' - \lambda X = 0$

(b) A *simple harmonic motion equations* $Y'' - \beta Y = 0$

(c) A *simple harmonic motion equations* $Z'' + (\lambda + \beta)Z = 0$

where λ and β are separation variables.

- In 2D polar coordinates:

$$[\, r^2R''/R + 2rR'/R] + [\, \Theta''/\Theta\,] = 0\,,$$

leading to:

(a) A *simple harmonic motion equation* $\Theta'' - \lambda\Theta = 0$, and

(b) An *homogeneous Euler equation* of the form $r^2R'' + 2rR' - \lambda R = 0$,

where λ is a separation variable.

- In 3D spherical coordinates:

$$\left[r^2 sin^2\phi \frac{R''}{R} + 2r sin^2\phi \frac{R'}{R}\right] + \left[cos\phi sin\phi \frac{\Phi'}{\Phi} + sin^2\phi \frac{\Phi''}{\Phi}\right] + \left[\frac{\Theta''}{\Theta}\right] = 0$$

where:

(a) The third term can be reduced by a constant, leading to an ordinary differential *simple harmonic motion equation* of the form $\Theta'' - \lambda\Theta = 0$.

(b) Division of the equation by $sin^2\phi$ allows replacement of the first term by another constant, leading to an ordinary differential equation of the form $r^2R'' + 2rR' - \beta R = 0$, also called the *homogeneous Euler equation*, and

(c) Replacement of the above two constants leads to another ordinary differential equation, the *associated Legendre equation* of the form

$(sin^2\phi)\Phi'' + (cos\phi sin\phi)\Phi' + (\beta sin^2\phi - \lambda)\Phi = 0$.

C.2.3. Solutions to some ordinary differential equations

Using separation of variables, the Laplace equation in Cartesian, polar and spherical coordinates is replaced by a system of ordinary differential equations, amongst which the *simple harmonic equation*, the *homogeneous Euler equation* and the *associated Legendre equation*, have known analytical solutions.

Simple harmonic motion equation

For a *simple harmonic motion equation* of the form $\Theta'' + \omega^2\Theta = 0$, the solution depends on the value of ω^2:

if $\omega^2 = 0$, then $\Theta(\theta) = A_\Theta + B_\Theta\theta$,

if $\omega^2 > 0$, then $\Theta(\theta) = C_\Theta cos(\omega\theta) + S_\Theta sin(\omega\theta)$, with ω integer for periodicity,

and if $\omega^2 < 0$, then $\Theta(\theta) = E_\Theta^+ exp(\omega\theta) + E_\Theta^- exp(-\omega\theta)$,

where the coefficients A_Θ, B_Θ, C_Θ, S_Θ, E_Θ^+, and E_Θ^- are derived from initial and boundary conditions.

Homogeneous Euler equation

For an *homogeneous Euler equation* of the form $r^2R'' + brR' - \beta R = 0$, the solution depends on the values of the b and β and particularly of the roots α_1 and α_2 of $\alpha(\alpha - 1) + b\alpha - \beta = 0$:

if $(b-1)^2 + 4\beta = 0$, the roots are equal and $R(r) = |r|^\alpha(C_R + D_R ln|r|)$,

if $(b-1)^2 + 4\beta > 0$, the roots are real and $R(r) = C_R|r|^{\alpha_1} + D_R|r|^{\alpha_2}$, and

if $(b-1)^2 + 4\beta < 0$, the roots are complex, and

$$R(r) = |r|^{\Re(\alpha)}\left(C_R cos(\Im(\alpha) ln|r|) + D_R sin(\Im(\alpha) ln|r|)\right),$$

where coefficients C_R, and D_R are derived from initial and boundary conditions and where $\Re(\alpha)$ and $\Im(\alpha)$ are the real and imaginary parts of complex root respectively.

Associated Legendre equation

The equation of the form $(sin^2\phi)\Phi'' + (cos\phi sin\phi)\Phi' + (\beta sin^2\phi - \lambda)\Phi = 0$ can be transformed using the change of variable $t = cos\phi$. Substituting $\Phi(\phi) = P(t)$, $\Phi' = \sqrt{1-t^2}P'$ and $\Phi'' = (1-t^2)P'' - tP'$, and dividing by $(1-t^2)$, the equivalent equation for $P(t)$ may be written:

$$(1-t^2)P'' - 2tP' + \left(\beta - \frac{\lambda}{(1-t^2)}\right)P = 0$$

where $P(t)$ is a Legendre polynomial of degree n as follows:

$$P_n(t) = \sum_{k=0}^{int(n/2)}(-1)^k \frac{(2n-2k)!}{2^n k!(n-k)!(n-2k)!} t^{n-2k} \text{ and } P_n^m(t) = (1-t^2)^{m/2}\frac{d^m P_n(t)}{dt^m}$$

C.2.4. Solutions to the Laplace equation

3D Cartesian coordinates

The solution to the Laplace equation in 3D Cartesian coordinates can be written as the sum of the combinations of all three solutions to the *simple harmonic motion equation* for all possible λ and β. The Laplace operator being linear, the sum of known solutions is also a solution.

The boundary conditions of the general problem define the most appropriate cases for these separation variables. For instance, assuming $\beta = -\lambda > 0$ is possible in a practical problem, then a subset of the solution may be written:

$$\varphi = \sum_{\sqrt{\beta}=1}^{\infty}\left(C_X cos(\sqrt{\beta}x) + S_X sin(\sqrt{\beta}x)\right)\left(E_Y^+ exp(\sqrt{\beta}y) + E_Y^- exp(-\sqrt{\beta}y)\right)(A_Z + B_Z z)$$

where the coefficients C_X, S_X, E_Y^+, E_Y^-, A_Z and B_Z are derived from initial and boundary conditions.

2D polar coordinates

Again, the Laplace operator being linear, the sum of the combinations of all possible solutions is also a solution. By definition, $r \geq 0$ and the solution is periodic in θ so that $\lambda \geq 0$ with $\sqrt{\lambda}$ integer and $b = 1$ in the *homogeneous Euler equation* with opposite roots $\alpha = \pm\sqrt{\lambda}$. The resulting solution is:

$$\varphi = C_0 + D_0 ln(r) + \sum_{\sqrt{\lambda}=1}^{\infty} \left[\left(C_R r^{\sqrt{\lambda}} + D_R r^{-\sqrt{\lambda}} \right) \left(C_\Theta cos(\sqrt{\lambda}\theta) + S_\theta sin(\sqrt{\lambda}\theta) \right) \right]$$

where the coefficients C_0, D_0, C_R, D_R, C_θ and S_Θ are derived from initial and boundary conditions.

3D spherical coordinates

To ensure a well-defined solution (even at a point where the spherical coordinates degenerate, on the z-axis at $\phi = 0\ [\pi]$) β should be of the form $\beta = n(n+1)$ with $n \geq 0$ integer, which leads to real and distinct roots for the Euler equation. The periodic nature of θ also leads to $\lambda = m^2$ with $n \geq m \geq 0$ integer. With this, the solution to the Laplace equation in spherical coordinates may be written as the sum of the combinations of all possible solutions:

$$\varphi = \sum_{n=1}^{\infty} \sum_{m=0}^{n} [(C_{nm} r^n + D_{nm} r^{-n-1}) P_n^m(cos\phi)(C_m cos(m\theta) + S_m sin(m\theta))]$$

where P_n^m is the associated Legendre polynomial, and where the coefficients C_{nm}, D_{nm}, C_m and S_m are derived from initial and boundary conditions.

As a particular case of the spherical coordinates, the cylindrical solution ($m = 0$) is:

$$\varphi = \sum_{n=0}^{\infty} (C_n r^n + D_n r^{-n-1}) P_n(cos(\phi)) .$$

C.3.Extension to the diffusion equation

An equation that is similar to the Laplace equation, found in linear wave theory for instance, is the diffusion equation (also called the *heat equation*), which can be written: $\frac{\partial \varphi}{\partial t} = \kappa \, \Delta\varphi$, for the spatial and temporal variable φ, where κ is a physical property of the material or the fluid modelled. Separation of variables (i.e. assuming a solution φ of the form $T(t).\Gamma(x,y,z)$ and replacing in the equation) leads to: $(T'/\kappa T) = (\Gamma''/\Gamma)$, which in turn leads to an exponential decay equation for T of the form $T' - \lambda\kappa T = 0$, the solution of which was of exponential form.

In linear wave theory, for instance in a 2D vertical Cartesian space, φ can be written as $T(t).X(x).Z(z)$, where X and T are solutions $(XT)'' - \lambda(XT) = 0$, and where Z is of exponential form, solution of $Z' - \lambda\kappa Z = 0$.

C.4.Potential flow theory applications

Under certain approximation, analytical solutions of the shallow water equations and of the continuity and Navier-Stokes equations can be established.

C.4.1. 1st order linear waves in finite depth

In a 1st order approximation, the non-linear terms of the dynamic and the kinematic free surface boundary conditions (see Section C.1.4) are here ignored by approaching their variations around the equilibrium state η_0 leading to:

$$\frac{\partial \eta}{\partial t} - \frac{\partial \varphi}{\partial z} = 0 \text{ and } \rho \frac{\partial \varphi}{\partial t} + \rho g \eta = 0$$

This system of boundary conditions can be further transformed taking the temporal

derivative $\partial./\partial t$ of the dynamic condition and eliminating $\partial h/\partial t$ between the two conditions, thus reducing the system to only one linear boundary condition for the velocity potential:

$\frac{\partial^2\varphi}{\partial t^2} + g\frac{\partial\varphi}{\partial z}$, which is of the form of the diffusion equation (see Section C.3), with Z as the solution of an exponential form, verifying $Z'|_{z=\eta} - (\lambda/g)Z|_{z=\eta} = 0$.

Because φ is also solution of the Laplace equation, X is solution of $X'' + \omega^2 X = 0$ and Z solution of $Z'' - \omega^2 Z = 0$, the sign of ω^2 defines the form of these solutions.

With Z the solution of an exponential decay equation at the free surface, it could be assumed that Z is of an exponential form throughout the domain, i.e. of the form $E_Z^+ exp(\omega z) + E_Z^- exp(-\omega z)$, which implies that $\omega^2 > 0$ hence that X is of the form $C_X cos(\omega x) + S_X sin(\omega x)$. Again the coefficients E_Z^+, E_Z^-, C_X and S_X are derived from initial and boundary conditions.

In finite depth, the impermeable bottom is represented using the method of images. With the origin of the vertical axis placed at the bottom of the tank, symmetry in z leads to: $Z(z) = E_Z^+ exp(\omega z) + E_Z^- exp(\omega z)$, or $E_Z cosh(\omega z)$. Thus, the velocity potential may be written as: $\varphi = T(t).E_Z cosh(\omega z).(C_X cos(\omega x) + S_X sin(\omega x))$. Using this expression for the velocity potential, the condition on the function $Z(z)$ at the free surface leads to $E_Z\omega.sinh(\omega\eta_0) - (\lambda/g)E_Z cosh(\omega\eta_0) = 0$, and hence $\lambda = \omega g.tanh(\omega\eta_0)$. With this, it is noted that $\lambda > 0$ whatever the sign of ω, which in turn implies that T is of the harmonic form $C_T cos(\lambda t) + S_T cos(\lambda t)$.

Finally:

$$\varphi = (C_T cos(\lambda t) + S_T cos(\lambda t)).E_Z cosh(\omega z).(C_X cos(\omega x) + S_X sin(\omega x)), \text{ and}$$

$$\lambda = \omega g.tanh(\omega\eta_0)$$

where the constants C_T, S_T, E_Z, C_X and S_X are defined through the boundary and initial conditions.

C.5.Solutions to the 1D shallow water equations

The 1D shallow water equations result from depth integration of the continuity and Navier-Stokes equations. In their conservative form, they are formulated as follows:

$$\frac{\partial h}{\partial t} + \frac{\partial (hu)}{\partial x} = 0 \qquad \text{and} \qquad \frac{\partial (hu)}{\partial t} + \frac{1}{2}\frac{\partial (hu^2)}{\partial x} + \frac{1}{2} g \frac{\partial (h^2)}{\partial x} = 0$$

where h is the water depth, u the longitudinal velocity component along the 1D x-axis and g is the gravitational constant acceleration.

C.5.1. Linearised solution (1^{st} order approximation)

Considering a finite water body, the non-linear terms of the 1D shallow water equations can be transformed into linear terms by considering their variations about the equilibrium solution $\frac{\partial h}{\partial t} + h_0 \frac{\partial u}{\partial x} = 0$ and $h_0 \frac{\partial u}{\partial t} + (hu)_0 \frac{\partial u}{\partial x} + g h_0 \frac{\partial h}{\partial x} = 0$ where the equilibrium is defined as still water, $(hu)_0 = 0$, in a basin of constant water depth h_0. These assumptions result in the linearised equations:

$$\frac{\partial h}{\partial t} + h_0 \frac{\partial u}{\partial x} = 0 \qquad \text{and} \qquad \frac{\partial u}{\partial t} + g \frac{\partial h}{\partial x} = 0.$$

In order to solve these equations, one can separate the variables by removing the term $\frac{\partial^2 h}{\partial t \partial x}$ after deriving the set by $\frac{\partial}{\partial x}$ and $\frac{\partial}{\partial t}$, and doing exactly the opposite to remove the term $\frac{\partial^2 u}{\partial t \partial x}$. Two equations follow:

$$\frac{\partial^2 u}{\partial t^2} - g h_o \frac{\partial^2 u}{\partial x^2} = 0 \qquad \text{and} \qquad \frac{\partial^2 h}{\partial t^2} - g h_o \frac{\partial^2 h}{\partial x^2} = 0.$$

Both equations are of the form of a *simple harmonic motion equation* $Y'' + \mu_y Y = 0$, the solution of which depends on the value of the separation variable $\mu_y = -g h_0$ (see Section C.2), after having separated the dependent variable with $Y(x,t) = T(t).X(x)$. It

should be noted that there are two sets of coefficients, one for each *simple harmonic motion equation*, for $Y \equiv u(x,t)$ and for $Y \equiv h(x,t)$.

Having said that, the solutions are known and in the form of:

$$T(t) = C_{Ty}\cos\left(t\sqrt{\mu_y}\right) + S_{Ty}\sin\left(t\sqrt{\mu_y}\right), \text{ and}$$

$$X(x) = C_{Xy}\cos\left(x\sqrt{\mu_y/gh_o}\right) + S_{Xy}\sin\left(x\sqrt{\mu_y/gh_o}\right),$$

where the coefficients C_{Ty}, S_{Ty}, C_{Xy}, S_{Xy}, and μ_y are defined through the boundary and initial conditions.

Finally, a solution for the linearized 1D shallow water equation is:

$$h(x,t) = \left[C_{Th}\cos\left(t\sqrt{\mu_h}\right) + S_{Th}\sin\left(t\sqrt{\mu_h}\right)\right]\left[C_{Xh}\cos\left(x\sqrt{\frac{\mu_h}{gh_o}}\right) + S_{Xh}\sin\left(x\sqrt{\frac{\mu_h}{gh_o}}\right)\right]$$

$$u(x,t) = \left[C_{Tu}\cos\left(t\sqrt{\mu_u}\right) + S_{Tu}\sin\left(t\sqrt{\mu_u}\right)\right]\left[C_{Xu}\cos\left(x\sqrt{\frac{\mu_u}{gh_o}}\right) + S_{Xu}\sin\left(x\sqrt{\frac{\mu_u}{gh_o}}\right)\right]$$

where the coefficients C_{Th}, S_{Th}, C_{Xh}, S_{Xh}, C_{Tu}, S_{Tu}, C_{Xu}, S_{Xu} and μ_h and μ_u are defined through the boundary and initial conditions.

It is noted that the form of the 2D averaged velocity is compatible with the form found for the velocity potential in a 2D vertical space (see Section C.4.1).